

CAD – INTEGRATED SIZE AND SHAPE OPTIMIZATION OF STEEL
LATTICE ENERGY TRANSMISSION LINE TOWERS USING SIMULATED
ANNEALING

A THESIS SUBMITTED TO
THE GRADUATE SCHOOL OF NATURAL AND APPLIED SCIENCES
OF
MIDDLE EAST TECHNICAL UNIVERSITY

BY

SERKAN ŞAHİN

IN PARTIAL FULFILLMENT OF THE REQUIREMENTS
FOR
THE DEGREE OF DOCTOR OF PHILOSOPHY
IN
CIVIL ENGINEERING

SEPTEMBER 2016

Approval of the thesis:

**CAD – INTEGRATED SIZE AND SHAPE OPTIMIZATION OF STEEL
LATTICE ENERGY TRANSMISSION LINE TOWERS USING
SIMULATED ANNEALING**

submitted by **SERKAN ŞAHİN** in partial fulfillment of the requirements for the degree of **Doctor of Philosophy in Civil Engineering Department, Middle East Technical University** by,

Prof. Dr. Gülbin Dural Ünver
Dean, Graduate School of **Natural and Applied Sciences**

Prof.Dr. İ. Özgür Yaman
Head of Department, **Civil Engineering**

Prof. Dr. Oğuzhan Hasaebi
Supervisor, **Civil Engineering Dept., METU**

Examining Committee Members

Assoc. Prof. Dr. Afşin Sarıtaş
Civil Engineering Dept., METU

Prof. Dr. Oğuzhan Hasaebi
Civil Engineering Dept., METU

Assoc. Prof. Dr. Eray Baran
Civil Engineering Dept., METU

Asst. Prof. Dr. Ercan Gürses
Aerospace Engineering Dept., METU

Asst. Prof. Saeid Kazemzadeh Azad
Civil Engineering Dept., Atılım University

Date: 20.09.2016

I hereby declare that all information in this document has been obtained and presented in accordance with academic rules and ethical conduct. I also declare that, as required by these rules and conduct, I have fully cited and referenced all material and results that are not original to this work.

Name, Last name : Serkan ŞAHİN

Signature :

ABSTRACT

CAD – INTEGRATED SIZE AND SHAPE OPTIMIZATION OF STEEL LATTICE ENERGY TRANSMISSION LINE TOWERS USING SIMULATED ANNEALING

Şahin, Serkan

Ph.D, Department of Civil Engineering

Supervisor: Prof. Dr. Oğuzhan Hasançebi

September 2016, 197 pages

Energy transmission grids have been undergoing drastic changes due to increasing energy demand throughout the world in the recent years. As a result of this trend, sufficient electricity should be transferred from production centers to consumption areas. Therefore, overhead transmission lines (OHTL) gain high importance to be designed on the land reliably and economically. A significant amount of overhead transmission lines is constituted by steel lattice towers. Transmission line towers serve to keep the conductors above the ground transferring electricity from the energy sources to the communities. The new conductor types, increased public awareness on aesthetics and environmental consciousness, and the need for higher capacity lines have resulted in great pressure on designers to develop economic and optimally designed towers. Additionally, optimization of transmission line towers is particularly important in the sense that these structures are designed once as either suspension or tension towers in several different types for each line, yet multitudes of them are erected along transmission lines extending to several hundreds of kilometers. Accordingly, even a small percentage of weight reduction

that can be achieved in the design of a single tower may add up to hundreds or thousands of tons of material when the entire transmission line is considered. This thesis presents a new optimization tool for automated design of steel lattice transmission line towers in real-world engineering practice. This tool has been developed by integrating the simulated annealing (SA) optimization algorithm into the commercial PLS-Tower software to optimize steel lattice towers for minimum weight according to ASCE 10-97 (2000) design specification using both size and shape design variables. In this context, a novel two-phase SA algorithm is specifically developed and compared with a typical SA formulation in four weight minimization problems of real-world steel lattice towers for high voltage overhead transmission lines between 110 and 400 kV. The optimized designs and the CPU time required by the two SA variants are reported for each test problem and then compared with the currently available structural configurations resulting from a conventional design process in order to quantify material saving achieved through optimization. According to results, two-phase SA algorithm converges the optimum solution as good as SA does; however, it requires much less time to converge the optimum solution.

Keywords: Structural Optimization, Steel Lattice Transmission Line Towers, Simulated Annealing, Sizing and Shape Optimization, PLS-Tower Software

ÖZ

ÇELİK KAFES ENERJİ NAKİL HATTI DİREKLERİNİN BENZETİMSEL TAVLAMA YÖNTEMİ KULLANILARAK BİLGİSAYAR DESTEKLİ OPTİMİZASYONU

Şahin, Serkan

Doktora, İnşaat Mühendisliği Bölümü

Tez Yöneticisi: Prof. Dr. Oğuzhan Hasaebi

Eylül 2016, 197 sayfa

Son yıllarda enerji iletim şebekeleri dünya çapında artan enerji talebi yüzünden geniş kapsamlı deęişiklikler geçirmektedir. Artan enerji ihtiyacı sonucunda yeterli miktarda elektrik enerjisi üretim merkezlerinden tüketim alanlarına taşınmalıdır. Bu nedenle havai enerji iletim hatlarının (HEİH) arazi üzerinde düzgün ve ekonomik olarak tasarlanması büyük önem göstermektedir. Havai iletim hatlarının büyük bir kısmını iletim hattı direkleri oluşturmaktadır. İletim hattı direkleri elektrięi üretim merkezlerinden tüketim alanlarına nakleden elektirik iletim kablolarını taşımak için tasarlanan yapılardır. Yeni iletim kablo tipleri, toplumların yapısal sistemler üzerindeki estetik kaygıları ve çevresel duyarlılıklar, daha yüksek kapasiteli enerji nakil hattı ihtiyacı direk tasarımcılarının üzerinde daha ekonomik ve optimum direk tasarımları yapma konusunda büyük baskı oluşturmaktadır. Buna ek olarak, iletim direkleri bir hat boyunca birkaç tip içerisinden askı ya da gerilim tipi direk olarak birkez tasarlanmasına rağmen bunların yığınlarının yüzlerce kilometre boyunca uzanan bir hat üzerinde dikilmesi bu yapıların optimizasyonun önemini bir kez daha göstermektedir. Tüm

iletim hattı dikkate alındığında bir iletim direğinde yapılacak olan küçük bir ağırlık azaltması fazladan yüzlerce hatta binlerce ton malzeme kullanımını önleyecektir. Bu tez pratik mühendislik uygulamalarında çelik kafes iletim direkleri için otomatikleştirilmiş optimizasyon aracı sunmaktadır. Bu araç çelik kafes iletim hattı direklerinin minimum ağırlık optimizasyonu için kesit ve şekil tasarım değişkenlerini dikkate alacak şekilde ve ASCE 10-97 (2010) şartnamesine uygun direkler tasarlamak üzere benzetimsel tavlama (BT) optimizasyon tekniği ile PLS-Tower ticari yazılımını entegre edilerek geliştirilmiştir. Bu kapsamda, yeni bir yöntem olan iki-aşamalı benzetimsel tavlama tekniği özel olarak geliştirilmiş ve tasarım ofisleri tarafından daha önce 110 ve 400 kV voltaj seviyesi aralığında tasarlanmış dört iletim direği yeni geliştirilmiş bu yöntem ve tipik BT yöntemiyle sonuçları karşılaştırmak adına optimize edilmiştir. Minimum ağırlık optimizasyonu sonucunda bu dört iletim direği için optimize edilmiş yapıların yapısal eleman dağılımları ve optimum sonuca ulaşılan kadar ihtiyaç duyulan CPU zamanı hem iki-aşamalı BT hem de tipik BT için belirtilmiştir. Ayrıca tasarım ofisleri tarafından tasarlanmış olan yapıların yapısal eleman dağılımları da optimizasyon sonucu ortaya çıkan sonuçlarla karşılaştırmak adına eklenmiştir. Sonuçlara göre, iki-aşamalı BT tipik BT kadar iyi sonuç vermekte fakat BT'nın optimum sonuca ulaşana kadar ihtiyaç duyduğu zamana oranla çok daha az zamana ihtiyaç duymaktadır.

Anahtar Kelimeler: Yapısal Optimizasyon, Çelik Kafes Enerji Nakil Hattı Direkleri, Benzetimsel Tavlama, Kesit ve Şekil Optimizasyonu, PLS-Tower Programı

To My Family

ACKNOWLEDGMENTS

This study was conducted under the supervision of Prof. Dr. Oğuzhan Hasançebi. I would like to express my earnest thanks and gratitude for his support, guidance, encouragement and criticisms at all levels of this research. It was a great honor and pleasure for me to work under his kind and enlightening supervision.

Also, I would like to express my deepest appreciation to my director in my office and almost (unofficial) co-supervisor Dr. Cenk Tort for his support, advice, comments, and tremendous encouragement throughout the thesis work. He is not only my director and more experienced researcher than I, he is also my elder brother. It was a great honor and privilege for me to work with him.

I want to thank to my manager Cenap Cenk Alkan for his help and encouragement throughout the thesis work.

I want to extend my thanks to Dr. Berk Taftalı for his valuable comments and help. Also, special thanks go to Dr. Ahmet Kuşyılmaz, Ömer Burak Yücel, Cihangir Dikici for their help and friendship.

I wholeheartedly express my grateful feelings to my parents Kerim and Dilhoş Şahin for their endless support, understanding and love. My love for them is eternal. Also, many thanks due my sisters, Semiha and Ülkü Şahin, for their priceless support during my lifetime. My family enthusiasm about this study was always my main source of motivation.

Finally, part of the research presented here is supported by The Scientific Research Council of Turkey under 1501 - Industrial R&D Projects Grant Programme Project No. 3110254, which is gratefully acknowledged.

TABLE OF CONTENTS

ABSTRACT.....	v
ÖZ.....	vii
ACKNOWLEDGMENTS.....	x
TABLE OF CONTENTS.....	xi
LIST OF TABLES.....	xv
LIST OF FIGURES.....	xvii
CHAPTERS	
1. INTRODUCTION.....	1
1.1. Energy Transmission Line Towers.....	1
1.2. Structural Optimization.....	8
1.2.1. Types (Models) of Structural Optimization.....	9
1.2.2. Techniques of Structural Optimization.....	11
1.3. Motivation of the Study.....	18
1.4. Content of the Thesis.....	20
2. ENERGY TRANSMISSION LINE TOWERS.....	25
2.1. General Information about Energy Transmission Line Towers.....	25
2.2. Type of Energy Transmission Line Towers.....	27
2.2.1. Tower Classification According to Function.....	28
2.2.2. Tower Classification According to Geometry.....	32
2.3. Components of Steel Lattice OHTL Towers.....	34
2.4. Clearance Requirements.....	35
2.4.1. Conductor Sag and Tension Calculation.....	35
2.4.2. Catenary Method: Supports at the Same Level.....	36
2.4.3. Catenary Method: Supports at Different Levels.....	47

2.5.	Loads on the OHTL Towers	50
2.5.1.	Self-Weight of Transmission Line Components	51
2.5.2.	Wind Load on Transmission Line Components	51
2.5.3.	Ice Load on Transmission Line Components	62
2.5.4.	Erection and Maintenance Loads	65
2.5.5.	Unbalanced Loading due to Broken Wire Condition	65
2.5.6.	Thermal Loads	65
2.5.7.	Earthquake Load.....	65
3.	LITERATURE SURVEY.....	67
3.1.	On Use of Simulated Annealing in Structural Optimization	68
3.2.	Literature Survey on Optimization of OHTL Towers	76
4.	FORMULATION OF DESIGN PROBLEM	87
4.1.	Design Variables	87
4.2.	Objective Function.....	89
4.3.	Constraints	89
4.3.1.	Compression Capacity	90
4.3.2.	Tension Capacity	93
4.3.3.	Maximum Slenderness Ratios	94
4.3.4.	Geometric Requirements	94
4.3.5.	Formulations of Constraints and Constraint Handling.....	95
5.	SIMULATED ANNEALING.....	97
5.1.	Introduction and Background	97
5.2.	Annealing in Thermodynamic and Simulated Annealing Analogy	101
5.3.	Metropolis Algorithm and Boltzmann Distribution.....	102
5.4.	Method of Simulated Annealing.....	105
5.4.1.	Definition of Simulated Annealing Terms	105
5.4.2.	The Outline of Simulated Annealing Algorithm	106
5.5.	Two-Phase Simulated Annealing Algorithm	114
5.6.	Strengths and Weaknesses of Simulated Annealing.....	121
5.7.	Simulated Annealing vs. Other Search Methods	121

6. PLS-TOWER INTEGRATED OPTIMIZATION SOFTWARE FOR OPTIMUM DESIGN OF TRANSMISSION LINE TOWERS	125
6.1. PLS-Tower	126
6.2. Integration of PLS-Tower with Optimization Algorithms	132
7. NUMERICAL EXAMPLES.....	139
7.1. The 337-Member, 110kV Suspension Tower	141
7.2. The 438-Member, 110kV Tension (Angle) Tower	148
7.3. The 397-Member, 220kV Suspension Tower	155
7.4. The 693-Member, 400kV Suspension Tower	162
8. CONCLUSION.....	171
8.1. Overview and Summary of Thesis	171
8.2. Future Recommendations.....	177
REFERENCES	179
APPENDICES	189
A. COMPONENT LIBRARIES OF PLS-TOWER.....	189
VITA.....	195

LIST OF TABLES

Table 7.1 The optimized weight of 110kV suspension tower and computing time in each run of the SA algorithm.....	144
Table 7.2 The optimized weight of 110kV suspension tower and computing time in each run of the two-phase SA algorithm.....	144
Table 7.3 Comparison of the optimized design weights of 110kV suspension tower with its existing design.	145
Table 7.4 The optimized weight of 110kV tension (angle) tower and computing time in each run of the SA algorithm.....	151
Table 7.5 The optimized weight of 110kV tension (angle) tower and computing time in each run of the two-phase SA algorithm.	151
Table 7.6 Comparison of the optimized design weights of 110kV tension (angle) tower with its existing design	152
Table 7.7 The optimized weight of 220kV suspension tower and computing time in each run of the SA algorithm.....	158
Table 7.8 The optimized weight of 220kV suspension tower and computing time in each run of the two-phase SA algorithm.....	158
Table 7.9 Comparison of the optimized design weights of 220kV suspension tower with its existing design.	159
Table 7.10 The optimized weight of 400kV suspension tower and computing time in each run of the SA algorithm.....	165
Table 7.11 The optimized weight of 400kV suspension tower and computing time in each run of the two-phase SA algorithm.....	165
Table 7.12 Comparison of the optimized design weights of 400kV suspension tower with its existing design.	166

Table 8.1 Design and geometrical data of example towers.	174
Table 8.2 Summary of example towers results.	176

LIST OF FIGURES

Figure 1.1 Parts of a transmission tower.....	1
Figure 1.2 Plan view of a typical transmission line.	2
Figure 1.3 Self-supporting towers.....	5
Figure 1.4 Guyed towers.....	5
Figure 1.5 Pole towers.	6
Figure 1.6 Lattice mast towers.....	7
Figure 1.7 Size optimization of 25-bar truss.....	10
Figure 1.8 Shape optimization of telecommunication tower.	10
Figure 1.9 Topology optimization of high-rise building (Stromberg et al., 2011).	11
Figure 2.1 An energy transmission line illustration (courtesy of Miteng.Inc).....	26
Figure 2.2 A typical energy transmission line tower (courtesy of Miteng Inc.)	27
Figure 2.3 Deviation angle of conductor, α	28
Figure 2.4 Typical suspension (tangent) tower examples (courtesy of Miteng Inc.).	29
Figure 2.5 Typical angle (tension) tower examples (courtesy of Miteng Inc.).....	29
Figure 2.6 Typical terminal (dead-end) tower examples (courtesy of Miteng Inc.).	30
Figure 2.7 Crossing-river towers (courtesy of Miteng Inc.).	30
Figure 2.8 Branching tower (courtesy of Miteng Inc.).	31
Figure 2.9 A typical energy transmission line (courtesy of Miteng Inc.).	31

Figure 2.10 Tower classification according to geometry (courtesy of Miteng Inc.).	33
Figure 2.11 Tower components for a delta-type tower.	35
Figure 2.12 Suspended conductor between equally leveled supports.	37
Figure 2.13 Infinitesimal extended portion of conductor.	37
Figure 2.14 Parameters of catenary.	42
Figure 2.15 Catenary method – supports at different levels.....	47
Figure 2.16 Negative x_1 condition.....	49
Figure 2.17 Definition of tower panel face (EN 50341, 2012).....	54
Figure 2.18 Definition of the angle incidence of wind (IEC 60826, 2003).....	56
Figure 2.19 Yawed wind illustration (ASCE 10-74, 2010).....	57
Figure 2.20 Wind forces on conductors (EN 50341, 2012).....	59
Figure 3.1 25-bar space truss	70
Figure 3.2 400kV double-circuit OHTL tower (Rao, 1995).....	78
Figure 3.3 218-member OHTL tower optimization (Tanikawi and Ohkubo,2004).	80
Figure 3.4 1053-primary member, 1000kV and 181.80 m. OHTL tower (Guo and Li, 2011).	83
Figure 3.5 400kV double-circuit and 41.20 m OHTL tower (Paris et. al, 2012). .	84
Figure 3.6 500kV double-circuit OHTL tower (Chunming et. al, 2012)	85
Figure 3.7 47-bar transmission tower.	86
Figure 4.1 The three shape variables (panel widths) considered to change geometry of a lattice tower.	88
Figure 4.2 The geometric requirements on steel sections of the leg members in a tower.	95

Figure 5.1 A typical heat treatment for a solid material.	98
Figure 5.2 Optimum solution stages of SA.....	100
Figure 5.3 Acceptance probability variance with time.	101
Figure 5.4 Physical analogy.	102
Figure 5.5 Sigmoid transformation function.....	112
Figure 5.6 A flowchart for Phase-1 of two-phase simulated annealing algorithm.	119
Figure 5.7 A flowchart for Phase-2 of two-phase simulated annealing algorithm.	120
Figure 6.1 Opening screen of PLS-Tower.	126
Figure 6.2 Comprehensive structure modeling with PLS-Tower.	127
Figure 6.3 The color-coded analysis result graphic.	129
Figure 6.4 The illustration of overstressed elements	130
Figure 6.5 The table of overstressed elements.....	130
Figure 6.6 The table of overstressed elements.....	130
Figure 6.7 The table of overstressed elements.....	131
Figure 6.8 Integration of the PLS-Tower and optimization algorithms.....	133
Figure 6.9 The user interface in the integrated optimization software to select the initial PLS-Tower model and angle profile database file.	135
Figure 7.1 The 337-member, 110kV suspension tower (all units are in mm).	142
Figure 7.2 Best feasible design weights obtained from SA and two-phase SA for 110 kV suspension tower.	146
Figure 7.3 Final best feasible towers obtained from SA and two-phase SA for 110kV suspension tower.	147

Figure 7.4 The 438-member, 110kV tension (angle) tower (all units are in mm).	149
Figure 7.5 Best feasible design weights obtained from SA and two-phase SA for 110 kV tension tower.....	153
Figure 7.6 Final best feasible towers obtained from SA and two-phase SA for 110kV tension tower.....	154
Figure 7.7 The 397-member, 220kV suspension tower (all units are in mm).....	156
Figure 7.8 Best feasible design weights obtained from SA and two-phase SA for 220 kV suspension tower.....	160
Figure 7.9 Final best feasible towers obtained from SA and two-phase SA for 220kV suspension tower.....	161
Figure 7.10 The 693-member, 400kV suspension tower (all units are in mm)...	163
Figure 7.11 Best feasible design weights obtained from SA and two-phase SA for 400 kV suspension tower.....	168
Figure 7.12 Final best feasible towers obtained from SA and two-phase SA for 400kV suspension tower.....	169
Figure A.1 Component libraries of PLS-Tower.....	193

CHAPTER 1

INTRODUCTION

1.1. Energy Transmission Line Towers

Towers of overhead power lines serve to keep conductors above the ground transferring electricity from the energy sources to the communities. They govern the aesthetic appearance of the transmission line and constitute the significant portion of the investment.

A typical transmission line tower structure consists of three parts; namely tower body, earth-wire peaks and cross arms (Figure 1.1). In general, the geometry of the transmission line towers is influenced by a high number of factors, such as the voltage level, the number of circuits, the required minimum ground clearance, etc.

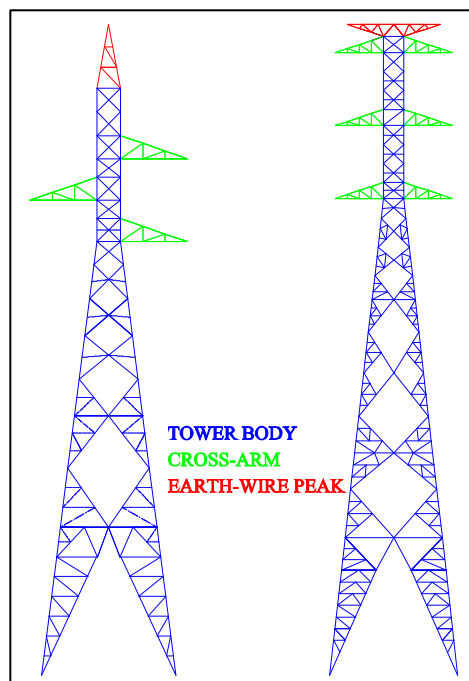


Figure 1.1 Parts of a transmission tower.

The towers in a transmission line can be classified into a number of groups according to their functions as follows (Figure 1.2):

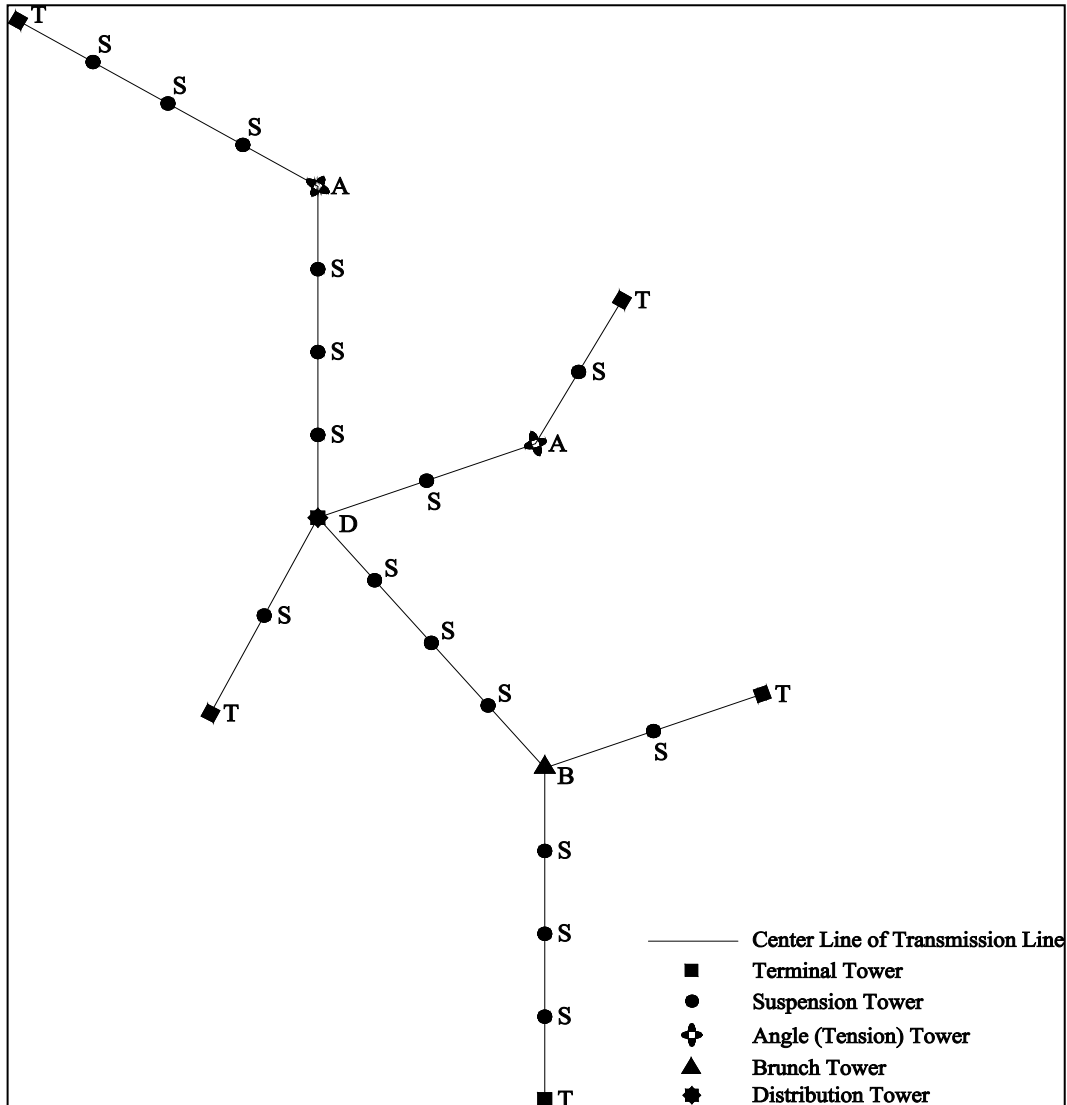


Figure 1.2 Plan view of a typical transmission line.

- **Suspension Towers:** They are intended to carry only weight of the conductor in straight line position or when the angle of line deviation is small. Majority of towers in a typical transmission line fall into this type. They are lightweight and more economical structures as compared to other types.

- ***Tension Towers:*** These towers, also referred to as angle towers, are designed to take the tension loads of the conductors. They are located between suspension towers as well as at turning points where the angle of line deviation is very high.

- ***Terminal Towers:*** They are located at the start and end of an energy transmission line. They are subjected to tension due to conductors or ground wires on one side. Accordingly, they are usually heavier and more costly structures than suspension and tension towers.

- ***Special Towers:***

▪ ***Transposition Towers:*** These towers are used when there is a need to change relative physical positions of the conductors in a transmission line.

▪ ***Crossing Towers:*** They are constructed at locations where there is a need to cross a long span, such as river crossing, lake crossings, other power line crossings and vally crossings.

▪ ***T-off (Branch and Distribution) Towers:*** These towers are placed at locations where the main line branches into multiple lines. If line is divided into two different lines, brunch towers are used to divide the main line. However, if the line is divided into more than two lines, distribution towers are utilized.

In transmission line towers the conductors are attached to the structures through insulators and attachment hardware. The type of hardware used for the conductors is selected based on the position and function of the tower in the transmission line. In the case of suspension towers, suspension insulator sets in the form of I string or V string are utilized. They predominantly transfer forces in the vertical direction and also in the transverse direction with respect to the line direction. On the other hand, in tension towers, the conductors are attached with the tension

insulator set and the conductors exert forces both in the transverse and longitudinal directions.

Other than their function in a line, towers can also be classified according to their structural characteristics. The selection of structural types used for transmission towers is a complicated phenomenon and is affected by several factors as listed below:

- The cost of right of way for the lines;
- Environmental effects of electromagnetic field and impact of the line on the surrounding nature;
- The planned service time of the line;
- Geotechnical considerations; such as weak soil condition, swamp or rocky areas, etc.;
- Manmade or geographical features along the line such as highways, railways, pipelines.

Self-supporting towers (Figure 1.3) are often preferred and widely used. They offer advantages due to reduced right of way. They are often designed in multiple configurations to adopt the structures into different terrains to meet the electrical clearances.

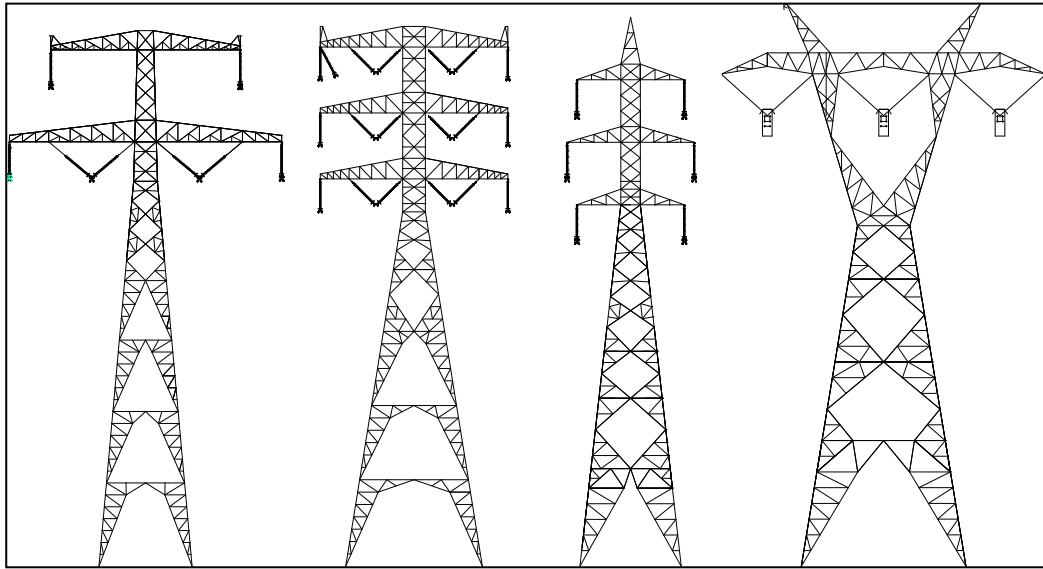


Figure 1.3 Self-supporting towers.

Guyed towers (Figure 1.4) consist of free-standing basements and are supported by guy wires to provide their stability. They are usually preferred if there is no strict limitation about right of way of the line. Although guyed towers require larger landing compared to other types of towers, they are lightweight and economical structures.

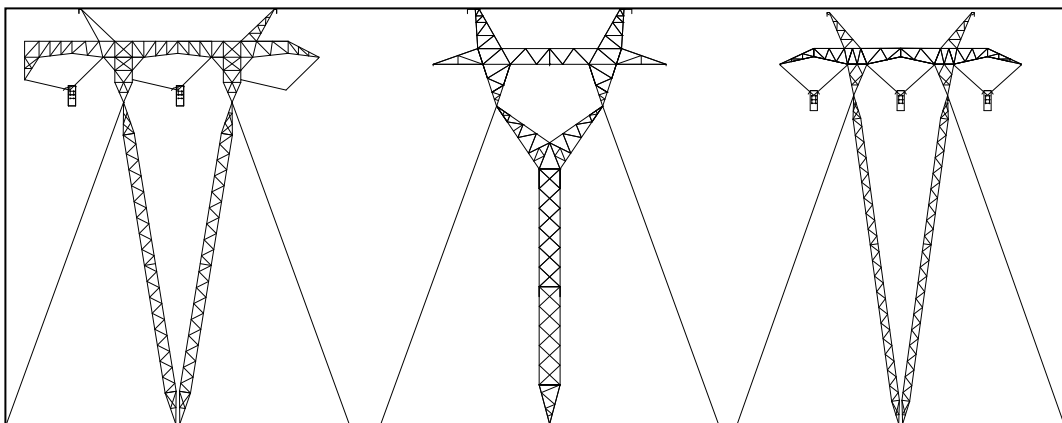


Figure 1.4 Guyed towers.

Pole towers (Figure 1.5) consist of tapered polygonal sections with hollow core. They are usually preferred in urban areas owing to their narrow base dimensions.

Nevertheless, the fact that they have narrow base dimensions does not mean that they are the most economical structures. Pole towers are usually heavier compared to self-supporting towers under the same design considerations.

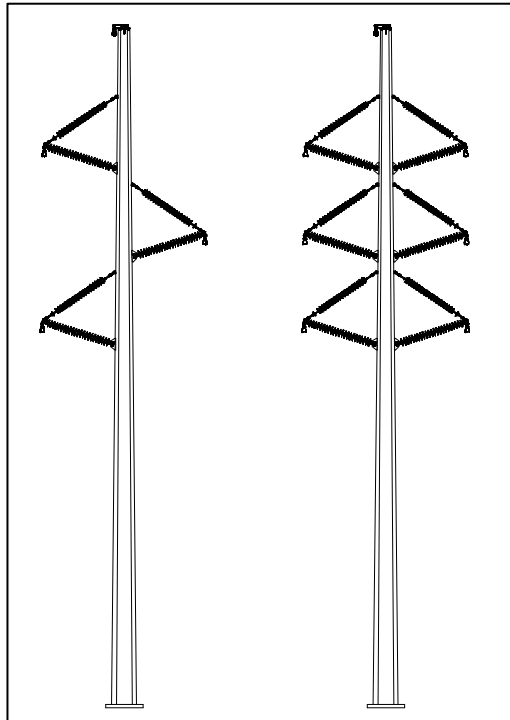


Figure 1.5 Pole towers.

Lattice mast towers (Figure 1.6) are formed by bolting steel angle sections or welding steel pipe sections to create a framework.

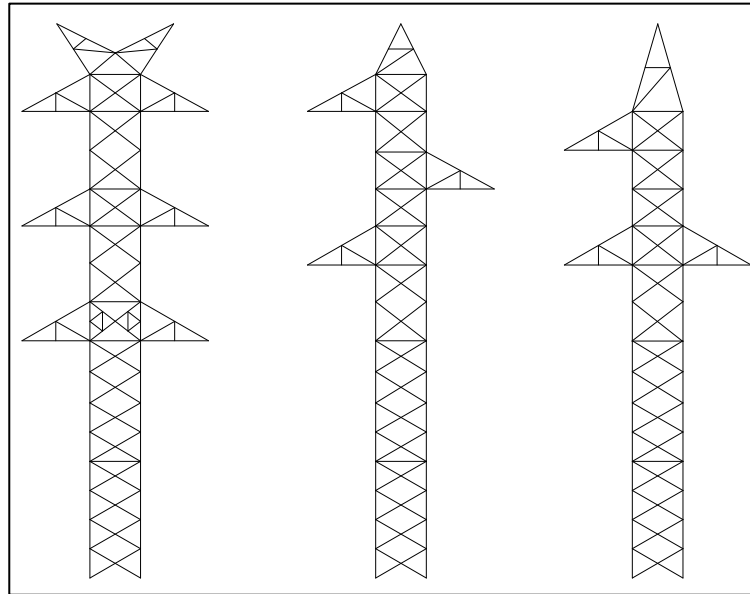


Figure 1.6 Lattice mast towers.

The selection of structure type has a significant influence on tower geometry. In addition, the tower geometry is affected by certain limitations such as electrical clearance requirements. Maintaining electrical clearances around conductors or energized equipment is a must to ensure the public and worker safety. The minimum distances between steel and conductors are taken into consideration while determining tower dimensions. Therefore, the maximum sag and swing of the conductors and earth wires are important parameters in tower design. The maximum sag affects the tower height and hereby the tower weight. The sag and tension calculation for conductors, earth wires and optical ground wires (OPGW) are explained in Chapter 2 broadly.

The sag of conductors and earth wires directly depend on the amount of tension in the cables. However, the tension in the cable is affected by environmental conditions. For instance, if the transmission line is built in or passes through a glacial topography, the ice load should be taken into consideration while conducting sag and tension calculations. Additionally, the towers must be designed according to various load effects as well as their combinations, which are listed below:

- Load due to structural member's self-weight of the tower;
- Load due to self-weight of the conductor, insulator, equipment, and hardware;
- Wind load on the tower;
- Wind load on the conductors, insulators, equipment, and hardware;
- Ice load on the tower;
- Ice load on the conductors, insulators, equipment, and hardware;
- Erection and maintenance load;
- Load due to pre-tension of the conductors;
- Unbalanced loading affects due to broken wire condition;
- Thermal loads;
- Earthquake loads.

1.2. Structural Optimization

The idea of structural optimization can be defined as the finding the solution to a design problem such that the maximum benefit can be derived from the available resources. Structural optimization has been studied widely by researchers since the development of finite element techniques in the mid-1950s. Since structural optimization requires performing repetitive design and analysis studies, the number of finite element runs gets significantly high for optimization of large systems. However, the advances in computer technology nowadays has paved way for integration of structural optimization theory with engineering practice in industry to develop software which are automated to achieve optimized solutions for design of engineering systems.

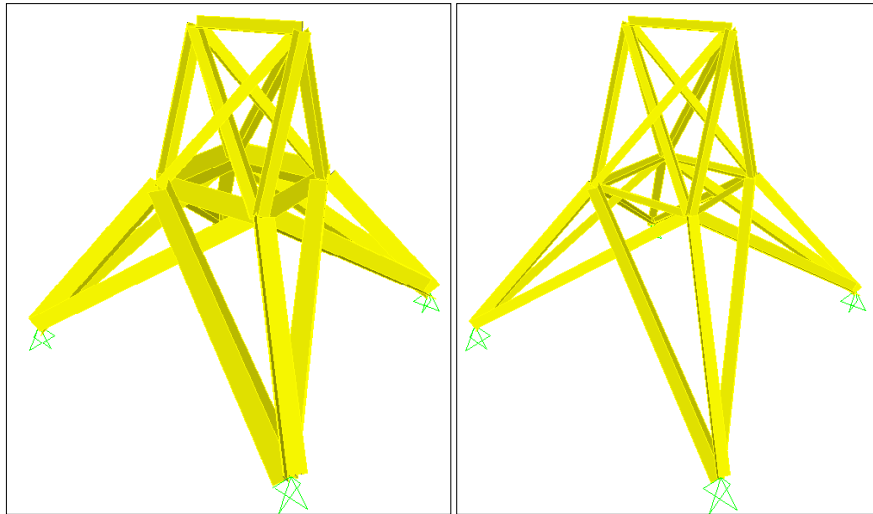
Structural optimization has found plenty of applications in various fields of engineering including:

- Design of aircraft structures;

- Design of civil structures;
- Design of mechanical components;
- Logistics and etc.

1.2.1. Types (Models) of Structural Optimization

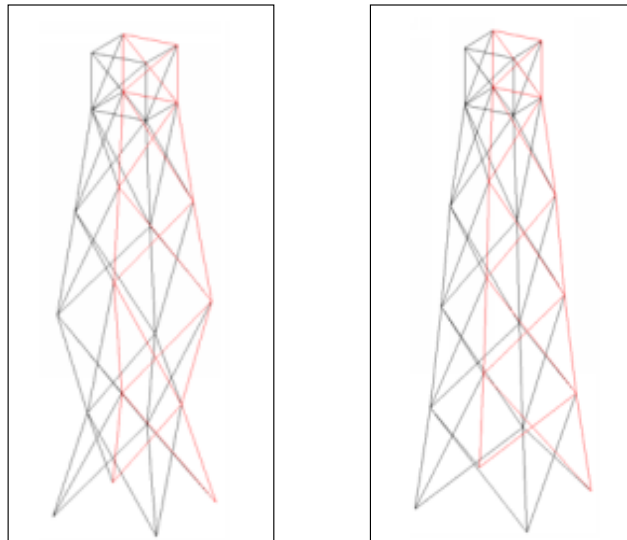
The types (models) of structural optimization can be grouped as size, shape and topology. The distinction of these types is associated with the nature of design variables used during the optimization process. In size optimization (Figure 1.7), the objective is to find cross-sectional areas of structural members that form up a finite element mesh. The boundary of the domain or the range of values of optimization variables is not allowed to vary. In shape optimization (Figure 1.8), the optimization algorithms decide on the geometric dimensions of the finite element mesh without changing the connectivity of the members existing in the model. In topology optimization (Figure 1.9), the aim is to find the best distribution of a material for a continuum media or the best element connectivity configuration for a skeletal structure. This optimization model requires less information available prior to optimization. Only the design domain and boundary conditions are provided at the beginning. It seeks for the optimum solution by investigating the whole feasible domain such that the finite element mesh is restructured and the most advantageous material distribution or member connectivity configuration is captured. The nodes and finite elements in the given domain may be removed and restored successively in the course of optimization process.



a) Before size optimization

b) After size optimization

Figure 1.7 Size optimization of 25-bar truss.



a) Before shape optimization

b) After shape optimization

Figure 1.8 Shape optimization of telecommunication tower.



Figure 1.9 Topology optimization of high-rise building (Stromberg et al., 2011).

1.2.2. Techniques of Structural Optimization

The search methods used to solve structural optimization problems can coarsely be divided into three general groups as gradient-based, metaheuristic and enumerative techniques.

1.2.2.1. Gradient- Based Methods

In gradient-based methods, the numerical procedures involve the first or higher order derivatives of the objective function and constraints with respect to design variables. This is numerically the most expensive procedure of such techniques. Nevertheless, their main advantage is that with a good initial guess, they have fast convergence characteristics. For complicated problems, however, the derivative computation may not be viable. Accordingly, they may suffer from divergence issues or the algorithms might be trapped in a local optimum point. Therefore,

global optimum is not guaranteed and the initial guess plays an important role in the success of the optimization process.

Mathematical programming methods are typical gradient based search algorithms, which are considered as one of the automated design procedures used for optimization (Fiacco and McCormick, 1990; Snyman, 2005). The optimum design is found between the upper and lower bound values under nonlinear inequality constraints. The two main operators of the mathematical programming include direction and step length. The direction is obtained from the gradient of the objective function. Along the direction vector, the step length is determined by one dimensional search techniques and the new design is computed. The updated design is checked against the stopping criteria until convergence is achieved. Belegundu and Arora (1985) studied on the different mathematical programming algorithms in structural optimization. The basic idea of the study was to illustrate the applicability of the mathematical programming methods for structural design area.

“Optimality criteria” methods are other gradient based search techniques, which work on the basis of updating design variables with the use of Lagrangian multipliers (Terai, 1974). First a Lagrangian function is defined combining the objective function, upper and lower bounds of the design variables and also the constraints. The optimum design is determined when the derivative of the Lagrangian function becomes zero with respect to the design variables. Several iterative procedures can be defined for update of the design variables and Lagrange multipliers. Optimality criteria method is preferred with large systems with fewer constraints. Terai (1974) applied optimality criteria to optimize 9-bar, 10-bar, 25-bar, and 72-bar truss structures successfully. Also, Patnaik et. al (1993) utilized optimality criteria to optimize several truss structures in their study.

1.2.2.2. Metaheuristics Search Methods

Metaheuristic techniques are often considered as random search procedures, yet they employ intelligent and imitated search strategies while exploring the design space. They are often inspired from natural phenomena. These techniques may utilize simple local search strategies as well as complex learning procedures. They have randomized and non-deterministic nature and employ special strategies to avoid local optima.

Genetic Algorithm (GA) is one of such techniques, which was pioneered by Holland (1992). The technique was made popular worldwide through the study of Goldberg and Samtani (1986). The technique is inspired from evolution phenomena observed in nature. The basic operators of GA include selection, evaluation, cross-over and mutation. It is a population based method, where a number of initial designs are created and evaluated. GA does not operate on design variables directly. Instead, it works with decoded binary representations of the design variables. From the evaluation of candidate designs, the best designs are predominantly selected. Upon performing cross-over and mutation operations, a new population is created. This process continues through a predefined number of generations or alternatively till the entire population reaches to the optimum design. GA has been applied to a large variety of structures ranging from bridges and truss structures in the literature. A detailed review of GA in structural design applications can be found in Leite and Topping (1998).

Simulated Annealing (SA) is another metaheuristic approach inspired from the annealing process of thermodynamics. In thermodynamics, as a metal cools down, its atoms move to new configurations to attain the minimum energy level. Similarly, the rationale in SA is to attain minimum value of an objective function by mimicking the steps in actual annealing process. The technique uses an iterative process where all the design variables are perturbed sequentially and randomly. Upon evaluation of their fitness, the successful designs are accepted automatically. The technique does not reject unsatisfactory or non-improving

designs instantly because such an approach may lead to convergence to a local optimum. Rather, to escape from a local optimum, a probability function in the form of Boltzmann distribution is introduced such that even the non-improving designs may be accepted. The parameters of Boltzmann distribution are updated throughout the optimization cycles using objective function values and current temperature. This process was called as Metropolis test, which was first introduced by Metropolis (1953). In this test, a random number is created according to a uniform distribution between 0 and 1. If this value is less than the acceptance probability, the candidate design is accepted even though it is a non-improving solution. SA can be applied to a wide range of optimization problems with both continuous and discontinuous design variables. It is not a population based technique; rather each time it works with a single design. Due to its enhanced search characteristics and success in locating the global or near global optimum solution it has gained popularity in structural optimization as well as in other disciplines. Balling (1991) Lamberti (2008), Hasancebi et al. (2010a) deserve significant credit in the application of SA for optimization of steel structures with SA.

Tabu Search (TS) is another metaheuristic method that iteratively searches for the optimum solution. At each step of the algorithm candidate designs are created such that the design variables are perturbed around their close vicinity. This is termed as “move”. The best design among the moves replaces the current design even though it is a non-improving solution. In order to prevent the algorithm from cycling through the same subset of the design domain, a tabu list is created, where the recently visited moves are recorded. If the best design is already in the tabu list, it is not accepted and the algorithm continues with the current design. Only a predefined number of successful moves are stored in the tabu list and the list is continually updated throughout the search. Bland (1994) utilized tabu search for size optimization of truss structures under displacement and reliability constraints. The same problem solved by Bland (1994) was also optimized by Connor et. al (1999) with improved tabu search algorithm.

Evolution Strategies (ES), originated by Schwefel (1965), is another metaheuristic approach being similar to GA conceptually and implementation-wise. The algorithm also takes advantage of idea of natural evolution, yet it involves strategy parameters that lead the search process in the design domain. First, an initial population of designs are created and evaluated according to their fitness values. A recombination operator is utilized to yield an offspring population where not only the design vectors but also the strategy parameters are subjected to recombination. It is followed by mutation of the offspring population. Then, the best individuals are selected according a selection scheme to yield the new generation. Papadrakakis et. al (1998) combined ES with neural network (NN) model to apply size and shape optimization. Two benchmark problems (i.e. a connecting rod and a square plate with central cut) were optimized to illustrate the applicability of proposed methodology in terms of shape optimization. Additionally, two benchmark problems (i.e. six and twenty stories space frames) were solved to show efficiency of the proposed methodology in sizing optimization. Hasancebi et. al (2011) parallelized the ES to increase the convergence time and applied the ES on high-rise steel building for sizing optimization.

Harmony Search (HS) algorithm is derived from the process that musicians follow while searching for the most pleasing harmony. It was first developed by Lee and Gem (2005). This technique also uses a design population called harmony matrix. The harmony consists of a predefined number of design vectors (or so-called harmonies) and it is initially created at random. The design vectors in the harmony matrix are evaluated and sorted in the increasing order with respect to their objective functions. A new harmony is created through selection of design variables either from the harmony matrix or from the whole design domain. A probability parameter exists to derive this process of new harmony selection. The newly generated harmony is checked against the existing ones in the harmony matrix. Depending on the value of its objective function value, it is either placed in the harmony matrix or discarded. Saka (2009) applied the HS algorithm to

optimize sway frames in accordance with BS5950 design specification rules. The results revealed that HS was a robust and powerful optimization algorithm to optimize sway frames. Hasancebi et. al (2010b) proposed an adaptive harmony search methodology to optimize large-scale steel frame structures and applied the algorithm on the two numerical examples.

Particle swarm optimization (PSO) method is another metaheuristic optimization technique taken place in literature and derived by Kennedy and Eberhart (1995). The algorithm is developed by inspiring from animals' herding, flocking, and schooling. Firstly; similar to genetic algorithm, the algorithm generates a random population and new generations are updated to search optimum solution in design space. Each solution is named as "particle" in the algorithm. The basic idea of algorithm is that each particle is a possible solution and moving with a specific velocity to find optimum solution. Each particle remembers its position and its best fitness value. The particles remember their best since each particle should decide search place to search optimum solution. For this reason, the particles exchange information they obtained in their position. The exchanging mechanism is very simple. A particle has a neighbourhood and knows the all fitness value in that neighbourhood. The position having the best fitness is used to adjust particle velocity to search optimum solution. At each step, particles move to new positions. Perez and Behdinan (2007) utilized PSO for structural optimization under design constraints. Three benchmark problems were selected to observe robustness and efficiency of the algorithm. According to results, PSO showed well performance compared to other algorithms. Zeng and Li (2012) combined PSO with group search optimization (GSO). The hybrid algorithm was tested on 25-bar truss structure.

Ant colony (AC), developed by Colorni et al. (1991) and Dorigo (1992), is another nature inspired metaheuristic method that simulates the behavior of ants while they search for food. The ants are social insects and they live in colonies. When they search for food, they always identify the shortest path from the colony

to the food source. As the ant goes from the colony to the food source it deposits an enzyme called pheromone. The other ants follow the pheromone to find the food source. However, they decide on the path based on the density of pheromone and it is always the shortest path that has the most amount of pheromone. In structural optimization; for example, each path corresponds to a steel section in the profile database. The suitability of the steel section is defined by the pheromone level and it is stored in a matrix called Trail Matrix. Following the construction of the Trail Matrix, selection probabilities are assigned to the paths. An ant colony is constructed by selecting a specified number of ants based on the selection probabilities. The ants in the colony are evaluated and following a global pheromone update rule the elitist ant is selected. This process is repeated for specified number of iterations. Zecchin et. al (2006) applied AC algorithm to optimize water distribution systems to minimize the total cost of the systems. Hasancebi and Carbas (2011) studied on size optimization of truss structures with AC algorithm. Two truss structures were considered to optimize and only ready sections were selected for each member.

1.2.2.3. Enumerative Search Methods

Finally, enumerative optimization techniques explore the design space by subdividing it into branches. The typical example of this technique is the branch and bound method (Scholz, 2011). The design space is considered as an inverted tree with branches containing the candidate designs and the full domain is placed in the root. The algorithm searches the branches of this tree. Each node in a branch is considered as a discrete solution and its objective function is evaluated. The solutions are either discarded or accepted depending on the upper and lower bound of the optimum solution. Bremicker et. al (1990) combined the branch and bound method with a sequential linearization procedure. The new algorithm was tested on several structures and the results were compared with the results of branch and bound method. Tseng et. al (1995) improved branch and bound method to speed up the convergence rate of the algorithm for the problems

including the large number of mixed discontinuous and continuous design variables. The improved algorithm was applied on truss type structures.

1.3. Motivation of the Study

Energy transmission line (ETL) or overhead transmission line (OHTL) towers are special structures utilized for safe and economic transmission of electricity to the communities. Due to their large quantity and critical role for people, the design process of these systems requires refined engineering studies.

A standard design procedure of transmission line towers requires that each particular tower is designed with different combinations of body and leg extensions. The various body extensions of a tower are required to increase its height and thus to obtain the required minimum ground clearance as well as clearances for road or river crossings. On the other hand, leg extensions are used to spot the tower on the land according to various geographic and surface conditions along the line. Therefore, during the design process of a particular tower type, a family of finite element (FE) models is generated corresponding to different combinations of body and leg extensions of the tower. The cross-arms as well as tower body that invariably present in every combination are referred to as basic-body, which is jointly shared by all tower family. Different body and leg extensions are added to the basic body of the tower to generate the family. The member groups in the basic body are grouped and designed together according to the maximum forces and strength utilization values across the tower family. On the other hand, the members that belong to a particular combination of body and leg extension, should be grouped internally and sized independently during the design process. To this end, a practical design application of a transmission line tower involves sizing of a high number of member groups, and requires concurrent analyses of finite element models of the entire tower family.

The lattice steel towers resist the applied loadings in the form of truss action.

Therefore, they are modeled and analyzed as space trusses, in which the members are assumed to carry primarily axial compression or tension forces. The structural analysis of a tower is usually performed using finite element method, in which the tower geometry is discretized into a certain number of elements (members) and nodes (joints). Today, various finite element computer programs and software packages are used by the designers working in the industry to analyze towers under ultimate design loads.

Optimization of truss structures with various optimization algorithms has been long studied in the literature. Now, there exists a significant number of powerful search algorithms which are available for optimum design of truss-type structures (and thus transmission-line towers), some of which are discussed in the previous section. However, despite significant theoretical developments in the field of structural optimization as well as emergence of new optimization techniques in the last few decades, the popularity of structural optimization in engineering design practice is still limited. This situation may be attributed to several reasons. Firstly, most of the optimization methods developed in the literature has certain drawbacks as far as their applications to real engineering problems are concerned. Some earlier methods, such as mathematical programming (MP) techniques, were not able to effectively meet the design requirements imposed in practical applications (Belegundu and Arora, 1985). On the other side, the recently developed methods, such as metaheuristic search techniques, can handle all requirements of practical design problems owing to their simple and easy-to-implement optimization algorithms (Saka, 2007; Lamberti and Pappalettere, 2011; Saka and Geem, 2013) yet they often require prohibitively long computing time to converge to a solution especially for large-scale structures subjected to numerous load combinations. Secondly, the researchers have not sufficiently exhibited power and usefulness of structural optimization techniques in real-design problems chosen from the industry practice. Therefore, more effort is required to integrate optimization concepts in real-life engineering applications.

It is also important to emphasize that optimization of steel transmission line towers is particularly important in the sense that these structures are designed once as either suspension or tension towers in several different types for each line, yet multitudes of them are erected along transmission lines extending to several hundreds of kilometers. Accordingly, even a small percentage of weight reduction that can be achieved in the design of a single tower may add up to hundreds or thousands of tons of steel material when the entire transmission line is considered.

1.4. Content of the Thesis

This thesis addresses practical optimum design of steel lattice transmission line towers in real-world engineering practice. The considered optimum design problem was formulated as achieving the minimum weight design of steel lattice towers using both size and shape design variables simultaneously under a set of strength and serviceability constraints imposed according to ASCE 10-97 (2000) design specification. Besides, all the fabrication, detailing and assembly requirements of steel lattice towers were taken into consideration as geometric constraints in order to produce optimized designs of the towers which are viable and directly applicable in real-life practice. The resulting design optimization problem was solved using simulated annealing optimization algorithm.

As discussed in Section 1.2.2.2, SA is a nature inspired meta-heuristic optimization technique which mimics the cooling mechanism of metallic atoms to attain the minimum energy state. The SA algorithm used in this study is essentially based on the improvement of the technique as formulated in Hasançebi et al. (2010a). In addition, a so-called two-phase SA algorithm was proposed in this thesis as an exclusive method for acquiring optimum design of steel transmission towers more rapidly with an annealing algorithm. In the first phase of this method, only the shape parameters are optimized by the annealing algorithm while the steel members are sized with a fully stressed design based heuristic approach. The objective of the first phase is to improve the initial design rapidly in relatively less number of iterations (cooling cycles). In the second

phase, the best design obtained in the prior phase is utilized as the initial solution, and the annealing algorithm is implemented anew for both shape and size variables together under a new set of annealing parameters.

The simulated annealing based algorithms developed for optimum size and shape design of steel lattice transmission line towers were integrated with PLS-Tower software to offer practicing engineers a useful tool which gives them ability to utilize full design and analyses features of PLS-Tower during automated optimum design process as well as to pre- and post-process tower models using its graphical user interface. The PLS-Tower, which is available in every design office working on energy transmission line structures, is the most well-known and recognized software by private corporations as well as state authorities. The software was specifically developed for analysis and design of steel lattice towers used in energy transmission lines. It allows for structural analyses of steel towers considering geometric nonlinearities, where the steel members can be sized according to almost all major design specifications in the world. In the study, the integration of simulated annealing algorithm with the PLS-Tower software is performed such that the optimization module modifies the current solution and generates an alternative design with a new set of size and shape variables. A new finite element model is generated in PLS-Tower for this new design with the help of model generating module that has been specifically developed by the authors to automate construction of a new model in PLS-Tower without any user interaction. The finite element solver of PLS-Tower is then executed to analyze the new design and obtain member forces, joint support reactions and joint displacements. Depending on the size of the model and type of analyses chosen (i.e., linear or nonlinear), the whole analysis process may take from a fraction of second to several minutes. The results of the analyses are collected in group summary tables, which display all details of member and connection design for the most critical element of each member group. The PLS-Tower is also automated to perform all design checks and calculate the resulting weight of the structure. The results obtained from PLS-Tower design module is sent back to optimization

module for objective function calculations in conjunction with an integrated penalty function.

The numerical performances of the SA based optimization algorithms developed here were investigated on four real-world examples of transmission line towers with capacities ranging from 110 kV to 400 kV chosen from the conventional industry practice. In each example, a transmission line tower of steel lattice type was optimized to attain its minimum weight using three shape variables and a selected number of member-size groups in line with the practical design of such structures. The members in the towers were selected from European angle profile database and the design checks were performed as per ASCE 10-97 (2000) specification. The optimized design weights of the towers by the two annealing algorithms (SA and two-phase SA) were reported along with total computing time required for optimization process in each design example. The optimized tower's weights were also compared with the results of conventional design process in order to quantify material saving owing to optimization process.

The thesis is organized in eight chapters. Chapter 2 presents detailed information on transmission towers. The types of towers utilized around the world are discussed. The various geometries of the towers are compared with pros and cons. The conductor mechanics is also explained including sag-tension calculations and clearance requirements. The operational and environmental load cases acting both on the tower structures and also on the conductors are also mentioned.

Chapter 3 provides a detailed literature survey on optimization methods used in the field of structural optimization. Particularly, the simulated annealing algorithm and its variations on optimization of truss structures are discussed. In addition, the existing literature is reviewed for studies on optimization of steel transmission line towers.

Chapter 4 presents a mathematical formulation of design optimization problem of transmission line towers, where objective function, design variables, ready profile lists for discrete optimization, constraints, and penalty functions used are described in detail.

In chapter 5, the SA algorithm employed is introduced in detail along with the proposed two-phase SA algorithm developed in this thesis. Both methods are compared and the need for the proposed two-phase SA algorithm for practical use of optimization in transmission line towers design is underlined. The methodology adopted for generation of candidate designs, evaluation, and metropolis test and constraint handling are provided.

Chapter 6 introduces the software platform through which transmission lines towers are optimized in this study. PLS-Tower software and its features, the developed software platform and its integration with PLS-Tower are explained. The type and quantity of data transferred between PLS-Tower software and optimization routine are specified.

The efficiencies of the annealing algorithms are investigated and quantified in Chapter 7 through real-world numerical instances of transmission line towers. The optimized design weights of the towers by both annealing algorithms are reported along with total computing time required for optimization process in each design example. The optimized towers' weights are also compared with the results of conventional design process in order to quantify material saving owing to optimization process.

Section 8 summarizes the main findings of this study and concludes the thesis with recommendations for future studies.

CHAPTER 2

ENERGY TRANSMISSION LINE TOWERS

2.1. General Information about Energy Transmission Line Towers

Energy transmission line (ETL) towers or, in other words; overhead transmission line (OHTL) towers serve to keep the conductors above the ground transferring the electricity from the energy sources to the communities. In the recent years, the electric transmission grids have been undergoing drastic changes due to increasing energy demand throughout the world. The new conductor types, increased public awareness on aesthetics and environmental consciousness, and the need for higher capacity lines have resulted in great pressure on designers to develop economic and optimally designed towers. Various types of towers are used in the transmission grids, including steel lattice, steel polygonal, concrete, wood and hybrid types (Kießling et al., 2003). However, due to their high strength-to-weight ratios steel lattice type is often preferred by majority of the utilities. Typically, the heights of steel lattice transmission line towers range from 15 meters to more than 300 meters.

The characteristic feature of a transmission line tower is its height. Since the towers are usually constructed on a narrow land, these structures can be identified as slender structures. Another important feature of these structures is that their design is predominantly controlled by wind loading. Wind load on the insulators and conductors should be taken into consideration as well as wind load on the tower. Lattice towers have an advantage in this sense because they not only have sufficient bending rigidity but also have smaller surface areas in terms of wind pressure exposure. The members of a lattice tower are usually selected from single or double steel angle profiles.

A typical overhead transmission line shown in Figure 2.1 consists of conductors, towers and insulators. The electricity is transmitted through the conductors. The conductors are usually made up of all aluminum strands (AAC) or aluminum strands with steel core (ACSR). Towers serve as supporting structures to hold the conductors at a certain height above the ground level. Finally, insulators ensure connection between conductors and towers, and also isolate the conductors electrically.

In a typical tower there exist several hardware components serving to attach conductors to the cross-arms and also to keep the conductors stable under environmental loads. Among these hardware components, insulators prevent electricity to flow through the tower structure, spacer keeps conductors touching each other. Dampers prevent resonance of conductors under wind loading. Jumpers function to transmit electricity over the cross-arm without any loss. Aircraft warning spheres are attached to the conductors to prevent collision of air vehicles to the transmission line. Some these components are illustrated in Figure 2.2.

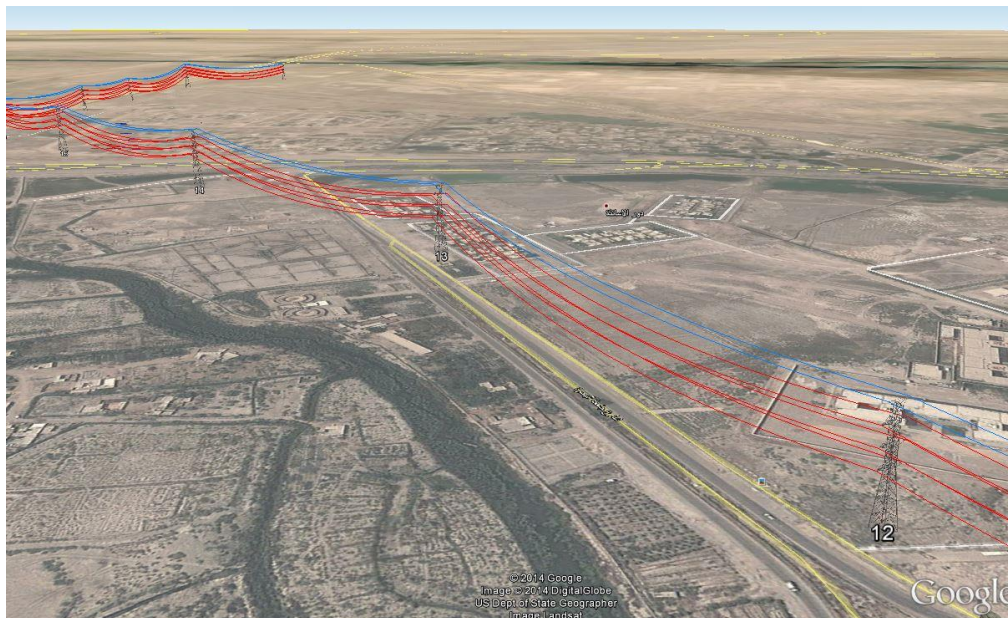


Figure 2.1 An energy transmission line illustration (courtesy of Miteng.Inc)

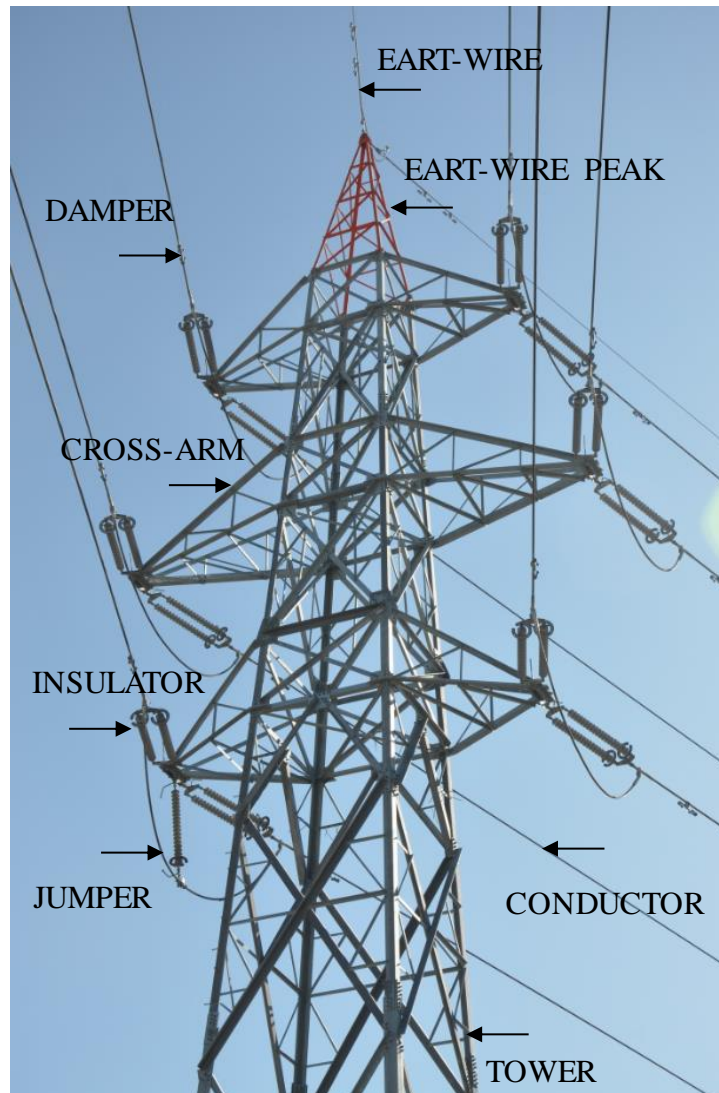


Figure 2.2 A typical energy transmission line tower (courtesy of Miteng Inc.)

2.2. Type of Energy Transmission Line Towers

Energy transmission lines are classified as low, high and very high voltage lines according to voltage level. Since low voltage lines are assigned for local or inner-city transmission, they can also be built underground. Although underground lines are more expensive and need much more insulation than over-head transmission lines, they are often preferred from the standpoint of aesthetic and safety. On the other hand, very high and high voltage lines are usually constructed overhead

between electricity production centers to consumption areas. Classifications of energy transmission line towers can be carried out according to many different criteria. However, the function, and geometry are more frequently used for their classification.

2.2.1. Tower Classification According to Function

Different types of towers are used in an energy transmission line depending on their locations and functions. Since usually multitudes of towers need to be used in an energy transmission line, classifications of them are carried out to shorten the design time, manufacturing of the tower members as well as overall erection time of a tower. Besides, the classification simplifies the design process and is highly advantageous from economical point of view.

The OHTL towers are usually named according the angle of line deviation (α). A typical top view of tower cross-arm is illustrated to show the angle of line deviation in Figure 2.3. At locations where the angle of line deviation is between 0° to 2° degrees, *suspension (tangent) towers* are utilized to carry the loads of conductors. It follows that the suspension towers are designed to carry the conductors in a straight or almost-straight routes (Figure 2.4). Therefore, under normal conditions they are not subjected to high longitudinal forces because the conductors' tensile loads acting on both sides of a suspension tower counteract with each other.

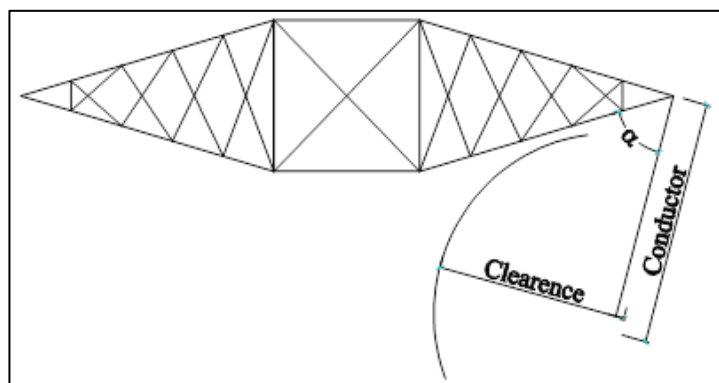


Figure 2.3 Deviation angle of conductor, α .



Figure 2.4 Typical suspension (tangent) tower examples (courtesy of Miteng Inc.).

At locations where the angle of line deviation is between 2° to 20° degrees, *angle suspension towers* or *angle (tension) towers* are used as illustrated in Figure 2.5. Angle suspension towers carry the conductors with an inclined position of insulator sets. Since unfavorable tower top geometry results, angle suspension towers are not considered as a part of line project for over than 110 kV lines (Kiessling et. al., 2003). Therefore, usually angle (tension towers) are utilized more often at locations where the angle of line deviation is higher than 2° up to 60° . The angle towers are designed to carry the unbalanced tensile forces resulting from significant changes in line direction.



Figure 2.5 Typical angle (tension) tower examples (courtesy of Miteng Inc.).

There should be some insurance points in a line to prevent destruction of a line as a whole if a tower collapses. Hence, angle towers are introduced at certain locations in a line so as to separate the whole line into certain segments to prevent an overall line destruction.

Finally, *terminal towers (dead-end)* are located at the start and end of an energy transmission line. These towers are subjected to high unbalanced tensile loads due to conductors on one side of the tower only (Figure 2.6).



Figure 2.6 Typical terminal (dead-end) tower examples (courtesy of Miteng Inc.).

Apart from the commonly used tower types mentioned above, there exists some special energy transmission line towers that should be designed exclusively to avoid extreme challenges, such as branch towers, crossing-river towers, and etc. Typical examples are shown in Figure 2.7 and Figure 2.8 for crossing towers and branching tower, respectively.

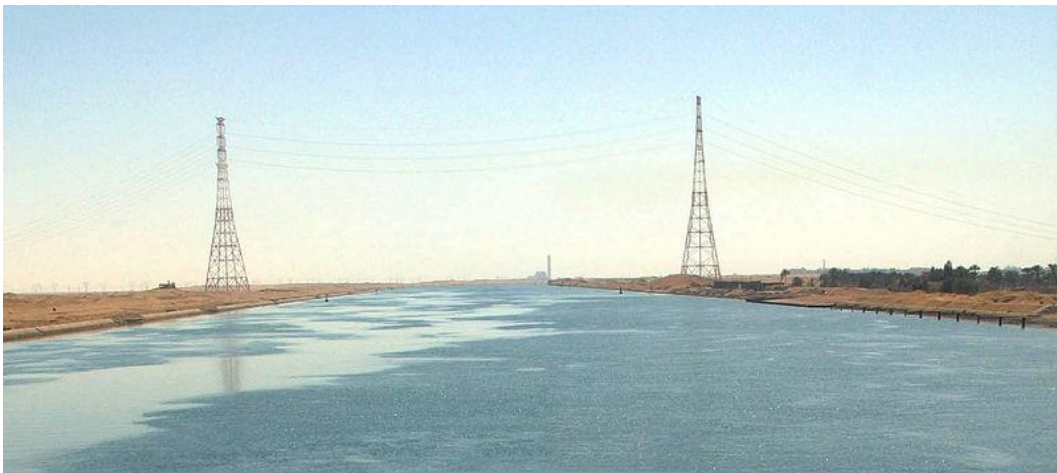


Figure 2.7 Crossing-river towers (courtesy of Miteng Inc.).

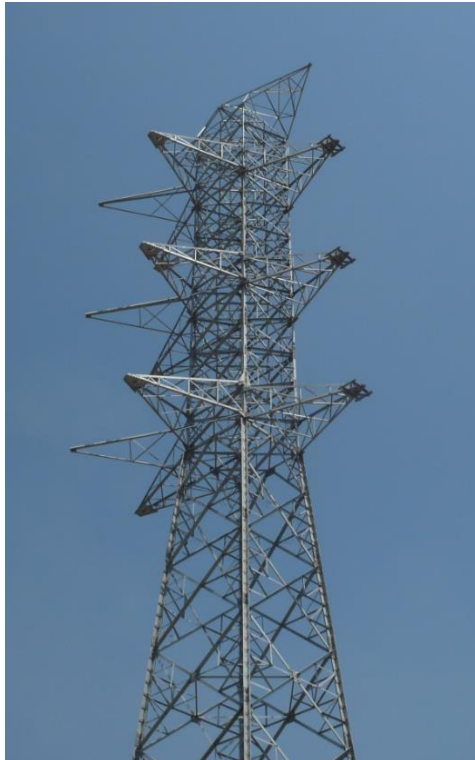


Figure 2.8 Branching tower (courtesy of Miteng Inc.).

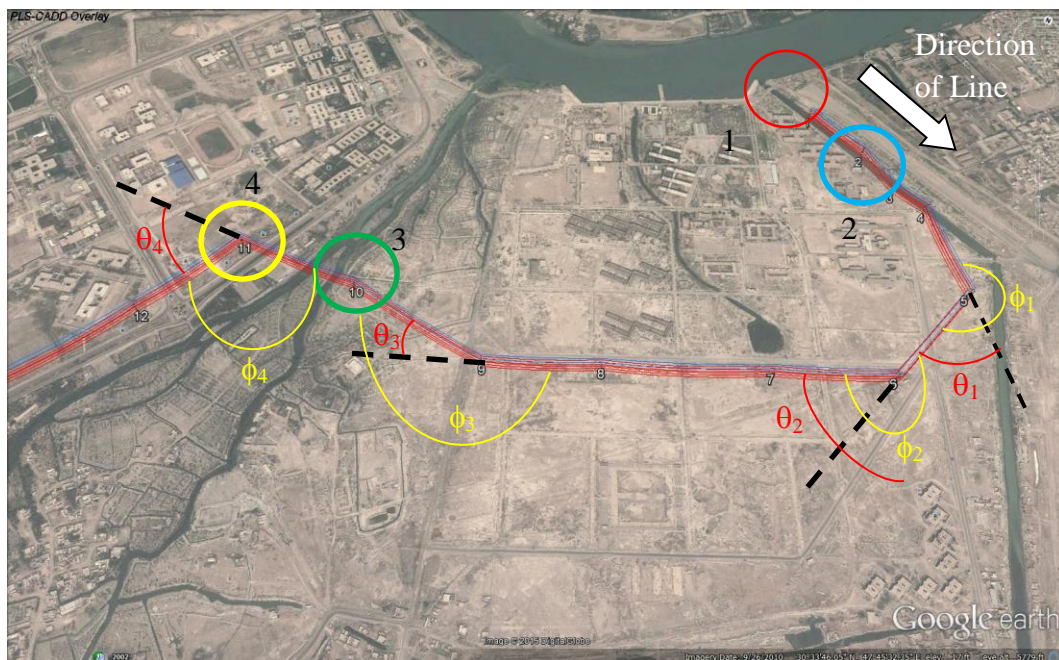


Figure 2.9 A typical energy transmission line (courtesy of Miteng Inc.).

Different types of OHTL towers in an energy transmission line are illustrated in Figure 2.9. Tower 1 is the terminal tower; tower 2 is a suspension tower; and towers 3 and 4 towers are angle suspension and angle towers, respectively. The tower angle (θ) is defined as the angle (ϕ) measured in clockwise direction from the back-span of the tower towards the a-head span of the tower minus 180 degrees as illustrated in Figure 2.9.

2.2.2. Tower Classification According to Geometry

The energy transmission line towers can be designed in various structural characteristics; such as self-supporting towers, pole towers, lattice towers. Amongst them, lattice towers have the following superiorities over the others,

- i) Easily adopted for any height and form;
- ii) Easily separated for transportation and re-erection;
- iii) Easily strengthened, repaired, shortened or extended;
- iv) Have long life if they are well protected against corrosion.

The steel lattice towers can be classified as delta, pine or guyed towers in terms of their geometrical appearance. The choice of towers' geometry to be used in a newly designed transmission line is affected by various considerations. For instance, since energy loss is significant for long span energy transmission lines, horizontally arranged conductors; namely delta-type towers, are usually preferred for these lines. If the tower construction land is not limited, guyed towers may be encouraged for less material use. Hence, conductor arrangement (i.e. horizontal or vertical arrangement) and landing limitations usually govern the choice of geometry for towers used in energy transmission lines.

Typical examples of delta, pine and guyed towers can be found in Figure 2.10.



a) Delta-type tower examples



b) Pine-type tower examples



c) Guyed tower examples

Figure 2.10 Tower classification according to geometry (courtesy of Miteng Inc.).

2.3. Components of Steel Lattice OHTL Towers

The geometrical dimensions of a tower are governed by electrical specifications and limitations. However, all transmission line towers consist of the following three main components, which are illustrated in Figure 2.11:

- i) Cross-arms (consoles) and/or bridges;
- ii) Earth wire peak;
- iii) Tower body and legs.

The portion above the top cross-arm or bridge is called the earth wire peak. The earth shield wire is connected to the tip of the peak. The cross-arms and bridge hold transmission conductors. The dimensions of cross arms depend on voltage level and configuration and electrical specifications. The portion of the tower from the ground level up to the top cross arm or bridge constitute tower body and legs. This portion of the tower plays a vital role for maintaining required ground clearance of the bottom conductor of the transmission line.

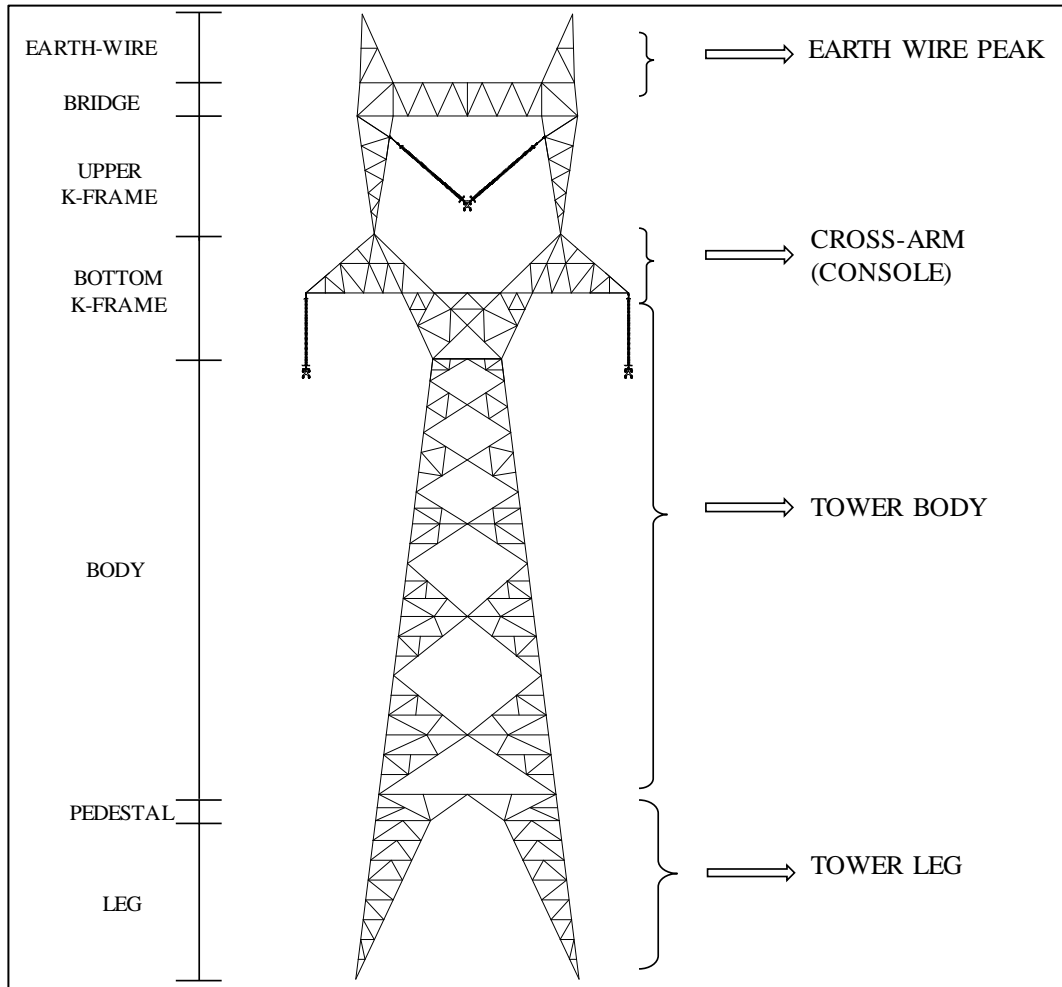


Figure 2.11 Tower components for a delta-type tower.

2.4. Clearance Requirements

2.4.1. Conductor Sag and Tension Calculation

For the sustainability and the safety of the overhead transmissions, one of the most important considerations is the analysis of sag and tension of the conductors. The conductors should be properly installed for the efficiency of the overhead transmission. Therefore; in the first place, the amount of sag and tension of the relevant conductor has to be determined under daily temperature, extreme temperatures, operational wind, and ice loading if applicable. In general, the

factors affecting the design and stringing of the conductors can be listed as follows:

- i) Conductor load per unit length;
- ii) Conductor tension;
- iii) Span length between supports (i.e. OHTL towers);
- iv) Temperature.

The conductor load per unit length needs special consideration beside the conductor self-weight per unit length. The factors that affect the conductor load are as follows:

- i) Conductor self-weight;
- ii) Weight of ice or snow clinging to the conductor;
- iii) Wind blowing against the conductor.

It is preferable to minimize the sag of conductor to avoid the need for designing very tall towers. Besides, a sufficient ground clearance is required under the bottom conductors.

2.4.2. Catenary Method: Supports at the Same Level

Figure 2.12 illustrates a suspended conductor between two equally leveled supports which are located a horizontal distance, D (m), away from each other. In this figure, O is the lowest point of the suspended conductor; the catenary length of the conductor is L (m); W (N/m) is assumed as the unit weight of the conductor per unit length; T (N) is the tensile force of the conductor at any point P in the direction of the curve, and finally H (N) is the horizontal tensile force at the origin point O .

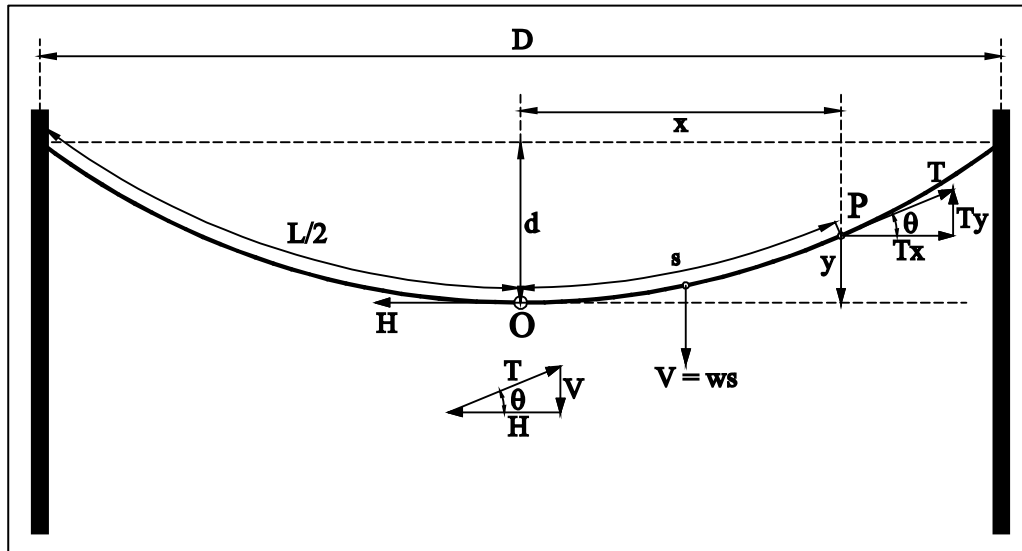


Figure 2.12 Suspended conductor between equally leveled supports.

The following equilibrium equations can be written for the conductor portion OP under the tensile force T, self-weight $w \times s$, and horizontal force H.

$$T_x = H \tag{2.1}$$

$$T_y = w \times s \tag{2.2}$$

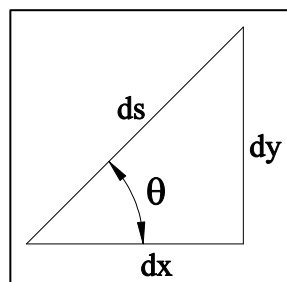


Figure 2.13 Infinitesimal extended portion of conductor.

If an infinitesimal point is selected around point P and the conductor distance between O and P, s is extended in an amount of ds as shown in Figure 2.13, the following equation can be written;

$$\tan \theta = \frac{dy}{dx} = \frac{V}{H} = \frac{w \times s}{H} \quad (2.3)$$

From the geometry,

$$ds^2 = dx^2 + dy^2$$

$$\left(\frac{ds}{dx}\right)^2 = 1 + \left(\frac{dy}{dx}\right)^2 \quad (2.4)$$

Using the Eqn. (2.3) and Eqn. (2.4), the following equation is obtained:

$$dx = \frac{ds}{\sqrt{1 + \left(\frac{ws}{H}\right)^2}} \quad (2.5)$$

Integrating the both sides of the Eqn. (2.5),

$$x = \int \frac{ds}{\sqrt{1 + \left(\frac{ws}{H}\right)^2}} \quad (2.6)$$

The result of the integration of the Eqn. (2.5) is that

$$x = \frac{H}{w} \sinh^{-1}\left(\frac{ws}{H}\right) + C \quad (2.7)$$

where C is the integration constant, which is determined by solving the equation when x=0.

Noting that when x=0, s=0, and as a result C=0. Therefore, the Eqn. (2.7) converts into the Eqn. (2.8).

$$s = \frac{H}{w} \sinh\left(\frac{wx}{H}\right) \quad (2.8)$$

When $s = \frac{L}{2}$, $x = \frac{D}{2}$, substituting this into the Eqn. (2.8),

$$\frac{L}{2} = \frac{H}{w} \sinh\left(\frac{wD}{2H}\right) \quad (2.9)$$

$$L = \frac{2H}{w} \sinh\left(\frac{wD}{2H}\right)$$

or the Eqn. (2.9) can be written as

$$L = \frac{2H}{w} \left[\frac{1}{1!} \left(\frac{wD}{2H}\right) + \frac{1}{3!} \left(\frac{wD}{2H}\right)^3 + \dots \right] \quad (2.10)$$

or approximately,

$$L = D \left(1 + \frac{w^2 D^2}{24H^2} \right)$$

From the Eqn. (2.3) and the Eqn. (2.8),

$$\frac{dy}{dx} = \frac{ws}{H} = \sinh\left(\frac{wx}{H}\right) \quad (2.11)$$

$$dy = \sinh\left(\frac{wx}{H}\right) dx$$

Integrating the both sides of the Eqn. (2.11), we obtain

$$y = \int \sinh\left(\frac{wx}{H}\right) dx$$

$$y = \frac{H}{w} \cosh\left(\frac{wx}{H}\right) + C_1 \quad (2.12)$$

If the lowest point of the catenary is considered as the origin, $x=0$, $y=0$, and then

$$C_1 = -\frac{H}{w}, \text{ since by the series, } \cosh(0) = 1.$$

Hence,

$$y = \frac{H}{w} \left[\cosh\left(\frac{wx}{H}\right) - 1 \right] \quad (2.13)$$

The Eqn. (2.13) is called as equation of catenary and can be written as;

$$y = \frac{H}{w} \left[\left\{ 1 + \frac{1}{2!} \left(\frac{wx}{H}\right)^2 + \dots \right\} - 1 \right]$$

or approximately,

$$y = \frac{wx^2}{2H} \quad (2.14)$$

From Figure 2.11 Figure 2.12, the tensile force on the conductor is,

$$T = \sqrt{H^2 + V^2} \text{ or } T = H \sqrt{1 + \left(\frac{V}{H}\right)^2} \quad (2.15)$$

From Eqn. (2.14) and Eqn. (2.15),

$$T = H \sqrt{1 + \left(\frac{dy}{dx}\right)^2} \quad (2.16)$$

From Eqn. (2.12) and Eqn. (2.16),

$$T = H \cosh\left(\frac{wx}{H}\right) \quad (2.17)$$

The total tension in the conductor at $x = D / 2$ is;

$$T = H \cosh\left(\frac{wD}{2H}\right) \quad (2.18)$$

or

$$T = H \left[1 + \frac{1}{2!} \left(\frac{wD}{2H}\right)^2 + \frac{1}{4!} \left(\frac{wD}{2H}\right)^4 + \dots \right]$$

when $x = D / 2$, $y = d$ from Eqn. (2.13)

$$d = \frac{H}{w} \left[\cosh\left(\frac{wD}{2H}\right) - 1 \right] \quad (2.19)$$

or

$$d = \frac{L}{2} \left[\frac{1}{2} \left(\frac{wD}{2H}\right) + \frac{1}{4!} \left(\frac{wD}{2H}\right)^3 + \frac{1}{6!} \left(\frac{wD}{2H}\right)^5 + \dots \right]$$

or approximately,

$$d = \frac{wD}{8H} \quad (2.20)$$

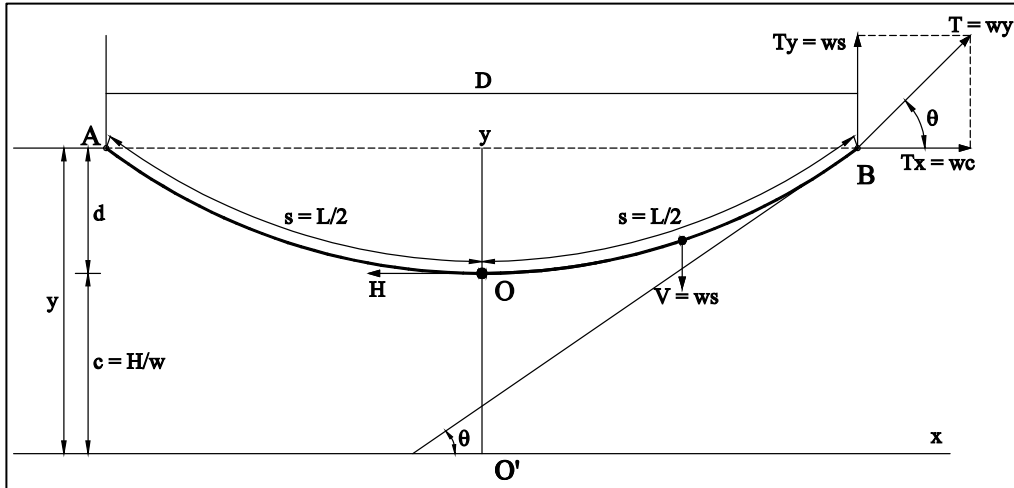


Figure 2.14 Parameters of catenary.

From Figure 2.14, O is the lowest point of the catenary curve.

$$T_y = \frac{L}{2} w \text{ or } s = \frac{L}{2} \quad (2.21)$$

Then,

$$T_x = wc \text{ and } T_y = ws \quad (2.22)$$

where c is the length of an arbitrary part of the conductor.

At the equilibrium condition;

$$T_x = H \text{ and } T_y = V \quad (2.23)$$

where H and V are the horizontal conductor tension and the weight of the conductor per meter of span times distance from maximum sag to support, respectively.

The calculation of T can be simplified as

$$T = \sqrt{H^2 + V^2} \quad (2.24)$$

$$T = \sqrt{(wc)^2 + (ws)^2} \quad (2.25)$$

$$T = \left(\sqrt{c^2 + s^2}\right)w \quad (2.26)$$

From Eqn. (2.22) and Eqn. (2.23), one can write

$$c = \frac{H}{w} \quad (2.27)$$

If Eqn. (2.27) is inserted into the Eqn. (2.8), we obtain

$$s = c \sinh\left(\frac{x}{c}\right) \quad (2.28)$$

From Eqn. (2.12) and Eqn. (2.27),

$$y = c \left[\cosh\left(\frac{wx}{c}\right) \right] + C_1 \quad (2.29)$$

From Figure 2.14, when $x = D / 2$ (i.e. at point O),

$x = 0$ and $y = 0$.

Equation (2.29) at $x = D/2$ becomes,

$$c = c[\cosh(0)] + C_1 \longrightarrow C_1 = 0$$

Therefore,

$$y = c \left[\cosh \left(\frac{x}{H} \right) \right] \quad (2.30)$$

Squaring both sides of Eqn. (2.28) and Eqn. (2.30), we obtain

$$s^2 = c^2 \left[\sinh^2 \left(\frac{x}{c} \right) \right] \quad (2.31)$$

$$y^2 = c^2 \left[\cosh^2 \left(\frac{x}{H} \right) \right] \quad (2.32)$$

Subtracting Eqn. (2.31) from Eqn. (2.32) leads to the following equations:

$$\begin{aligned} y^2 - s^2 &= c^2 \left[\cosh^2 \left(\frac{x}{H} \right) - \sinh^2 \left(\frac{x}{c} \right) \right] \\ y^2 - s^2 &= c^2 \\ y &= \sqrt{c^2 + s^2} \end{aligned} \quad (2.33)$$

From Eqn. (2.26) and Eqn. (2.33), one can write

$$T_{\max} = wy \quad (2.34)$$

Eqn. (2.34) shows that the maximum tension takes place at the supports.

According to Figure 2.13,

$$y = c + d \quad (2.35)$$

From Eqn. (2.33) and Eqn. (2.35),

$$c + d = \sqrt{c^2 + s^2} \longrightarrow c = \frac{s^2 - d^2}{2d} \quad (2.36)$$

If Eqn. (2.35) is inserted into Eqn. (2.34), we obtain

$$T_{\max} = w(c + d) \quad (2.37)$$

Substituting Eqn. (2.36) into Eqn. (2.37), one obtains the maximum value of the conductor tension, which is expressed as follows:

$$T_{\max} = \frac{w}{2d} (s^2 + d^2) \quad (2.38)$$

Maximum sag occurs at point O. At this point, the vertical component of the conductor tension is zero. Therefore, the minimum tension takes place in Eqn. (2.39) at where the point of maximum sag and that tension force is equal to horizontal component of tension.

$$T_{\min} = H = wc \quad (2.39)$$

Substituting Eqn. (2.36) into Eqn. (2.39) yields

$$T_{\min} = w \left(\frac{s^2 - d^2}{2d} \right) \quad (2.40)$$

From Figure 2.3,

$$c = y - d \quad (2.41)$$

The total conductor length; L,

$$L = 2s \tag{2.42}$$

From Eqn. (2.28) and Eqn. (2.42),

$$L = 2c \sinh\left(\frac{x}{c}\right) \tag{2.43}$$

Also, from Eqn. (2.37) and Eqn. (2.39),

$$T_{\max} = T_{\min} + wd \tag{2.44}$$

2.4.3. Catenary Method: Supports at Different Levels

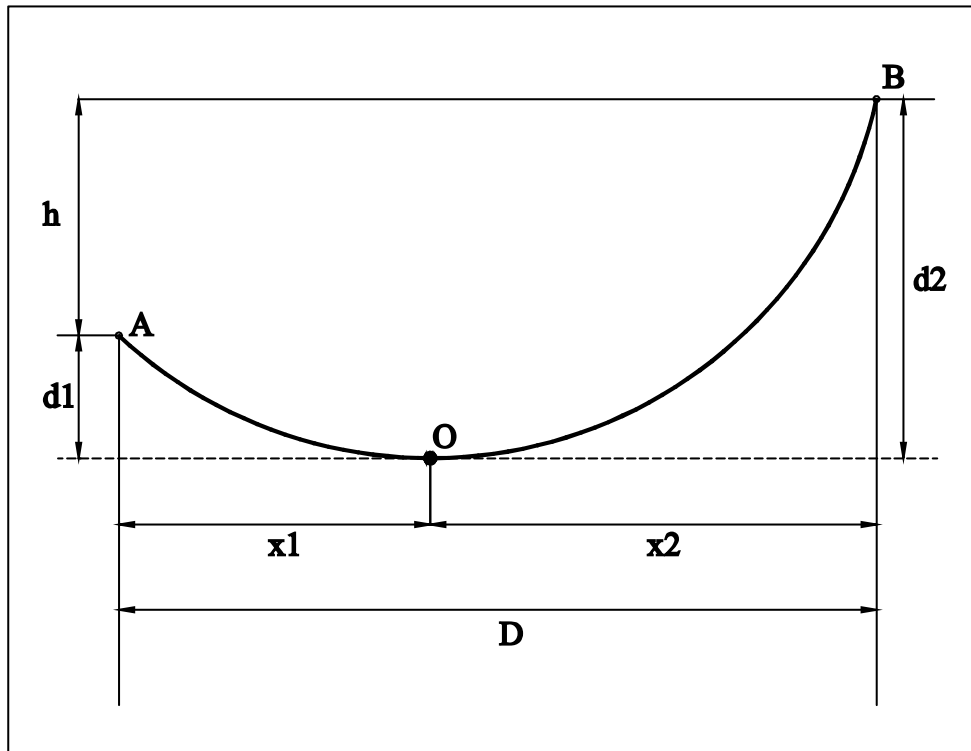


Figure 2.15 Catenary method – supports at different levels.

If the supports are at different levels as shown Figure 2.15, the following equations are used instead to calculate line sag, where D is the horizontal distance between supports; h is the height difference between two supports; x_1 and x_2 are the horizontal distance of the supports to the maximum sag point of the conductor, and finally d_1 and d_2 are the sag distance of the conductor from the top of the supports.

Using approximate formulation of catenary using simplified form on sag given in Eqn. (2.14) and for the small spans (i.e. small sag of the conductor), we obtain

$$y = \frac{wx^2}{2T} \tag{2.45}$$

When $y = d_1$, $x = x_1$

$$d_1 = \frac{w x_1^2}{2T} \quad (2.46)$$

and similarly,

$$d_2 = \frac{w x_2^2}{2T} \quad (2.47)$$

By using Eqn. (2.46) and Eqn. (2.47) in Eqn. (2.45)

$$h = \frac{w}{2T} (x_2^2 - x_1^2) \quad (2.48)$$

and $D = x_1 + x_2$ (2.49)

$$h = \frac{w}{2T} (x_2^2 - x_1^2) = \frac{w}{2T} (x_2 - x_1)(x_2 + x_1)$$

$$x_2 - x_1 = \frac{2Th}{w(x_1 + x_2)} \text{ or,}$$

$$x_2 - x_1 = \frac{2Th}{wD} \quad (2.50)$$

By solving Eqn. (2.49) and Eqn. (2.50) simultaneously, we obtain

$$x_1 = \frac{D}{2} - \frac{hT}{wD} \quad (2.51)$$

$$x_2 = \frac{D}{2} + \frac{hT}{wD} \quad (2.52)$$

In Eqn. (2.51),

If $\frac{D}{2} > \frac{hT}{wD}$, then x_1 is positive.

If $\frac{D}{2} = \frac{hT}{wD}$, then x_1 is zero.

If $\frac{D}{2} < \frac{hT}{wD}$, then x_1 is negative.

Negative x_1 means that the lowest point of the conductor (i.e. point O) is the outside of the span as shown Figure 2.16.

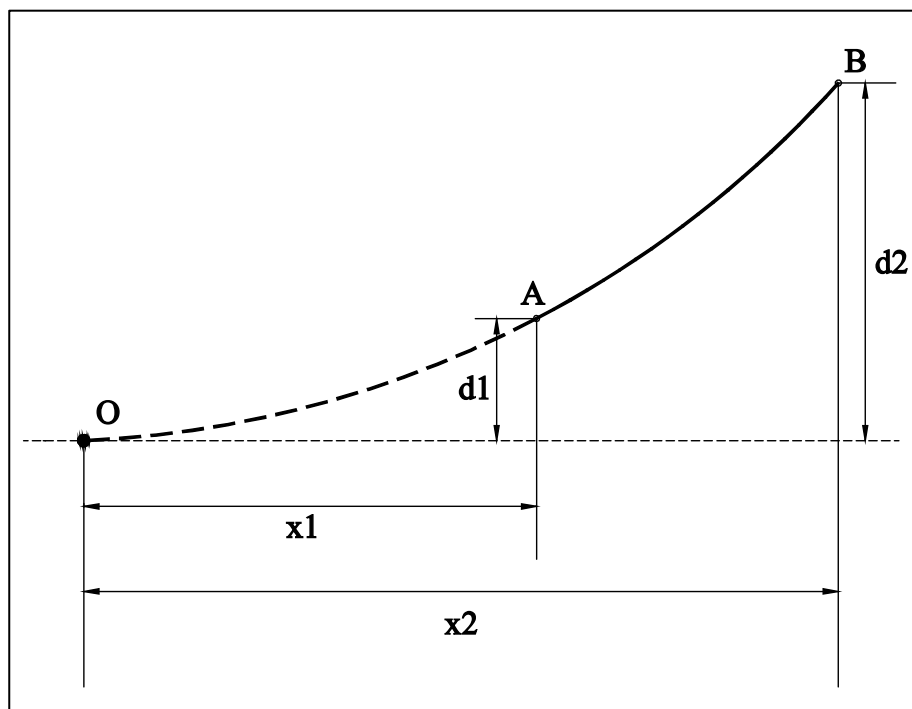


Figure 2.16 Negative x_1 condition.

2.5. Loads on the OHTL Towers

OHTL towers are subjected to various loads in three directions: vertical, transverse, and longitudinal. The transverse load is perpendicular to the line and the longitudinal loads act parallel to the line. Various international and national standards exist to calculate the forces transmitted to OHTL under various load effects. The key documents providing guidelines on calculating loads of OHTL towers are EN 50341, IEC 60826 and ASCE 74. EN 50341 is the European norm on design of OHTL towers. It covers all design concepts of OHTL over 45 kV. Guidelines are provided on conductor selection, earthing system, support design, load calculation, insulators and other line equipment. IEC 60826 is an international standard by International Electrotechnical Commission. It mainly focuses on calculation wind and ice loads on tower structures. ASCE 74 is developed by ASCE specifically for structural loads on OHTL tower. The formulations are provided to calculate wind, ice and operational loads. In general, the following load effects and their combinations are considered in these standards while designing OHTL towers:

- i) Load due to structural member's self-weight of the tower;
- ii) Load due to self-weight of the conductor, insulator, equipment, and hardware;
- iii) Wind load on the tower;
- iv) Wind load on the conductors, insulators, equipment, and hardware;
- v) Ice load on the tower;
- vi) Ice load on the conductors, insulators, equipment, and hardware;
- vii) Erection and maintenance load;
- viii) Load due to pre-tension of the conductors;
- ix) Unbalanced loading affects due to broken wire condition;
- x) Thermal loads;
- xi) Earthquake loads.

2.5.1. Self-Weight of Transmission Line Components

Self-weight of the structural members as well as those of conductor, insulator and permanently attached equipment and hardware cause vertical loads on the tower structure. The weight of structural members is distributed to every joint in the tower according to tributary weight of each member framing into the joint. On the other hand, self-weight of conductor, insulator and permanently attached equipment are directly acted at gravity loads at the joints where these components are connected in the tower.

2.5.2. Wind Load on Transmission Line Components

The calculation of wind loads on a transmission tower is a difficult problem and involves various approximations. The dynamic properties of the tower structure are very complex and almost impossible to quantify its true interaction with the wind during extreme events such as storms or hurricanes. The tower structures are designed with complicated geometry with irregularities in both plan and profile. The steel profiles making up the tower structure are often selected from angle shapes due to economy and constructability reasons. The angle shapes are asymmetrical and exhibit different response depending on the direction of loading. They are very weak under flexural or torsional loading conditions. When wind blows through the transmission tower, it exerts a pressure on the surface of the angle profiles. The wind pressure exhibits its full effect on the members located at the windward face of the towers. For members located inside the tower or at the leeward face, the effect of wind diminishes due to shielding at the windward face. Therefore, it is impossible to quantify the real effect of wind on the structural members and this is only handled by approximations.

While calculating the wind loads, depending on the geographical location of the OHTL, the basic wind speed is obtained from the meteorological maps. The wind speed can be obtained in different reliability levels. The reliability level varies depending on the structure of the grid, country code requirements and

consequences of probable failures. It is common that the wind speed for 50 year return period is obtained from the meteorological maps and reliability factors are introduced to achieve the desired level of safety.

The wind pressure calculations of OHTL components show slight variations due to their distinct geometries. In this section, the wind pressure calculations are provided only for the conductors, insulators, and hardware due to the fact that they constitute the majority of the loads governing the tower design. The details of the wind load calculations for other components can be found in the relevant load calculation document.

The wind speed is converted into wind pressure utilizing the formulations below for EN 50341, IEC 60826 and ASCE 74 as given equations. Since these three specifications are most widely used in the industry, the details of wind calculation equations are presented in this thesis.

2.5.2.1. Wind Load on Tower Structure

The equations of wind forces acting on tower structure can be calculated using the following equations:

a) Wind Loads on Tower – EN 50341 (2012)

Two methods are given for calculation of wind forces. Method 1 is used for regular geometries where the tower is assumed to be divided into sections. The shielding effect of members is taken into account. In Method 2, wind force acting on individual members is considered. The shielding effect is ignored. Method 2 is recommended for structures with irregular geometry.

Method 1:

$$Q_{wt} = q_p(h) G_t (1 + 0.2 \sin^2 2\phi) (C_{t1} A_{t1} \cos^2 \phi + C_{t2} A_{t2} \sin^2 \phi) \quad (2.53a)$$

where;

$q_p(h)$: the peak wind pressure (see EN 50341 (2012) Clause 4.3.4);

h : the reference height to be used for the conductor;

G_t : the structural factor for lattice tower. The recommended value is 1, but another value may be specified in the National Normative Aspects (NNAs) (see EN 50341 (2012) Clause 4.4.3.2 to calculate G_t);

C_{t1}, C_{t2} : the drag factor for lattice tower panel face 1 (respectively face 2) of the section being considered in a wind perpendicular to this panel (Figure 2.17);

A_{t1}, A_{t2} : the effective area of the elements of lattice tower panel face 1 (respectively face 2) of the section being considered (Figure 2.17);

ϕ : the angle between wind direction and the longitudinal axis of the cross-arm;

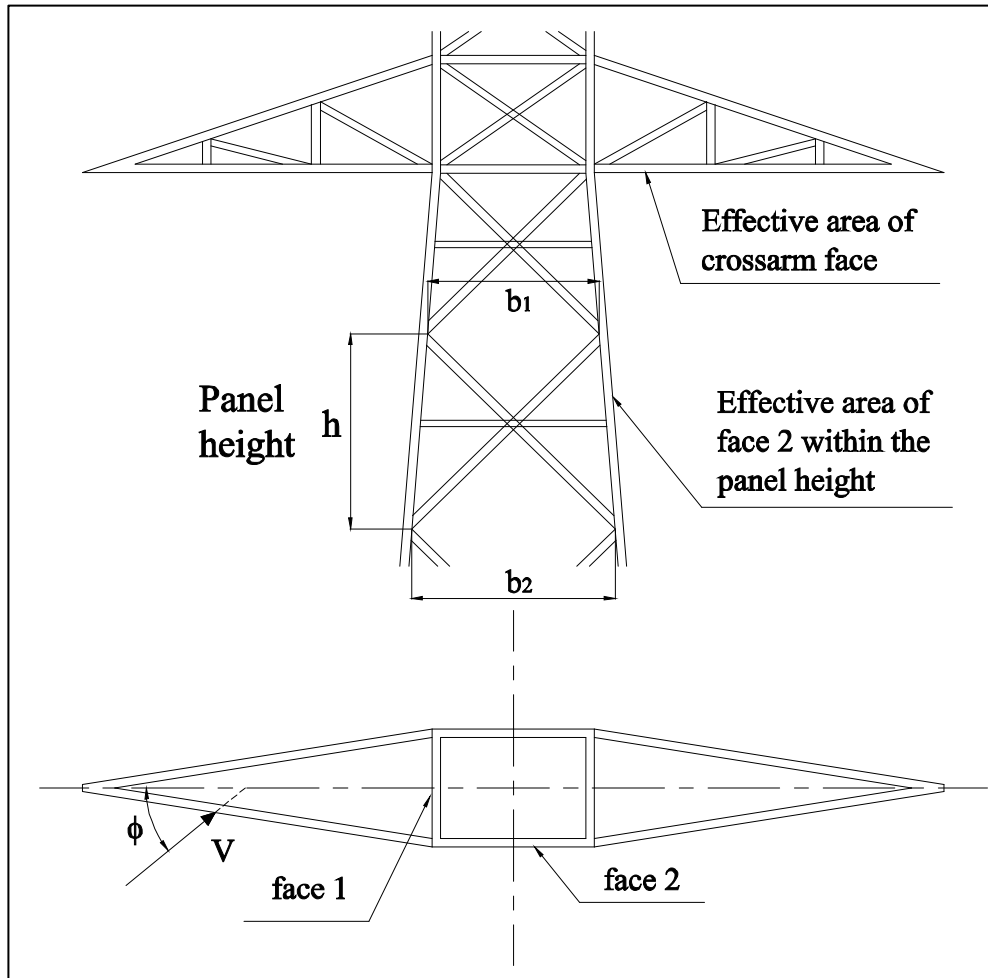


Figure 2.17 Definition of tower panel face (EN 50341, 2012).

Method 2:

$$Q_{wm} = q_p(h) G_m C_m A_m \cos^2 \phi_m \quad (2.53b)$$

where;

$q_p(h)$: the peak wind pressure (see EN 50341 (2012) Clause 4.3.4);

h : the reference height to be used for the conductor;

G_m : the structural factor for lattice tower. The recommended conservative value is 1, but another value may be specified in the NNAs (see EN 50341 (2012) Clause 4.4.3.3 to calculate G_m);

- C_m : the drag factor for each tower member. The recommended conservative value is 1.6 for an angle member but another value may be specified in the NNAs;
- A_m : the effective area of the tower member being considered and is equal to its length multiplied by its width;
- ϕ_m : the angle between wind direction and the normal axis plane of the tower member being considered.

b) Wind Loads on Tower – IEC 60826 (2003)

The wind loading according IEC 60826 is calculated for panels defined along the height of the structure. The formulation of the wind force is given as follow:

$$A_t = q_0 (1 + 0.2 \sin^2 2\theta) (S_{t1} C_{xt1} \cos^2 \theta + S_{t2} C_{xt2} \sin^2 \theta) G_t \quad (2.54)$$

where;

- q_0 : the dynamic reference wind pressure (see IEC 60826 (2003) Clause 6.2.5);
- ϕ : the angle of incidence of the wind direction with the perpendicular to face 1 of the plane in a horizontal plane (Figure 2.18);
- S_{t1} : the total surface area projected normally on face 1 of the panel;
- S_{t2} : the total surface area projected normally on face 2 of the supported members of face 2 of the same panel. The projections of the bracing elements of the adjacent faces and of the diaphragm bracing members can be neglected when determining the projected surface area of a face;
- C_{xt1}, C_{xt2} : the drag coefficients peculiar to faces 1 and 2 for a wind perpendicular to each face (see IEC 60826 (2003), Clause 6.2.6.4.1);

G_t : the combined wind factor for the supports (see IEC 60826 (2003), Clause 6.2.6.4.1).

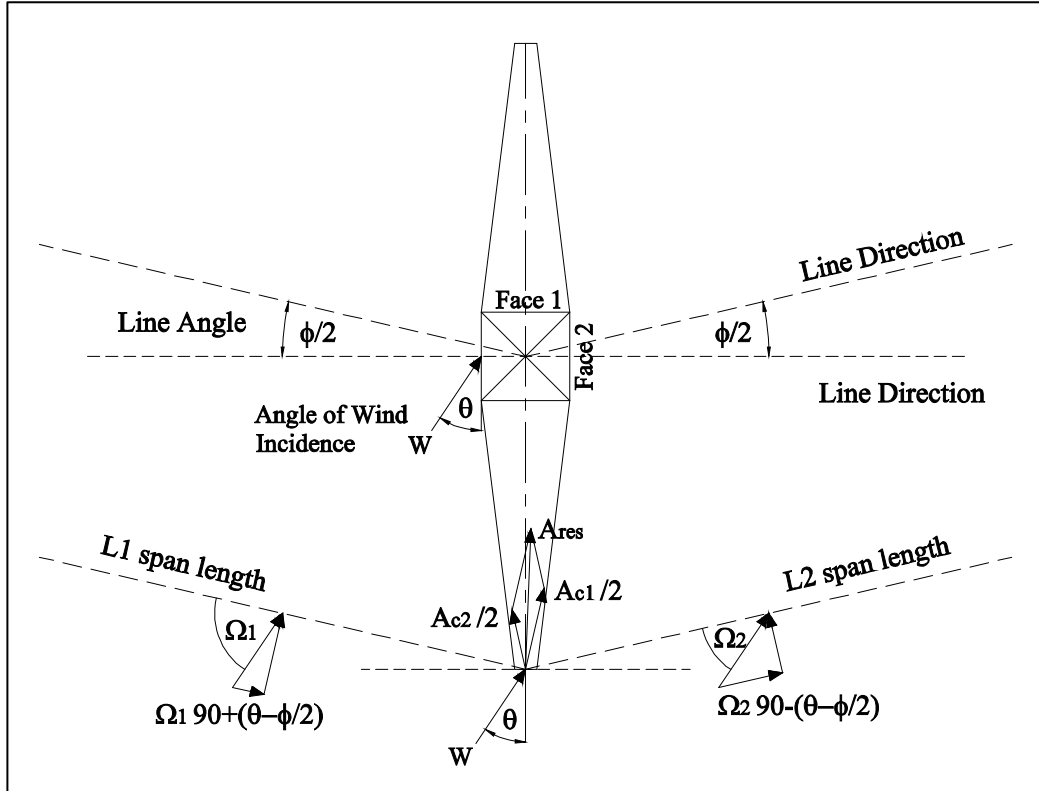


Figure 2.18 Definition of the angle incidence of wind (IEC 60826, 2003).

c) Wind Loads on Tower – ASCE 10-74

In ASCE 10-74 (2010), the wind forces are calculated using Eqns. 2.55a and 2.55b. The forces are obtained both for transverse and longitudinal for yawed wind conditions. Figure 2.19 illustrates the resultant yawed wind force directions on a transmission line. The shielding effect is taken into account in force coefficients.

$$F_t = \gamma_w Q K_z K_{zt} V^2 G_t \cos \Psi C_{ft} A_{nt} \quad (2.55a)$$

$$F_l = \gamma_w Q K_z K_{zt} V^2 G_t \cos \Psi C_{fl} A_{ml} \quad (2.55b)$$

where,

$F_{t,l}$: the wind force in the direction of transverse or longitudinal;

Ψ : the yaw angle measured in a horizontal plane;

A_{mt} : the area of all members in the face of the structure that is parallel to the line

A_{ml} : the area of all members in the face of the structure that is perpendicular to the line;

C_{ft} : the force coefficient associated with face of the structure that is parallel to the line;

C_{fl} : the force coefficient associated with face of the structure that is perpendicular to the line;

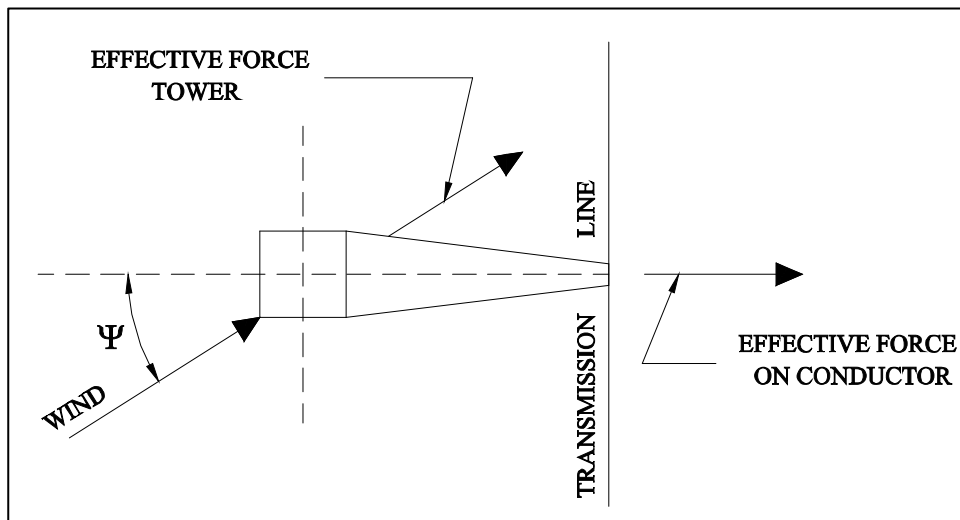


Figure 2.19 Yawed wind illustration (ASCE 10-74, 2010).

2.5.2.2. Wind Load on Conductor

a) Wind Loads on Conductors – EN 50341 (2012)

The formulation to obtain the forces acting on the conductors is given below. The formulations take into account the orientation of the line with respect to the wind direction.

i) In the direction of the cross-arm:

$$Q_{w_{c,v}} = q_p(h) G_c C_c d \left[\pm \frac{L_1}{2} \cos^2 \left(\phi + \frac{\theta_1}{2} \right) \cos \left(\frac{\theta_1}{2} \right) + \frac{L_2}{2} \cos^2 \left(\phi - \frac{\theta_2}{2} \right) \cos \left(\frac{\theta_2}{2} \right) \right]$$

ii) Perpendicular to the cross-arm:

$$Q_{w_{c,v}} = q_p(h) G_c C_c d \left[\pm \frac{L_1}{2} \cos^2 \left(\phi + \frac{\theta_1}{2} \right) \cos \left(\frac{\theta_1}{2} \right) + \frac{L_2}{2} \cos^2 \left(\phi - \frac{\theta_2}{2} \right) \cos \left(\frac{\theta_2}{2} \right) \right] \quad (2.56)$$

where;

$q_p(h)$: the peak wind pressure;

h : the reference height to be used for the conductor;

G_c : the span factor or structural factor for the conductor;

C_c : the drag factor or force coefficient for the conductor;

d : the diameter of the conductor;

L_1, L_2 : the lengths of the two adjacent spans;

ϕ : the between wind direction and the longitudinal axis of the cross-arm;

θ_1, θ_2 : $(\theta_1 + \theta_2) / 2 = \theta$ angle of the line direction change.

The orientation of wind load components is illustrated in Figure 2.20.

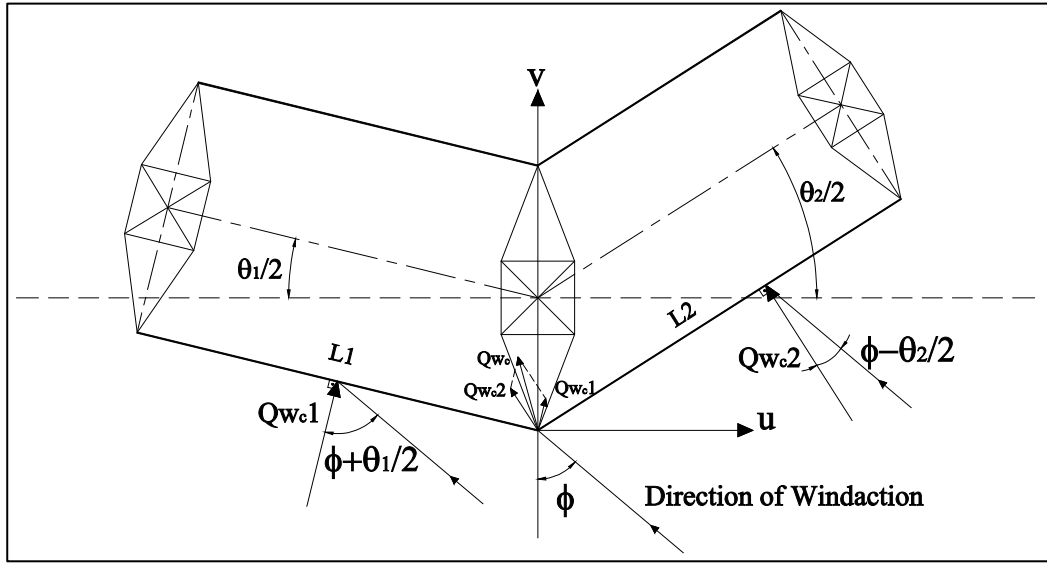


Figure 2.20 Wind forces on conductors (EN 50341, 2012).

b) Wind Loads on Conductors – IEC 60826 (2003)

IEC 60826 (2003) calculates the wind force on the conductors based on Eqn. (2.57) given below:

$$A_C = q_0(h) C_{XC} G_C G_L d L \sin^2 \Omega \quad (2.57)$$

where,

- q_0 : dynamic reference wind pressure ((see IEC 60826(2003) Clause 6.2.5)
- C_{XC} : drag coefficient of the conductor (generally taken equal to 1.00 for the stranded conductors and wind velocities. Other values can be used if derived from direct measurements or wind tunnel tests);
- G_C : combined wind factor for the conductors (see IEC 60826(2003) Clause 6.2.6.1);
- G_L : span factor (see IEC 60826(2003) Clause 6.2.6.1);
- d : diameter of the conductor;
- L : wind span of the support;
- Ω : angle between the wind direction and the conductor (Figure 2.18).

c) Wind Loads on Conductors – ASCE 10-74 (2010)

In ASCE 10-74 (2010) the wind force on the conductor can be calculated by Eqns. 2.58a and 2.58b below.

$$F = \gamma_w Q K_z K_{zt} (V_{50})^2 G C_f A \quad (2.58a)$$

or

$$F = Q K_z K_{zt} (V_{RP})^2 G C_f A \quad (2.58b)$$

where,

F : the wind force in the direction of wind unless otherwise specified

γ_w : the load factor to adjust the force, F, to the desired return period

V_{50} : basic wind speed, 50-year return period, 3-sec gust,

V_R : the 3-sec gust design wind speed, associated with the RP-year return period

K_z : the velocity pressure exposure coefficient, which modifies the basic wind speed for various heights above ground and for different exposure categories

K_{zt} : the topographic factor

Q : numerical constant

G : the gust response factor for conductors, ground wires, and structures

C_f : the force coefficient values

A : the area projected on a plane normal to the wind direction

2.5.2.3. Wind Load on Insulator

a) Wind Loads on Insulator– EN 50341 (2012)

EN 5041 (2012) provides the equation below to calculate the wind force on the insulators.

$$Q_{\text{Wins}} = q_p(h) G_{\text{ins}} C_{\text{ins}} A_{\text{ins}} \quad (2.59)$$

where;

$q_p(h)$: peak wind pressure (see EN 50341 (2012) Clause 4.3.4);

h : reference height above ground to be used for the insulator set which is the height of the attachment point in the support. Another reference height may be specified in the NNAs;

G_{ins} : structural factor for the insulator set. The recommended value is 1, but another value may be specified in the NNAs;

C_{ins} : drag factor for the insulator set. The recommended value is 1.2, but another value may be specified in the NNAs;

A_{ins} : area of the insulator set projected horizontally on a vertical plane parallel to the axis of the string.

b) Wind Loads on Insulator – IEC 60826 (2003)

The wind force on insulator is calculated according to formulation below. However, IEC 60826 (2003) suggests that the wind pressure on insulator can be taken the wind force on supports for the sake of simplicity.

$$A_i = q_0 C_{Xi} G_t S_i \quad (2.60)$$

where,

q_0 : dynamic reference wind pressure ((see IEC 60826(2003) Clause 6.2.6.3);

C_{Xi} : drag coefficient of the insulators, considered equal to 1.20;

G_t : combined wind factor for the insulators (see IEC 60826(2003) Clause 6.2.6.3);

G_L : area of the insulator string projected horizontally on a vertical plane parallel to the axis of the string. In case of multiple strings, the total area can be conservatively taken as the sum of all strings.

c) Wind Loads on Insulator – ASCE 10-74 (2010)

In ASCE 10-74 (2010), no specific equation is provided for the insulators. However, in Appendix G force coefficients are given for different cross-sectional shapes and they can be utilized for determining of force coefficient of insulators.

2.5.3. Ice Load on Transmission Line Components

Icing or glaciation causes not only an increase in self-weight of the tower components and conductor, insulator, hardware but also increase their surface area for wind application. That is to say, with the increase of the surface areas of the tower components and other members (i.e. conductor, insulator, hardware), the tower is exposed to the additional wind load. In addition, icing on conductors results in significant tension forces to develop at the attachment points of the structure. This tension forces may act both in transverse and longitudinal directions.

Ice loading is classified based on its method of formation. Precipitation icing is the mostly observed condition where freezing rain or drizzle conditions takes place. Ice-cloud icing, on the other hand, takes place when ice particles on the cloud precipitates on the conductor. Ice is also classified in groups according to its physical characteristics. In ASCE 74 (2010), ice is grouped as glaze, rime, wet-snow and hoarfrost in the order of decreasing density. Among these icing types, wet-snow reaches to the largest radial thickness values.

In all design codes, an equivalent radius is calculated based on precipitation of ice on the conductor. EN 50341 (2012), the formula to obtain equivalent diameter.

$$D = \sqrt{d^2 + \frac{4 I}{9.81 \pi \rho_I}} \quad (2.61)$$

where;

d : the diameter of conductor;

I : the ice load per length of the conductor according to the actual combination (see EN 50341 (2012), Clause 4.6.1);

ρ_I : the ice density according to type of ice deposit and drag factor (see EN 50341 (2012), Table 4.5);

In IEC (2003), two most critical, in general, conditions are considered to take into account of combined wind and ice loading. Eqn. (2.62a) and Eqn. (2.62b) provided for equivalent diameter. Annex A in IEC 60826 (2003) is referenced in case other conditions should be considered.

Condition 1: The highest value of ice load is combined with average of yearly maximum wind speed during ice persistence.

$$D_L = \sqrt{d^2 + \frac{4 g_L}{9.82 \pi \delta}} \quad (2.62a)$$

Condition 2: The highest value of wind speed during ice persistence is combined with average of yearly maximum ice load.

$$D_H = \sqrt{d^2 + \frac{4 g_H}{9.82 \pi \delta}} \quad (2.62b)$$

where;

D_L, D_H : the equivalent diameters;

d : the diameter of conductor;

g_L, g_H : the ice load per length;

δ : the highest density for type of ice being considered.

According to ASCE 74 (2010), the following equations are provided to obtain equivalent diameter.

If all dimensions are in imperial units;

$$W_i = 1.24 (d + I_z) I_z \quad (2.63)$$

In SI units;

$$W_i = 0.0282 (d + I_z) I_z \quad (2.64)$$

where;

W_i : weight of glaze ice per length;

d : bare diameter of the conductor;

I_z : design ice thickness

Ice load is sometimes considered as uniformly distributed through the line at each span. The radial thickness of the ice can be obtained from meteorological maps showing the estimates of ice thickness in different regions of the world. The ice thickness is often provided for average 20 or 50 years of glaze. However, this may not be the case always. Therefore, some design codes also consider the cases in which ice load might be different in adjacent spans since the intensity of icing may differ. This leads to appreciable unbalanced tension forces by the conductors on the two sides of the tower. The unbalanced condition is especially significant in case of in-cloud icing or wet snow.

2.5.4. Erection and Maintenance Loads

Special erection methods, such as lifting a structures, may result in overloads in some members. The erection loads result from supporting the weight of the truss in a different manner from how the weight is supported on an in-service nature. During erection and maintenance, some tower members are loaded in flexure by the vertical weight of the members and they must be considered during the design stages.

2.5.5. Unbalanced Loading due to Broken Wire Condition

Whenever the conductor or ground wire breaks, its force will be to cause unbalanced pull normally in the longitudinal direction which the tower has to withstand. During the design stage, this unbalanced longitudinal pull should be also considered in various scenarios of broken wire conditions.

2.5.6. Thermal Loads

Since the bolt connection type is usually considered for the tower structures, thermal effects on structural members are not usually taken into consideration to analyze and design towers.

2.5.7. Earthquake Load

Earthquake loads are not always considered during the design stages of OHTL towers. Some design codes exclude ground-induced vibrations caused by earthquake motion because it is known historically that transmission line towers have performed well under earthquake events. Besides, the other loads, such as wind/ice combinations or broken wire loads usually exceed earthquake loads. However, if a technical specification indicates to be taken into consideration of earthquake load, it is applied on the structure based on the given rules in technical specification.

CHAPTER 3

LITERATURE SURVEY

Modern optimization techniques have rightly attracted a substantial interest in research and applied fields of engineering. Structural optimization, which aims to produce the best solution to a structural design problem according to a chosen objective is one of such areas.

Actually a practical structure is governed by a large number of design variables (e.g., topology, shape and cross-sectional parameters), implicit constraints (e.g., those related to structural response, i.e., stresses and displacements, and stability) and possibility of multiple local minima. Thus, a computationally complex problem of this nature calls for an efficient and reliable optimization method. Conventionally, mathematical programming methods and optimality criteria techniques have overwhelmingly controlled the applications in this field. However, recently nature-inspired methodologies, commonly referred to as metaheuristic search methods in the literature, have found interesting applications showing certain advantages as compared to the conventional methods.

Simulated annealing, which utilizes concepts from annealing process of physical systems in thermodynamics, is one of such metaheuristic techniques. In this process, a physical system (a solid or a liquid) initially at a high-energy state is cooled down slowly to reach its lowest energy state, and thus to gain a perfectly regular, strong and stable structure. The idea that this process could be mimicked for the solutions of mathematical optimization problems was pioneered independently by Kirkpatrick et al. (1983) and Cerny (1985) by defining a parallelism between minimizing energy level of a physical system and lowering the objective function which utilizes concepts from annealing process of physical systems in thermodynamics. The technique soon gained a worldwide popularity

and found plenty of applications in various disciplines of science and engineering owing to its simple implementation and enhanced search characteristics.

In the following subsections, some applications of simulated annealing in the field of structural optimization are reviewed first. Then, design optimization of steel lattice towers with various optimization techniques in the literature are overviewed.

3.1. On Use of Simulated Annealing in Structural Optimization

Simulated annealing (SA) has found interesting and successful applications in a wide spectrum of problem areas, including optimum structural design.

Chen et al. (1991) implemented the SA in finding the optimal arrangement of active and passive members in complex truss type structures so as to augment the inherent damping. They classified members of a truss structure as active and passive members. Active members refer to those truss members used with sensors to observe disturbances and feedback control to decide a suitable corrective response. On the other hand, passive members refer to those truss members which provide energy dissipation without feedback control. The numerical applications were presented using two different truss structures. The first structure was a 150-member tetrahedral truss and the second one was a 1.8-m-long 54-member cantilevered boom. In conclusion, SA was proved as an efficient algorithm especially for complex large structures.

Balling (1991) has applied the SA and the linearized branch and bound techniques for the size optimum design of an asymmetric six-floor frame and concluded that SA was a more powerful technique in comparison to the other.

Theodoracatos and Grimsley (1995) utilized SA algorithm to achieve an optimum arrangement of shapes of material to reduce material cost in the manufacturing stage. They compared the SA results with the polynomial-time cooling schedules

and decrement rule results. Finally, the study was concluded that SA could reliably be utilized for the generalized geometric packing problems.

Bennage and Dhingra (1995) used SA for solving single and multi-objective structural optimization problems that have both discrete and continuous design variables. Two different truss structures were used to investigate the efficiency of SA algorithm. In the first case, a 25-member truss structure illustrated in Figure 3.1, which is considered as a benchmark problem in structural optimization literature, was optimized as single and multi-objective optimization problem. In single objective optimization the weight of the truss was minimized under a set of constraints imposed. However, in multi-objective optimization stage, not only the minimization of structural weight but also deflection of pre-defined joints as well as the maximization of the fundamental frequency of vibration of the truss were taken as problem objectives. As a second example, the weight of a 10-bar planar truss was optimized using SA algorithm. The study concluded that SA algorithm showed significantly better performance as compared to some gradient-based optimization methods. Despite its outstanding performance, the SA algorithm required an immense computational burden especially when continuous design variables were used. Therefore, they recommended an SA and gradient-based hybrid optimization technique for future works.

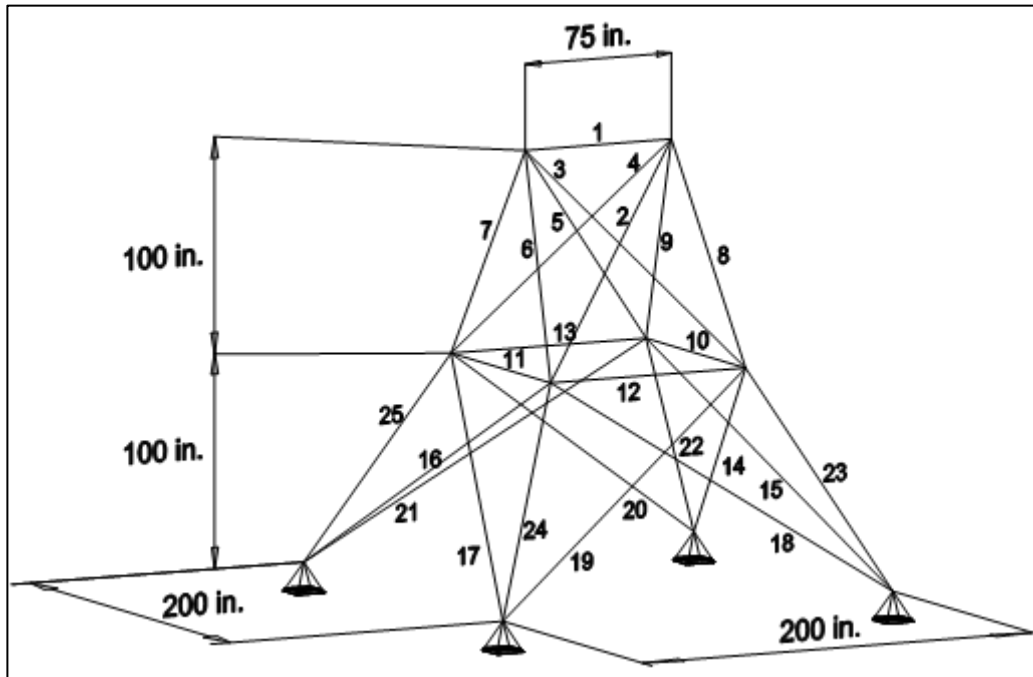


Figure 3.1 25-bar space truss .

Shim and Manoochehri (1997) applied a SA algorithm to topology design optimization of plates based on removal and restoring structural meshes described in the finite element models. The objective of the study was to minimize the material use, satisfying the constraints on maximum stress value and maintenance of connectivity between meshes. The authors used three large-scale, non-convex and nonlinear problems. To increase the computational efficiency, the nonlinear shape optimization problems were converted into linear shape optimization. A correction factor was used to reduce the error due to the linearization.

Shea et al. (1997) developed a shape annealing approach based on a shape grammar formalism and simulated annealing to optimize truss structures. Grammars are a generation system used to describe a set of designs through the transformations that map one design to another (Stiny, 1980). In the study, the shape annealing has been developed a stochastic optimization method in which a grammatical approach was employed for the modification of structural topology (Redy and Cagan, 1995) of trusses, while SA was used to optimize them. The

numerical application of the technique was demonstrated on two truss structures in conjunction with dynamic grouping of members. The results revealed that the method performed well in optimizing the structures.

Leite and Topping (1999) have drawn attention to the point that SA was not a population based search technique and the major drawback of this algorithm was its long convergence time in complex structures. Hence, they proposed a parallelization scheme for the implementation of the SA algorithm in parallel programming environment. They concluded that parallelization could be used to improve the computational time performance of SA; yet, there was no general parallelization approach of SA for any kind of structural optimization problem, implying that parallelization of SA was a problem dependent issue for structural optimization.

Manoharan and Shanmuganathan (1999) compared four stochastic search techniques, namely tabu search, simulated annealing, genetic algorithm (GA), and branch and bound in structural weight minimization problems using sizing design variables. A test suite consisting of three planar truss structures were used, and the optimized solutions to these problems using aforementioned search techniques were compared. They reported that tabu search, simulated annealing and genetic algorithms performed well for sizing optimization problems of truss structures and that tabu search converged to the best solution faster than both SA and GA.

Begg and Liu (2000) tested five algorithms for simultaneous optimal design of smart structural systems in which both structural layout and controller parameters are involved. These algorithms consisted of (i) simulated annealing (SA), (ii) genetic algorithm (GA), (iii) hybrid sequential linear programming and SA (SLPSA), (iv) hybrid sequential quadratic programming and SA (SQPSA) and (vi) sequential mixed integer continuous linear programming (SMLP). The performance of these five algorithms were quantified in two numerical examples,

namely a 2-bar planar truss and a 25-bar planar truss. It was reported that SLPSA led to better and more efficient results amongst the five methods employed.

Ceranic et al. (2001) applied the SA algorithm to obtain the minimum cost design of reinforced concrete retaining structures; in particular cantilever retaining walls. The optimum design problem was formulated such that concreting, reinforcing and formwork price were incorporated into the cost function. A modified SA algorithm was developed in the study to improve the convergence characteristics of the algorithm. The results indicated that SA could successfully be implemented for minimum cost design of reinforced concrete retaining walls.

Park and Sung (2002) developed a distributed optimization algorithm using both simulated quenching (SQ) and simulated annealing techniques to optimize steel structures. The main idea behind the study was to improve convergence time of SA. The distributed algorithm developed was based on two different levels of parallelism; namely a SQ algorithm distributed at design variable level and an SA algorithm distributed at candidate design variable level. The efficiency of the proposed algorithm was investigated numerically on two steel structures. Firstly, a 21-story steel braced frame was sized for minimum weight under stress, maximum displacement and inter-story drift constraints. Secondly, similar to first example a 21-story but irregular steel braced frame was optimized. It was shown that the proposed algorithm could reduce computational time requirement significantly.

Hasançebi and Erbatur (2002a) utilized SA algorithm for simultaneous size, shape, and topology optimization of steel trusses. First, the technique was reformulated in a way to be able to work more efficiently in complex structural design optimization problems. Next, the efficiency of the reformulated technique was tested on two large scale design example problems; namely a 224-member 3D steel pyramid and a physical design area problem. It was concluded that SA

was a fully competent algorithm to deal with complex design optimization problems efficiently.

Hasançebi and Erbatur (2002b) reformulated the working mechanism of Boltzmann parameter and applied SA to optimize complex truss type structures. The so-called weighted Boltzmann parameter and critical Boltzmann parameters were proposed to remedy implementation of classical Boltzmann parameter. Numerical applications were carried out on different truss structures that were sized for minimum weight using sizing variables. These problems were a 26-story and 942-member 3D truss tower, an 18-member planar truss structure, and a 47-member 2D truss tower were optimized. It was shown that the proposed reformulations of the SA enhanced the performance of the technique to a large extent.

Chen and Su (2002) proposed two approaches to overcome computational burden of SA during structural optimization. The first approach was defining the feasible region using linearized constraints so that SA would perform a search only in feasible region. The second approach was that SA started to search process in the region including design variables having high design values. The rationale behind the second approach was explained by the statement that the region including higher design variables contained the most feasible solutions. Three numerical examples were presented. They reported that the two proposed methods worked well, yet more numerical tests were needed to promote the conclusion.

Genovese et al. (2005) proposed an improvement of SA algorithm on the basis of the two-stage stochastic search; namely global and local annealing. In global annealing, all design variables were perturbed simultaneously, whereas design variables were perturbed one by one at a time in local annealing. The optimization algorithm was transferred from the global annealing to local annealing in the course of optimization based on the current best record at the beginning of each cooling cycle. The performance of the improved SA algorithm was investigated

on three numerical examples, in which the solutions produced to these problems with the improved SA were compared with those of classical SA and gradient based optimization techniques. It was reported that the improved SA gave rise to better results not only for weight optimization but also for computation burden than that of classical SA.

Degertekin (2007) studied optimization of nonlinear steel space frames optimization using SA and genetic algorithm. Three space frames were optimized by using both optimization methods. The study revealed that although GA required less convergence time than that of SA, SA achieved better solutions.

Venanzi and Materazzi (2007) combined SA algorithm with dynamic analysis to look for the optimum solutions of wind-excited structures. A guyed mast was also used to demonstrate the efficiency of algorithm under several structural analysis techniques.

Lamberti (2008) attempted to transform the simulated annealing algorithm from trial point approach to population based approach. Additionally, a multi-level annealing strategy consisting of perturbing design variables all at once and perturbing design variables individually was also implemented. A new software named Corrected Multi-Level & Multi-Point Simulated Annealing (CMLPSA) was developed for the application of the proposed approach. The efficiency of the proposed approach was investigated using six trusses where the trusses are optimally designed for minimum weight using size and shape design variables. The solutions obtained to these test problems with the proposed approach were compared with the classical SA, particle swarm optimization (PSO), and harmony search optimization (HS) techniques. It was shown that CMLPSA found better solutions than those of classical SA, and that CLMPSA arrived the best solution faster than PSO and HS did.

Hasançebi et al. (2010a) proposed an improvement of SA performance in structural design optimization. They proposed two new approaches; namely reformulation of the acceptance probability parameter of SA and updating of the Boltzmann parameter using a sigmoid function. Two steel frames were optimized with the improved SA according to AISC-ASD (1989) specification. The results revealed that the proposed improvements accelerated the efficiency of SA with respect to a standard implementation of the algorithm.

Garcia-Lopez et al. (2011) integrated SA with SIMP (solid isotropic material with penalization) for sizing and topology optimization of structures. SIMP is one of the homogenization methods used in topology optimization. In homogenization method, more than one type design variables are required and domain is divided into microstructures including voids. Materials are distributed based on the optimality criteria and therefore implementation of the method in structural optimization or complex problems is computationally expensive. In the study, SIMP was developed to overcome aforementioned drawback of the homogenization method. It required only one type design variable that reduced the computational burden significantly compared to homogenization method. Besides, implementation of SIMP was very easy and straightforward. Nevertheless, the results obtained by using SIMP showed that it converged to suboptimal solutions and sometimes the resulting topologies included physically meaningless areas. Therefore, the results obtained by SIMP needed to be refined by designers. In the study, SA was integrated with SIMP to obtain physically meaningful results. Four benchmark problems were optimized using SA-SIMP method and the results obtained were compared to those produced by SIMP only. It was reported that topologies obtained by SA-SIMP were more rigid and physically meaningful.

Marti et al. (2013) combined SA with genetic algorithm (GA) for cost optimization of prestressed concrete precast road bridges. The hybrid algorithm employed the neighborhood move feature of SA based on a mutation operator of GA to produce candidate solutions. The results revealed the potential applicability

of heuristic optimization algorithms on design of prestressed concrete precast road bridges.

Liu and Ye (2014) used SA algorithm with genetic algorithm (GA) to observe the collapse mechanism of dome structures under seismic loading. The study indicated two collapse mechanisms of dome structures as dynamic instability and strength failure. The optimization model was used to represent the collapse mechanisms for single-layer spherical shells. The authors proposed a combined optimization algorithm including GA and SA (GASA). A better performance of GASA was reported as compared to GA. Besides, the study was concluded that the proposed optimization method and optimization model could be used effectively to observe collapse mechanisms for single-layer spherical shells subjected to seismic loads.

3.2. Literature Survey on Optimization of OHTL Towers

The design optimization of lattice structures has always been a difficult task due to a large number of design variables, in which size, shape and sometimes topology design variables should be often considered simultaneously in order to minimize the weights of the structures. Therefore, it has attracted the attention of numerous researchers for a long time. Due to advancement in computing technology, in the recent years, the research on this topic has become even more popular. In the following, design optimization studies of transmission line towers available in the literature are reviewed briefly.

Mitra and Wolfenden (1968) introduced a dynamic programming algorithm for optimizing the transmission line routes. The towers were selected from a suite of available tower structures and the proposed method determined the arrangement of suspension towers producing the minimum overall cost for the transmission line. The height of the towers were also optimized during this process using an approach called discrete deterministic multistage decision technique. The numerical application of the technique was carried out using a 20-mile (32.2 km)

400 kW line. It was reported that the optimization led to a remarkable amount of saving from economical point of view.

Sheppard and Palmer (1972) developed a dynamic programming technique to optimize transmission towers, in which the algorithm sought for the number of panels and bracing configurations along the height of the tower to form the lightest structure. The results indicated that a significant cost saving could be achieved with the optimized design of transmission tower through dynamic programming method.

Rao (1995) optimized a 400 kV double-circuit OHTL tower (Figure 3.2) for structural weight using size and shape optimization. A computer program was developed to optimize the tower, where a systematic process was proposed to obtain minimized weight of the tower in crisp and fuzzy environments. A significant decrease was reported in weight of the tower following the optimization process.

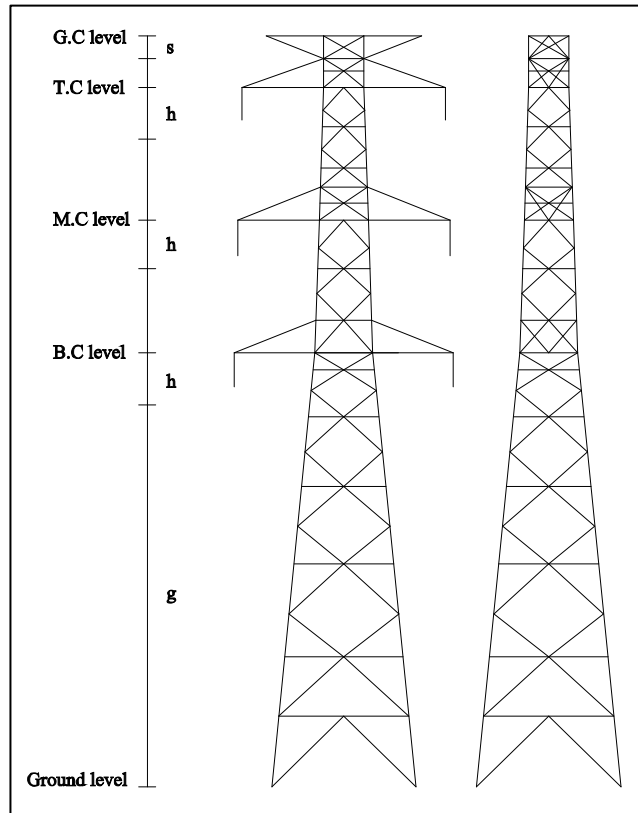
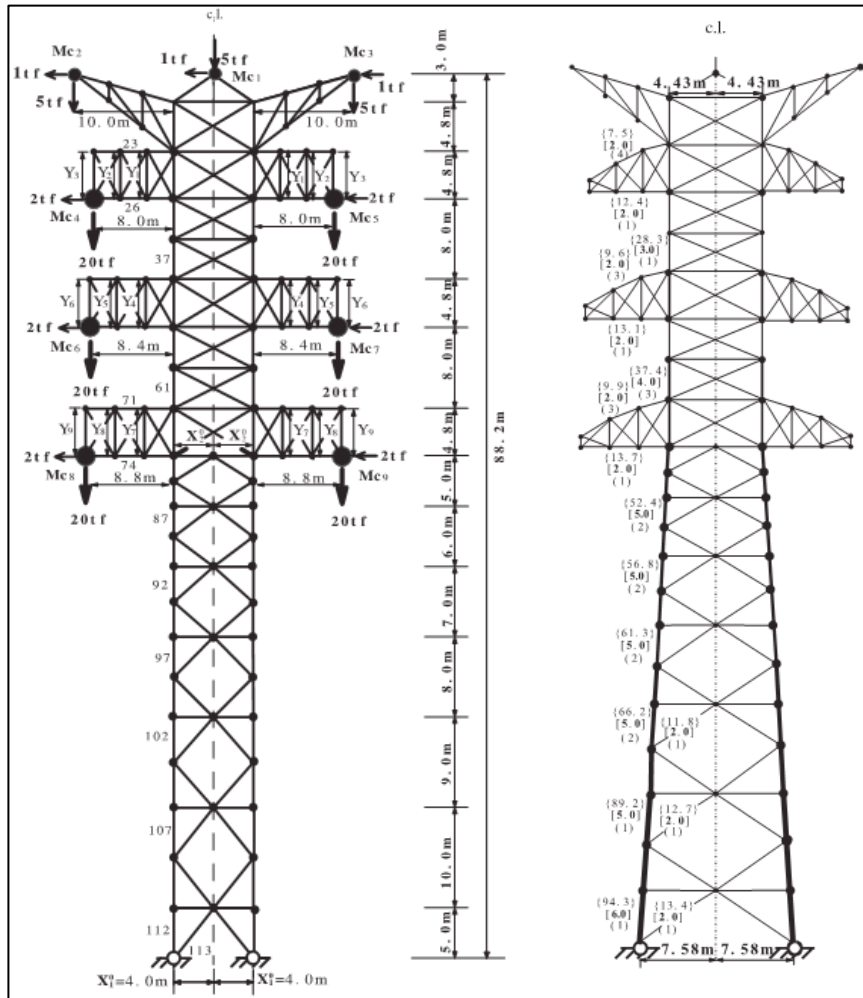


Figure 3.2 400kV double-circuit OHTL tower (Rao, 1995).

Natarajan and Santakumar (1995) addressed the failures of transmission line towers due to improper application of design specifications during the design stage of such structures. Also, they indicated the importance of reliability-based design to overcome the uncertainty factors in material properties and tower external loading. They developed four computer programs for component reliability, reliability analysis, optimization, and automation of failure mode generation. The developed programs were integrated to each other. A 110 kV and a 220 kV tangent towers were examined to optimize. The results obtained indicated that more economical tower design was achieved via the proposed methodology, and that the developed programs could be used to check reliability level of existing towers.

Tanikawi and Ohkubo (2004) performed a study to minimize the cost of transmission towers consisting of circular steel piped members subject to both

static and seismic loads. After transforming the primary optimum design problem into a convex and separable approximate subproblem by using the direct and reciprocal design variables, they solved the resulting subproblem by a dual method in a two-stage optimization process. The objective function was formulated as the cost of the tower, which considered both material cost and the cost of land. In the study, a 218-member tower was presented as a numerical example, where a simultaneous size and shape optimum design of the tower was sought under different scenarios for the cost of land. The sizing variables corresponded to cross-sectional areas of tower members, whereas nine nodal coordinates at cross-arms as well as base dimension and bottom cross-arm spacing were used as shape design variables (Figure 3.3). The results presented rigorousness, efficiency and reliability of their proposed approach, and indicated that the cost of land had a significant impact on the optimal shape, distribution of materials and cross-sectional areas of all tower members.



a) Before Optimization b) After Optimization

Figure 3.3 218-member OHTL tower optimization (Tanikawi and Ohkubo,2004).

Shea and Smith (2006) combined structural shape grammars with SA (STSA) for shape and topology optimization of energy transmission line towers. A suspension tower was optimized by using STSA. Four optimization approaches were applied on the transmission tower design; namely i) only size optimization (i.e. discrete cross-section optimization); ii) a combined size and shape optimization; iii) a combined size, shape and tower envelope optimization; and iv) a combined size, shape, tower envelope and topology optimization. The numerical example presented in the study a mass reduction in the order of 16.7% can be achieved by the virtue of combined size, shape and tower envelope optimization.

Kaveh et al. (2008) utilized a genetic algorithm to optimize transmission towers. The energy method was integrated with force method to reduce design unknowns and to eliminate the need of matrix inversion. It was highlighted that the proposed algorithm could easily be adopted for towers having a small number of members. However, for the complex tower structures as in practice, the convergence time of the algorithm was unreasonable. For that reason, neural networks were employed for approximate response analyses of designs sampled during the optimization process, rather than performing computationally expensive exact structural analyses. The resulting algorithm was applied to four different benchmark problems and the results obtained revealed that neural networks could efficiently be used as approximate analyses methods to overcome computational difficulties which stem from excessive analyses time of transmission towers during optimization process.

Shehata et al. (2008) articulated the importance of the microburst effect on the failure of the OHTL towers in a worldwide range. They stated that there were several parameters which resulted in a maximum internal force in a transmission tower member. The maximum internal force could vary for each member based upon the combination of those microburst parameters. Therefore, the challenging issue; according to the authors, was to determine the critical combination of those parameters. They utilized a genetic algorithm to determine the critical microburst configurations. As a result, they stated that GA optimization technique integrated with finite element analysis could be used to either design new towers or investigate the behavior of existing towers against the microburst loading.

Paris et al. (2010) employed sequential linear programming (SLP) with quadratic line search for shape optimization of energy transmission line towers. A pre-designed existing 110kV tension tower was optimized with SLP improved through quadratic line search algorithm. In the proposed algorithm the shape optimization is performed without changing the cross-section sizes of the initial design. Once shape optimization is completed, the cross-sections are revised according to the axial loads in the members. The approach does not guarantee the

optimum design since shape and cross-section variables are not modified simultaneously. However, it is an efficient technique for improving existing designs. The result showed that the optimized design of the tower in this case was 10% lighter than the existing one. The authors used the same initial geometry obtained from the first and second trial and changed member sizes for initial design in the fourth trial. The optimized design of the tower in this case was 13% lighter than the existing one. In the fifth and the final trial, the authors changed bracing configuration of the initial design manually. The new initial design was optimized using improved SLP algorithm, resulting in 17% reduction in the weight of the truss as compared to the original one.

In Guo and Li (2011) an adaptive genetic algorithm was introduced and implemented for four different optimization models of long-span transmission towers considering size, shape and topology design variables. A 1000 kV high-voltage OHTL tower (Figure 3.4) was presented for numerical illustration, where optimum designs produced to this tower using cross-section (size) optimization (CSSO), shape combination optimization (SCO), topology combination optimization (TCO), and layer combination optimization (LCO) were compared. LCO produced the least weight design for the tower out of four optimization scenarios tested.

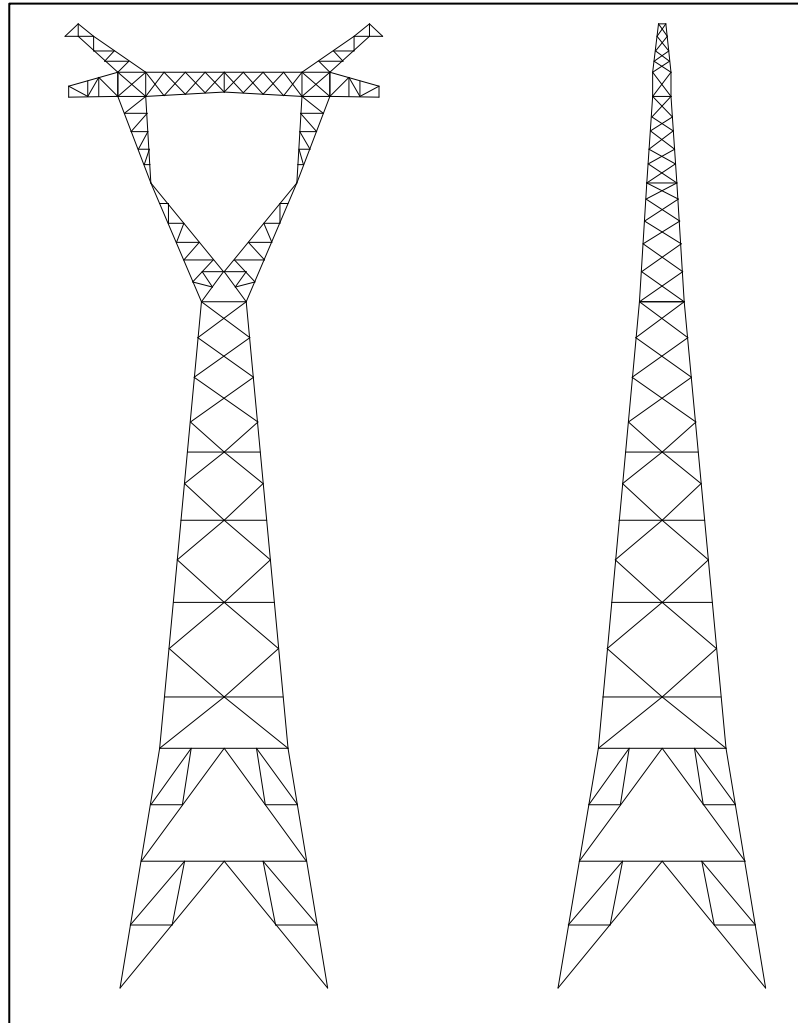
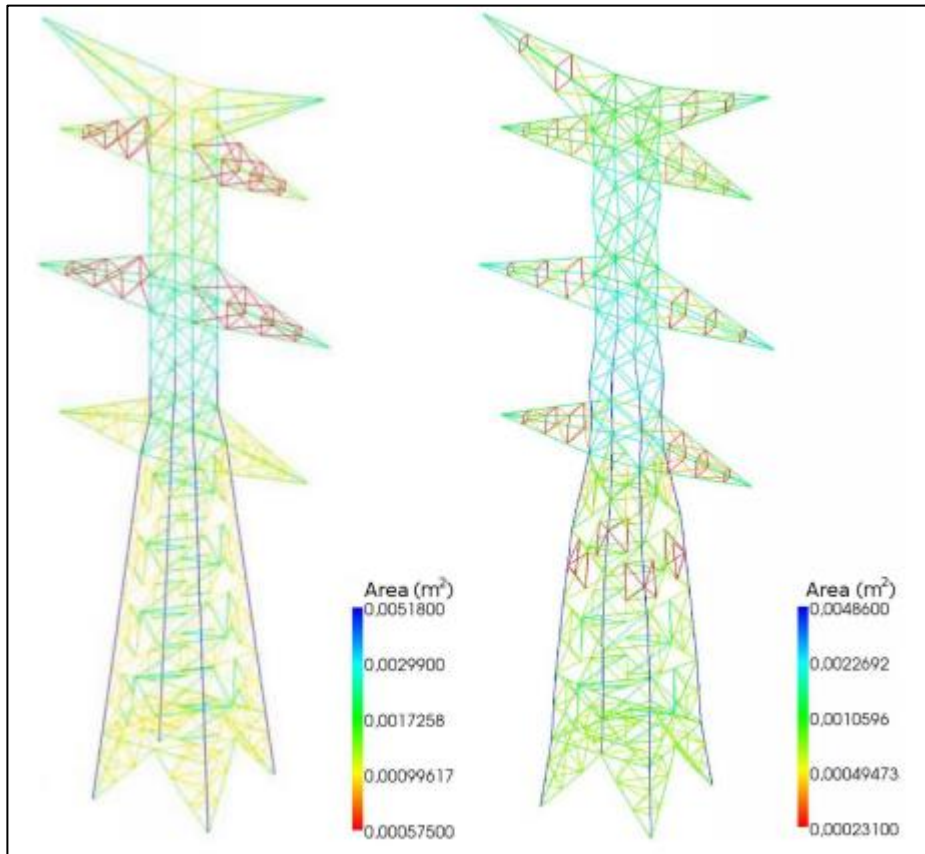


Figure 3.4 1053-primary member, 1000kV and 181.80 m. OHTL tower (Guo and Li, 2011).

Paris et al. (2012) proposed a size and shape optimization of transmission line towers using SA algorithm. Size design variables (i.e. member cross-sections) were taken into account as discrete design variable and geometrical design variables (i.e. joint locations) were defined as continuous design variables. A 400kV double circuit energy transmission line tower shown in Figure 3.5 was optimized for minimum weight through the proposed algorithm according to European and Spanish specifications. It was reported that the proposed method resulted in an optimized design of the tower which satisfied all design requirements with important material saving.



a) Before Optimization

b) After Optimization

Figure 3.5 400kV double-circuit and 41.20 m OHTL tower (Paris et. al, 2012).

Chunming et al. (2012) proposed an integrated structure and material multi-objective optimization model for ultrahigh-voltage transmission towers composed of high-strength steel material. A fast non-dominated sorting genetic algorithm was used as an optimizer. Member cross-section areas and materials were taken as design variables and the objective function was defined as minimum cost of structures. A 500 kV double circuit transmission tower shown in Figure 3.6 was used as a numerical example. They reported that their proposed method led to reasonable cost reduction in the design of the transmission tower.

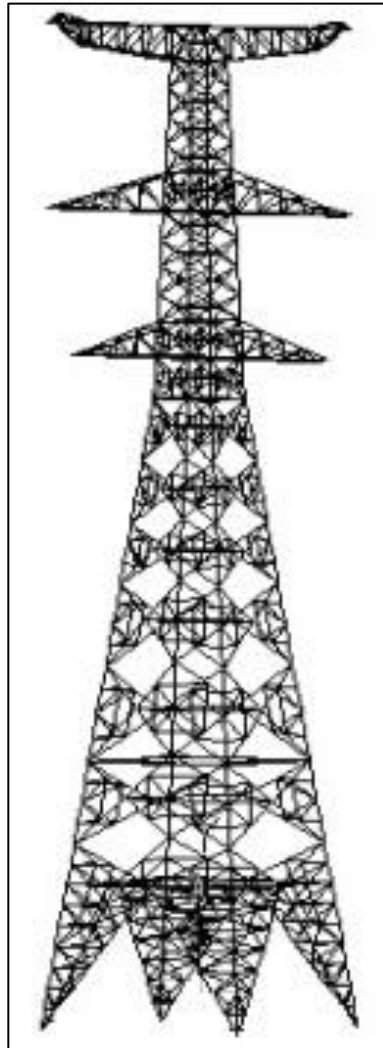


Figure 3.6 500kV double-circuit OHTL tower (Chunming et. al, 2012) .

Gomes and Beck (2012) declared that the minimum cost of a structure could be achieved by taking into consideration the consequences failure of the structure. The authors developed a design system including combination of nonlinear finite element analysis, structural reliability analysis, artificial neural network, and hybrid particle swarm optimization technique. 47-bar transmission line tower optimized considering nodal position configuration of tower and cross-section size of members constituting the tower (Figure 3.7). The authors indicated that the initial model had a steel mass of 837kg, a failure probability of 8.91×10^{-4} and 914 monetary units as expected cost. The tower solved by using deterministic volume minimization method and obtained 5% lesser expected cost compared to initial

one. However, the global risk optimization method obtained 10% lesser expected cost. The another important conclusion was that the global risk optimization method required optimization time more than 2000 times greater than that of the deterministic volume minimization problem required. Therefore, artificial neural networks were implemented into the global risk optimization to decrease optimization time.

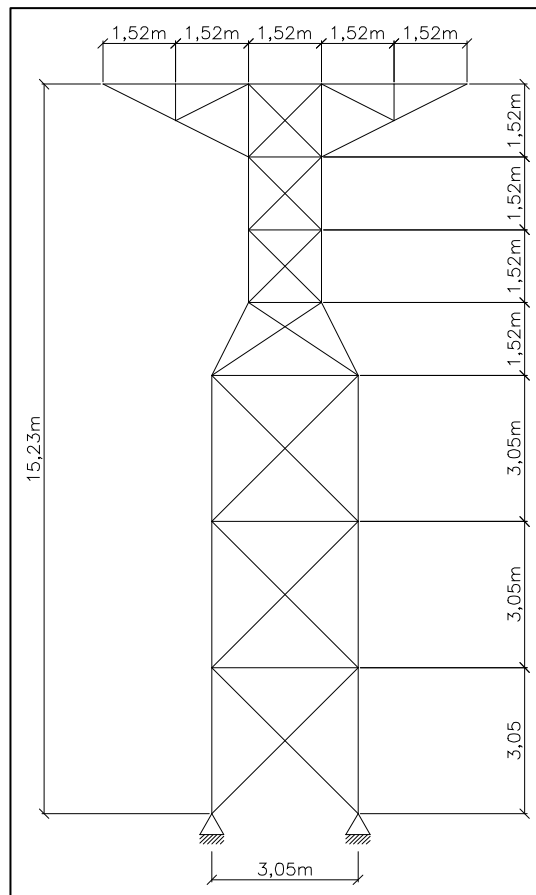


Figure 3.7 47-bar transmission tower.

CHAPTER 4

FORMULATION OF DESIGN PROBLEM

In the context of this thesis study, the steel lattice transmission line towers are optimized for minimum weight using both size and shape design variables under a set of strength and serviceability constraints imposed according to ASCE 10-97 (2000) design specification. A mathematical formulation of this problem is stated in the following.

4.1. Design Variables

The structural behavior of a transmission tower is governed by the cross-section sizes of the lattice members and geometry of the tower. Hence, the employed set of design variables consists of two design vectors represented as \mathbf{Xc} (Eqn. 4.1) and \mathbf{Xs} (Eqn. 4.2). The sizing design vector \mathbf{Xc} contains the cross-sectional sizes of all member groups (N_m) in a tower. The tower members are selected from a discrete profile database where discrete steel sections are sorted and indexed in the order of increasing cross-sectional areas. Hence, the sizing design vector \mathbf{Xc} is defined as a vector of N_m integer values, each corresponding to index number of a selected steel section in the profile database for a tower member. The shape design vector \mathbf{Xs} comprises all design variables (N_s) that are employed to alter the geometry of a tower.

$$\mathbf{Xc} = [X_{c1}, X_{c2}, \dots, X_{N_m}]^T \quad (4.1)$$

$$\mathbf{Xs} = [X_{s1}, X_{s2}, \dots, X_{N_s}]^T \quad (4.2)$$

In general, one can define numerous parameters defining the geometry of the tower, including overall tower height, cross-arm (console) widths, panel heights

and panel widths. Nevertheless, the required electrical clearances from conductors to the steel members and the ground necessitate determination of overall tower height and console widths priorly. Similarly, the panel heights are often determined by keeping the bracings at an angle of 45° degree from the horizontal. To this end, in this study only the panel widths along the height of a tower are selected as shape design variables during the optimization process in compliance with practical design requirements. Figure 4.1 displays the three shape variables defined for a typical pine-tree type transmission tower. Theoretically, one can define a panel width at every panel through the height of a tower, as implemented in some benchmark problems in the literature, such as 47-bar transmission tower truss (Ahrari and Deb, 2016). However, in practice the shape variables must be defined only at panels where the inclination of tower legs changes in order to ensure straightness of the tower body within different parts.

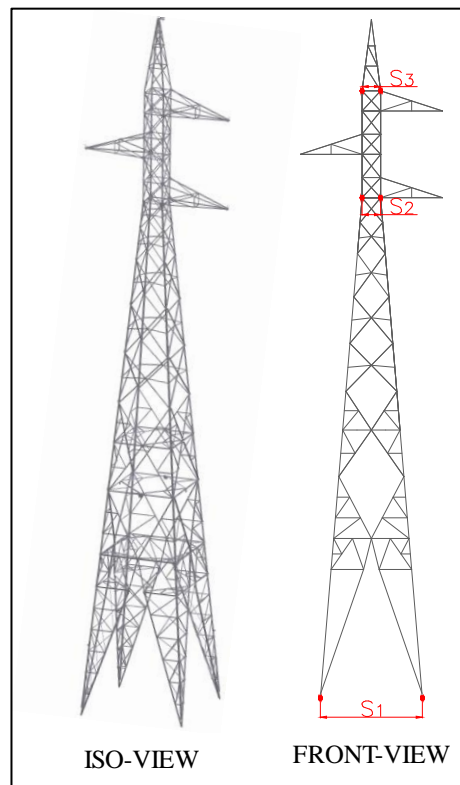


Figure 4.1 The three shape variables (panel widths) considered to change geometry of a lattice tower.

4.2. Objective Function

Usually the cost of steel structures cannot be directly associated only with the structural weight, as it is affected by many other factors, such manufacturing, erection, transportation costs, etc. However, there is a high level of correlation between weight and cost of a steel lattice tower. Accordingly, the objective function of the problem at hand is defined as minimizing the total element weight (W_s) of the tower, which is formulated as follows:

$$W_s = \sum_i^{N_m} \rho \cdot L_i \cdot A_i \quad (4.3)$$

where, ρ is the unit weight of steel, L_i and A_i are the length and cross-sectional area of i -th member of the tower.

4.3. Constraints

The members in transmission line towers must be sized to satisfy stress, stability, and slenderness limits according to a chosen code of design practice. In practice, the nodal displacements are usually not considered as a design criterion, although it can easily be integrated into optimization process, if required. A designer is responsible for triangulating the structural system of a steel lattice tower in a way to prevent instability and occurrence of significant bending moment in members. To this end, it is assumed that the tower members resist applied loads by developing tension or compression forces only, and they are not subjected to significant bending moments. Therefore, the design limit states consist of yielding and fracture for members in tension, and yielding and buckling for members in compression. In addition, ASCE 10-97 (2000) provides various slenderness limits on members for serviceability conditions.

4.3.1. Compression Capacity

The compression capacity P_c of an axially loaded member is obtained by multiplying its gross cross-section area A with the design (allowable) compressive stress F_c as calculated by Eqns. (4.4) through (4.6),

$$P_c = F_c \cdot A \quad (4.4)$$

$$F_c = \begin{cases} \left[1 - \frac{1}{2} \left(\frac{KL/r}{C_c} \right)^2 \right] F_{cr} & \text{if } \frac{KL}{r} \leq C_c \\ \frac{\pi^2 E}{(KL/r)^2} & \text{if } \frac{KL}{r} > C_c \end{cases} \quad (4.5)$$

$$C_c = \pi \sqrt{2E/F_y} \quad (4.6)$$

where, E represents the elastic modulus of steel, L is the unbraced length, r is the radius of gyration, K is the effective length coefficient, F_y is the yield stress, F_{cr} is the critical stress, and C_c is the critical slenderness ratio between elastic and inelastic buckling.

The critical stress F_{cr} corresponds to reduction of material's yield stress F_y based on width (w)-thickness (t) ratio of the cross-section, and is calculated using Eqn. (4.7)

$$F_{cr} = \begin{cases} F_y & \text{if } \frac{w}{t} \leq \frac{80\Psi}{\sqrt{F_y}} \\ \left[1.667 - 0.677 \frac{w/t}{(w/t)_{\min}} \right] F_y & \text{if } \frac{80\Psi}{\sqrt{F_y}} \leq \frac{w}{t} < \frac{144\Psi}{\sqrt{F_y}} \\ \frac{0.0332\pi^2 E}{(w/t)^2} & \text{if } \frac{w}{t} \geq \frac{144\Psi}{\sqrt{F_y}} \end{cases} \quad (4.7)$$

where, $\Psi = 1$ for F_y in ksi and $\Psi = 2.62$ for F_y in MPa

The effective slenderness ratios (KL/r) of members in Eqn. (4.5) are determined for leg members, other compression members and redundant members, as discussed in the following subsections.

4.3.1.1. Leg Members

For all leg members bolted in both faces at connections,

$$KL/r = L/r \quad 0 \leq \frac{L}{r} \leq 150 \quad (4.8)$$

4.3.1.2. Other Compression Members

For stocky members with a concentric load at both ends,

$$KL/r = L/r \quad 0 \leq \frac{L}{r} \leq 120 \quad (4.9a)$$

For stocky members with a concentric load at one end and normal framing eccentricity at the other end,

$$KL/r = 30 + 0.75L/r \quad 0 \leq \frac{L}{r} \leq 120 \quad (4.9b)$$

For stocky members with normal framing eccentricity at both ends,

$$KL/r = 60 + 0.5L/r \quad 0 \leq \frac{L}{r} \leq 120 \quad (4.9c)$$

For slender members unrestrained against rotation at both ends,

$$KL/r = L/r \quad 120 \leq \frac{L}{r} \leq 200 \quad (4.9d)$$

For slender members partially restrained against rotation at one end, and unrestrained at the other,

$$KL/r = 28.6 + 0.762L/r \quad 120 \leq \frac{L}{r} \leq 225 \quad (4.9e)$$

For slender members partially restrained against rotation at both ends,

$$KL/r = 46.2 + 0.615L/r \quad 120 \leq \frac{L}{r} \leq 250 \quad (4.9f)$$

4.3.1.3. Redundant Members

For all stocky redundant members,

$$KL/r = L/r \quad 0 \leq \frac{L}{r} \leq 120 \quad (4.10a)$$

For slender redundant members unrestrained against rotation at both ends,

$$KL/r = L/r \quad 120 \leq \frac{L}{r} \leq 250 \quad (4.10b)$$

For slender redundant members partially restrained against rotation at one end, and unrestrained at the other,

$$KL/r = 28.6 + 0.762L/r \quad 120 \leq \frac{L}{r} \leq 290 \quad (4.10c)$$

For slender redundant members partially restrained against rotation at both ends,

$$KL/r = 46.2 + 0.615L/r \quad 120 \leq \frac{L}{r} \leq 330 \quad (4.10d)$$

4.3.2. Tension Capacity

The tension capacity P_t of an axially loaded member is obtained by multiplying design tensile stress F_t of the member with its net area, A_{net} , as given by Eqn. (4.11).

$$P_t = F_t \cdot A_{net} \quad (4.11)$$

For an angle member, the design tensile stress F_t is calculated based on whether the member is connected by both legs or a single leg as follows:

$$F_t = \begin{cases} F_y & \text{if connected by both legs} \\ 0.90F_y & \text{if connected by a single leg} \end{cases} \quad (4.12)$$

The net area is calculated based on tearing of the member across its weakest section which passes through the holes using Eqn. (4.13),

$$A_{net} = A_{eff} - h \cdot t \cdot n_h \quad (4.13)$$

where h is diameter of the hole, t is member's thickness, n_h is the number of bolt holes to deduct from the cross-section, and A_{eff} , is the member effective area.

For an angle member, the member effective area A_{eff} , is calculated based on whether the member is connected by both legs, long leg or short leg as follows:

$$A_{eff} = \begin{cases} A & \text{if connected by both legs or long leg only} \\ A - (b - a) \cdot t \cdot n_a & \text{if connected by short leg only} \end{cases} \quad (4.14)$$

where b and a are the widths of long and short legs for unequal angle sections, respectively and n_a is the number of angles for a section; that is, $n_a = 1$ for single angle sections, and $n_a = 2$ for double angle sections, etc.

4.3.3. Maximum Slenderness Ratios

The leg, other and redundant members are required not to exceed the following limiting values of slenderness ratio:

$$\lambda_{\max} = \left(\frac{KL}{r} \right)_{\max} = \begin{cases} 150 & \text{for leg members} \\ 200 & \text{for other mebers} \\ 250 & \text{for redundant members} \end{cases} \quad (4.15)$$

4.3.4. Geometric Requirements

While sizing a transmission tower, it is required that the applied loads are safely carried from the earth-wire peak and cross-arms to the ground through the leg members. For a safe transmission of loads, the leg members should be designed such that the upper leg have an angle section with a flange width (w) and thickness (t) not larger than those of the angle section of the lower leg. In other words, both the flange width and thickness of angle sections used for leg members must increase, as one goes from top to the bottom through the height of the tower. These geometric requirements are stated mathematically in Eqns. (4.16) and (4.17) and are also illustrated in Figure 4.2 for a typical tower.

$$w_{i+1} \leq w_i \quad (4.16)$$

$$t_{i+1} \leq t_i \quad (4.17)$$

In Eqns. (4.16) and (4.17), w_i and w_{i+1} represent the widths of the angle sections used for lower and upper and leg members, respectively and t_i and t_{i+1} are the thicknesses of these angle sections.

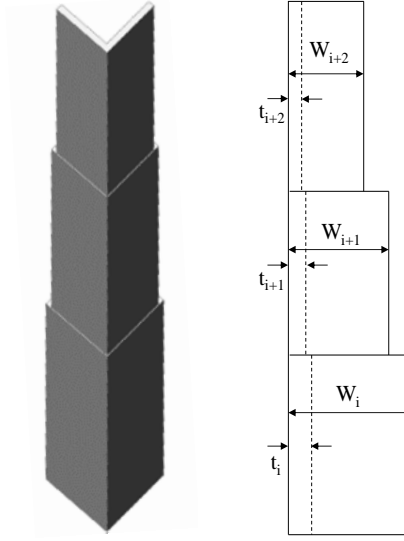


Figure 4.2 The geometric requirements on steel sections of the leg members in a tower.

4.3.5. Formulations of Constraints and Constraint Handling

The design limit states discussed above are normalized and expressed as a set of functions for constraint handling, as follows:

$$C_i^c = \max \left[\frac{(P_{mc})_i}{(P_c)_i} - 1.0, 0 \right] \quad (4.18a)$$

$$C_i^t = \max \left[\frac{(P_{mt})_i}{(P_t)_i} - 1.0, 0 \right] \quad (4.18b)$$

$$C_i^\lambda = \max \left[\frac{(\lambda)_i}{(\lambda_{max})_i} - 1.0, 0 \right] \quad (4.18c)$$

$$C_i = \sum_{i=1}^{N_m} \max(C_i^c, C_i^t, C_i^\lambda) \quad (4.18d)$$

where $(P_{mc})_i$, $(P_{mt})_i$, $(\lambda)_i$ are the compression and tension loads developed in the i -th member of the tower and its slenderness ratio, respectively; $(P_c)_i$, $(P_t)_i$, $(\lambda_{max})_i$,

are the allowable values of the preceding quantities according to ASCE10-97 (2000), C_i^c , C_i^t , and C_i^λ are constraint violations for compression capacity, tension capacity and slenderness ratio of the i -th member of the tower, and C_1 is the summation of maximally violated design limit state constraints for all the members.

Similarly, the geometric requirements are normalized and expressed as a set of functions for constraint handling, as follows:

$$C_i^w = \max \left[\frac{w_{i+1}}{w_i} - 1.0, 0 \right] \quad (4.19a)$$

$$C_i^t = \max \left[\frac{t_{i+1}}{t_i} - 1.0, 0 \right] \quad (4.19b)$$

$$C_2 = \sum_{i=1}^{N_{lm}} \max(C_i^w, C_i^t) \quad (4.19c)$$

where N_{lm} is the total number of leg members in the tower, C_i^w and C_i^t are the geometric constraint violations for the i -th leg member of the tower, and C_2 is the summation of maximally violated geometric constraint for all the leg members in the tower.

Finally, the constraints are handled in the present study using an external penalty function approach, where the modified objective function (W) is formulated as follows:

$$W = W_s \cdot (1 + r_1 \cdot C_1 + r_2 \cdot C_2) \quad (4.20)$$

where r_1 and r_2 refer to the penalty coefficients used for adjusting the degree of penalization for violations of design limit state and geometric constraints, respectively. Both penalty coefficients are set to a value of 1.0 during numerical examples.

CHAPTER 5

SIMULATED ANNEALING

In this thesis, the optimum design of transmission line towers is investigated using simulated annealing optimization technique. In the following, the underlying concepts of these techniques are presented first and the annealing algorithm employed in the study is outlined in more detail. It should be emphasized that the annealing algorithm used in this study is based on extension of the technique in Hasançebi et al. (2010a). In addition to this algorithm, a so-called two-phase SA algorithm is proposed in this thesis as an exclusive method for acquiring optimum design of steel transmission towers more rapidly with an annealing algorithm. The implementation of the two-phase SA algorithm is also explained in the last section of this chapter.

5.1. Introduction and Background

Annealing is a heating and cooling process of a physical system whereby the internal structure of the system is altered to change the physical and sometimes chemical properties of the system. The underlying purpose of the annealing process is to obtain an intended or a target configuration of a system from its present or randomly generated state by increasing temperature of the system first and then cooling it very slowly. Hence, the idea of annealing process comprises of two basic consecutive steps as heating and cooling of the physical system. Firstly, the physical system is heated up to increase its internal energy level so that its atomic configuration becomes more unstable where atoms diffuse freely to look for a target configuration. Secondly, the heated up system is cooled very slowly so that the system minimizes its energy level progressively. In this way, a change in the atomic configuration of the system is enabled at every manipulated temperature stage during which the atoms pass through different energy levels to

form more stable and perfectly ordered physical state of the system. At every energy level, the system obtains its newly formed properties. Therefore, the speed of cooling stage gains crucial importance to obtain perfectly ordered and stable state. The cooling process is continued till freezing (crystallization) condition. In other words, the cooling process is continued till the physical system has the minimum energy level (ground state) and more stable structural condition. The minimum energy level is obtained only if the initial or maximum temperature is high enough and the physical system is cooled very slowly. A typical heat treatment procedure for a solid material is displayed in Figure 5.1.

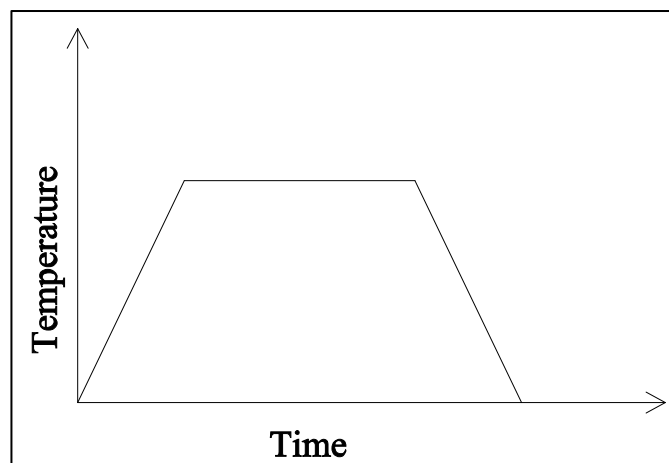


Figure 5.1 A typical heat treatment for a solid material.

The development of a numerical optimization algorithm to solve mathematical optimization problems is inspired by the theory of the annealing process of physical systems. The idea of gradual passing from high energy level to lower one is linked with the reducing of the objective function of the optimization problems.

An iterative-based or a local search optimization algorithm usually searches the global optima by generating a random solution and exploring the neighboring solutions in the search space systematically. Simulated annealing (SA) is a local search and stochastic optimization algorithm developed through inspiration by the

aforementioned annealing process in thermodynamic. Metropolis et al. (1953) laid the foundations of SA in their study which proposed the specific case of the canonical ensemble. The canonical ensemble illustrates the possible states of mechanical systems in a thermal equilibrium with a heat bath at a fixed temperature. In their study, the transition of a system between different energy levels to reach thermal equilibrium was investigated at a constant temperature. They have derived so-called Boltzmann distribution which is accepted as the key part of SA and used for the transition probability between energy levels. Based on Boltzmann distribution, Kirkpatrick et al. (1983) and Cerny (1985) independently developed the search algorithm of SA technique for solving numerical optimization problems

SA operates on the basis of using two solutions any time. The first one is the current solution and the other one is the candidate or the alternative solution of the optimization problem. The improving candidate solutions, which result in an improvement as compared to the current solution, i.e., downhill moves, are always accepted and replace the current solution, similar to a traditional local search algorithm. However, the prominent feature of SA is that it attempts to escape from local optima by occasional uphill moves, in which case non-improving candidate solutions are accepted even though their solutions are not any better than those of the current one. In the literature, this feature of SA is resembled as a bouncing ball over the mountain hill as depicted in Figure 5.2. In this figure, the initial condition of an optimization problem is illustrated in part (a). At this stage, the current solution is close to a local optimum solution designated as triangle; however, far from the global optimum solution shown as circle. In part (b), the current solution is the local optimum and better than its neighboring solutions. In traditional algorithms, the algorithms get stuck in at the sub-optimal point since the current solution is better than its neighboring solutions and hence, it cannot move away from the local optimum solution. In part (c), the current solution is at a different local optimum point. The algorithm can proceed to the global optima by jumping off those local optimums as shown in part (d).

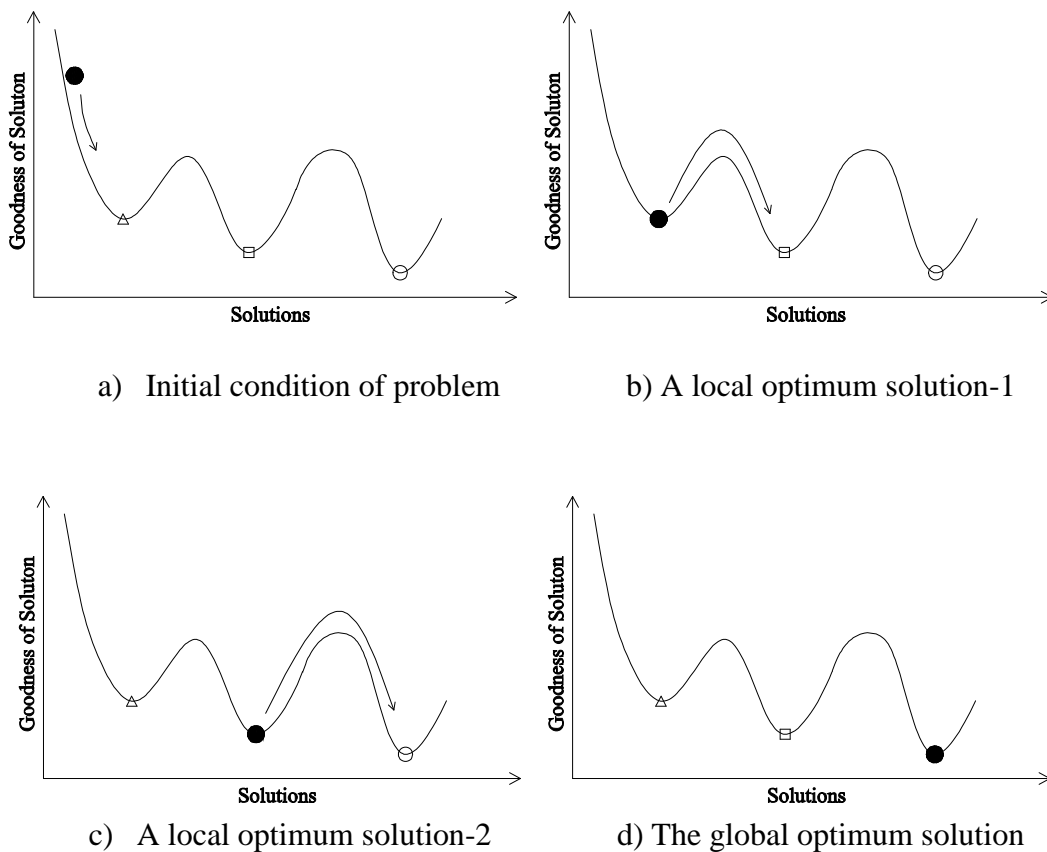


Figure 5.2 Optimum solution stages of SA.

It should be underlined that non-improving (poor) candidates are not always accepted. In fact, the rate of acceptance of poor candidate solution is fairly high in the early stages of optimization process. However, the rate of acceptance of poor candidate solutions decreases considerably as the cooling temperature approaches to the ground state, where the temperature is close to zero. This way, an explorative search is replaced gradually by exploitative one. Figure 5.3 shows the chance of acceptance probability of poor candidate solutions in a typical run of SA algorithm implemented over 300 cooling cycles (iterations).

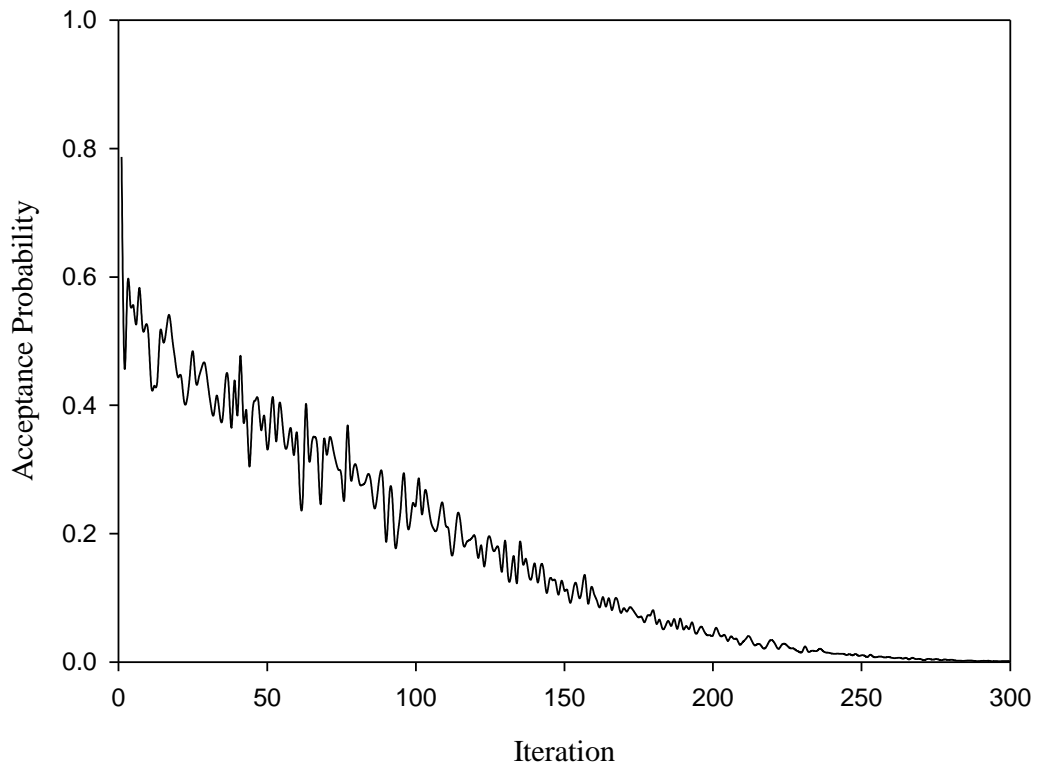


Figure 5.3 Acceptance probability variance with time.

SA can reach the global or a near-global optimum solution if the cooling is done successively by selection of proper temperature parameters. Similar to actual annealing process in thermodynamic, a slow cooling is essential to reduce the cost of an objective function to a satisfactory level at each temperature cycle, in order for a successfully implemented optimization process. The reduction of temperature at every cooling cycle and the number of iterations carried out at each temperature is called annealing schedule. Therefore, forming a proper annealing schedule is of vital importance to reach global or near-global optimum solutions with SA.

5.2. Annealing in Thermodynamic and Simulated Annealing Analogy

Working mechanism of SA is directly inspired from the annealing process of a physical system in thermodynamic based on the following similarities between the actual annealing procedure and optimization process. In the annealing procedure

the aim is to minimize the energy level which is conceptually similar to reducing objective function value in optimization process. The atomic configuration of the physical system corresponds to the set of design variables of the optimization problem. The energy state of the system is identical to every possible solution of the optimization problem. The current and candidate (alternative) states of the physical system coincide with current and candidate (alternative) solutions in optimization problem. The temperature in annealing process can be as a control and termination parameter in optimization process for determining level of convergence to a target solution. Finally, local and global minimum energy states correspond to the local and the global optimum solutions in optimization problem, respectively. Figure 5.4 illustrates the physical analogy between annealing process and SA.

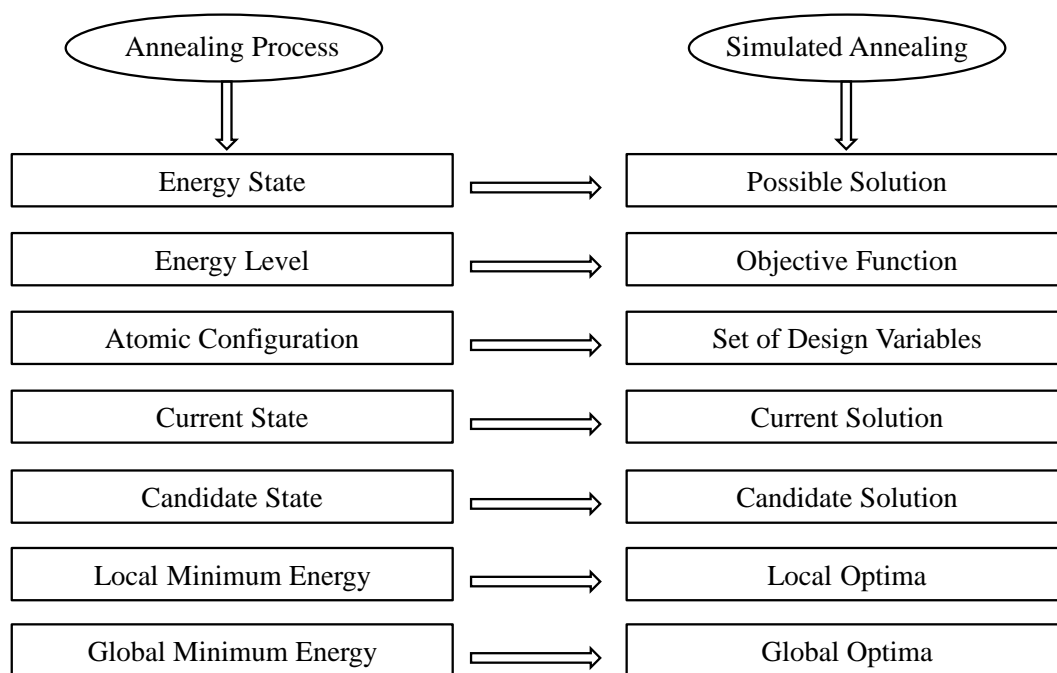


Figure 5.4 Physical analogy.

5.3. Metropolis Algorithm and Boltzmann Distribution

Metropolis algorithm is one of the most popular algorithms of Monte Carlo Markov Chain (MCMC) method. Metropolis et al. (1953) studied on the transition

of a system between different energy levels to reach the thermal equilibrium at constant temperature. They introduced an algorithm simulating the transition between different energy levels of a system in a heat bath to thermal equilibrium was introduced. Based on the results of this study and the principles of statistical mechanics, they derived the so-called Boltzmann distribution. In simulated annealing, all random moves depend on the Boltzmann distribution in the search space (Szewczyk and Hajela, 1993). Boltzmann distribution determines the probability of the system in a state “ θ ” at a given equilibrium temperature as follows:

$$P(\theta) = \frac{1}{\sum_{\Theta} \exp\left[-\frac{E(\theta)}{K * T}\right]} \cdot \exp\left[-\frac{E(\theta)}{K * T}\right] \quad (5.1)$$

In Eqn. (5.1), $P(\theta)$ is the probability of the system to be in a state (θ); T is the given temperature; $E(\theta)$ is the energy level of the state (θ); Θ is the all possible states at which the system endure at the given temperature and K is called as Boltzmann parameter which can be taken as constant or a dynamic value during the transition of the system between different energy levels. In Balling (1991), Boltzmann parameter (K) was described *as a normalization constant* and formulated as follows:

$$K^{(u)} = \frac{K^{(p)} N_a + \Delta\theta}{N_a + 1} \quad (5.2)$$

where; $K^{(p)}$ and $K^{(u)}$ refer to the values of Boltzmann parameter before and after it is updated by Eqn. (5.1), respectively; N_a is the number of poor candidates.

At a given constant temperature, different variations of the system are generated randomly with small perturbation each time. If the newly generated (perturbed) state has the better atomic configuration (i.e. lower energy level), the new state is

accepted as the current state immediately. However, if the perturbed state is in the higher energy level, it is only accepted based on the following ratio called as the Metropolis criterion (Hajela, 1999):

$$P_s = \frac{P(\theta_a)}{P(\theta_c)} = \exp \left\{ - \left[\frac{E(\theta_a) - E(\theta_c)}{K * T} \right] \right\} \quad (5.3)$$

In Metropolis criterion, P_s indicates the transition (acceptance) probability; θ_a and θ_c are the candidate (alternative) and current states, respectively. Note that θ_a is the higher energy level state than θ_c . $P(\theta_a)$ and $P(\theta_c)$ are the probabilities of states θ_a and θ_c , which are obtained from the Boltzmann distribution given in Eqn. (5.1); and $E(\theta_a)$ and $E(\theta_c)$ are the corresponding energy levels. The above transition probability works only if $E(\theta_a)$ is equal or greater than $E(\theta_c)$, i.e., $E(\theta_a) \geq E(\theta_c)$.

Metropolis et al. (1953) unearthed the Boltzmann distribution and transition probability with their study. The essence of this acceptance criterion, the so-called Metropolis algorithm, can be explained as follows:

- 1) The temperature should be set to a high initial value T_s so that almost all possible states are accepted at first.
- 2) The higher the T_s , the greater becomes the energy level of the initial state $E(\theta_c)$.
- 3) A small perturbation is given to the current state to change its atomic configuration and thus to generate an alternative (i.e. candidate) state at different energy level $E(\theta_a)$.
- 4) The difference between two energy levels is determined [$\Delta E = E(\theta_a) - E(\theta_c)$]. If the new state is in the lower energy level ($\Delta E < 0$), it is accepted as the current state immediately. However, if the difference between two energy levels has a non-negative value, the alternative state can still be accepted as the current state based on the result of the transition

probability. This process is continued till the system is brought to the thermal equilibrium at the same temperature.

- 5) Temperature is reduced slowly and aforementioned process is repeated till the system reaches the globally minimum energy level.

5.4. Method of Simulated Annealing

5.4.1. Definition of Simulated Annealing Terms

A typical SA algorithm basically consists of twelve parameters (terms) as “solution space, current solution, alternative (candidate) solution, objective function, current temperature, starting temperature, final temperature, cooling factor, perturbation limit, probability of acceptance of a candidate solution, iteration number of inner loop, Boltzmann parameter”. Before starting to explain the outline of SA algorithm, the parameters of SA will be introduced very briefly in the following:

1. A solution space \mathbf{S} including all possible solutions of the problem.
2. A current solution $\theta_c \in \mathbf{S}$, and a candidate (alternative) solution $\theta_a \in \mathbf{S}$. The θ_c and θ_a are generated randomly or based on pre-defined rules.
3. An objective function W defined on solution space \mathbf{S} ; i.e., $W(W_c, W_a): \mathbf{S} \rightarrow \mathbb{R}$. It is worth mentioning that W_c and W_a are the objective functions of the current and the candidate solutions, respectively.
4. Cooling schedule parameters T , T_s , T_f , and η which refer to current temperature, starting temperature, final temperature, and cooling factor, respectively. The value of the cooling factor is in the range of zero and one. $\eta \in (0,1) \in \mathbb{R}^+$.
5. The amount of small perturbation δ applied to one design variable of the current solution while generating a candidate solution.
6. Probability of acceptance of a candidate solution P based on the Metropolis acceptance criterion (Metropolis et al., 1953).

7. The iteration number I of inner loop, a single iteration of which corresponds to the case where all design variables are selected once and perturbed to generate a candidate solution.
8. Boltzmann parameter can be taken as a constant value. However, Hasançebi et al. (2010a) have stated that in a usual SA algorithm, Boltzmann parameter (K) is manipulated as the working average of the objective function difference (ΔW) values for non-improving candidates, i.e., $K = \Delta W_{ave}$.

5.4.2. The Outline of Simulated Annealing Algorithm

A number of variations and enhancements of the SA algorithm have been proposed in the literature to improve its search performance. The SA algorithm employed in this thesis for the size and shape optimum design of steel lattice transmission line towers is based on the improvement of the technique as formulated in Hasançebi et al. (2010a). In the following, this algorithm is presented first in the form a pseudo-code and then the implementation and computational steps of this algorithm are explained in detail.

Simulated Annealing Algorithm:

```

Module SA
  Sub main()
    'BEGIN
    Initialize ( $\theta_c$ ) 'Initialize Current Design Randomly
    'Where  $\theta_c = [X_c^c, X_s^c]$ 
    ' $X_c^c = (X_{c1}^c, X_{c2}^c, \dots, X_{ci}^c, \dots, X_{Nc}^c) =$  cross-section variables,  $i=[1, \dots, N_c]$ 
    ' $X_s^c = (X_{s1}^c, X_{s2}^c, \dots, X_{sj}^c, \dots, X_{Ns}^c) =$  shape variables,  $j=[1, \dots, N_s]$ 
    'Calculate objective function of current design ( $W_c$ )
    T=Ts
    Do While (T>Tf) 'Loop till Final Temperature

      Do While (I<If) 'Loop till Final Inner Loop

        Do While (k<Nc+Ns)
          'Perturb  $\theta_c$  by  $\delta$  to create  $\theta_a$ 
          'Where  $\theta_a = \theta_c + \delta = [X_c^a, X_s^a]$ 
          ' $X_c^a = (X_{c1}^a, X_{c2}^a, \dots, X_{ci}^a, \dots, X_{Nc}^a) =$  cross-section variables,
           $i=[1, \dots, N_c]$ 
          ' $X_s^a = (X_{s1}^a, X_{s2}^a, \dots, X_{sj}^a, \dots, X_{Ns}^a) =$  shape variables,  $j=[1, \dots, N_s]$ 
          If k ≤ Nc Then
             $\theta_k^a \in X_c^a$ 
            For i = 1 to Nc
               $X_{ck}^a = X_{ck}^c + \delta_k$  if i = k
               $X_{ck}^a = X_{ci}^c$  if i ≠ k
            Next i
             $\forall j \in [1, \dots, N_s] : X_{sj}^a = X_{sj}^c$ 
          Else
             $\theta_k^a \in X_s^a$ 
            For i = 1 to Ns
               $X_{sk}^a = X_{sk}^c + \delta_k$  if i = k
               $X_{sk}^a = X_{si}^c$  if i ≠ k
            Next i
             $\forall j \in [1, \dots, N_c] : X_{cj}^a = X_{cj}^c$ 
          End If
          'Calculate objective function of candidate design ( $W_a$ )
          If ( $\Delta W = W_a - W_c \leq \theta$ ) Then
             $X_c^c = X_c^a \wedge X_s^c = X_s^a \wedge W_c = W_a$ 
          Else
            If Rnd() ∈ (0,1) < P Then
               $X_c^c = X_c^a \wedge X_s^c = X_s^a \wedge W_c = W_a$ 
            Else
              'Keep the same current design
            EndIf
          EndIf
          k = k + 1
        Loop
        I = I + 1
      Loop
      T = T*η
    Loop
  End Sub
End Module

```

Step 1: Initialization (Current Design) and Setting Annealing Schedule

The first step is initialization and setting of an appropriate cooling schedule. As for the initialization, a profile database is assigned for sizing variables and upper and lower bounds are determined for shape variables. The profile database consists of a predefined number of steel angle sections where the sections are sorted and indexed in the order of increasing cross-sectional areas. The annealing schedule parameters are calculated using the formulas in Eqn. (5.4) based on selection of a starting acceptance probability (P_s), a final acceptance probability (P_f), and the number of cooling cycles (N_c).

$$T_s = -\frac{1}{\ln(P_s)}, \quad T_f = -\frac{1}{\ln(P_f)}, \quad \eta = \left[\frac{\ln(P_s)}{\ln(P_f)} \right]^{1/N_c - 1} \quad (5.4)$$

In Eqn. (5.4), T_s , T_f , and η are referred to as starting temperature, final temperature, and the cooling factor, respectively. The starting temperature is assigned as the current temperature, i.e., $T = T_s$. It is important to emphasize that the starting acceptance probability P_s and thereby the starting temperature T_s should be assigned high enough to allow acceptance of non-improving candidates at a high rate in order to encourage an extensive exploration of the design space in the early stages of optimization process.

Step 2: Generation of Initial Design

The initial design is generated randomly such that sizing design variables are set to some integer values between 1 and the number of discrete steel sections available in the profile database, and shape design variables are initialized to any real values between their predefined lower and upper limits. A finite element model (FEM) of the tower is generated automatically for the initial design in PLS-Tower using the model generating module, as discussed in the following chapter. The member, material and geometrical properties as well as load assignments in

the FEM are also carried out automatically. Optionally a linear or geometrically nonlinear finite element solver of PLS-Tower is then executed to analyze the design and to obtain force and deformation responses of the tower under the applied load cases. The design limit states as well as geometric requirements are checked to identify any possible constraint violation in the initial design, and the modified objective function value of the current design (W_c) is calculated.

Step 3: Generating Candidate Designs

A number of candidate designs are generated in the vicinity of the current design. This is performed as follows: (i) a design variable is selected, (ii) the selected variable is given a small perturbation in a predefined neighborhood (Eqn.5.5), and (iii) finally, a candidate design is generated by assuming the perturbed value of the variable, while keeping all others same as in the current design. It follows that a candidate design differs from the current one in terms of one design variable only. It is important to note that each design variable is selected only once in a random order to originate a candidate design. Hence, the total number of candidate designs generated in a single iteration of a cooling cycle is equal to the total number of design variables, i.e. $N_c + N_s$.

$$\theta_k^a = \theta_k^c + \delta_k \quad (5.5)$$

In Eqn. (5.5), θ_k^c denotes a selected sizing (X_{ci}) or shape (X_{sj}) variable of current design, δ_k is the amount of perturbation applied to the selected variable, and θ_k^a refers to the perturbed value of the variable of candidate design

For each sizing variable the δ_k is set to a randomly chosen integer value within a predefined neighborhood $[-n_{w1}, n_{w1}]$, which is defined in this study as follows:

$$n_{w1} = \text{int}(\sqrt{N_{\text{sec}}}) \quad (5.6)$$

For each shape variable the δ_k is set to a randomly chosen real value within a predefined neighborhood $[-n_{w2}, n_{w2}]$, which is defined in this study as follows:

$$n_{w2} = \frac{S_{\text{upp}} - S_{\text{low}}}{10} \quad (5.7)$$

In Eqns. (5.6) and (5.7), N_{sec} denotes the number of steel sections in discrete profile database, S_{low} and S_{upp} represent the predefined lower and upper bounds for a shape variable, respectively.

Step 4: Evaluating a Candidate Design and Metropolis Test

Each time when a candidate design is generated, its objective function (W_a) is computed according to Eqn. (4.20) and is set to compete with the objective function of current design (W_c). If the candidate provides a better solution (i.e., $\Delta W = W_a - W_c \leq 0$), it is automatically accepted and replaces the current design. Otherwise, the so-called Metropolis test is resorted to determine the winner in which the probability of acceptance P of a poor candidate design is assigned using Eqns. (5.8) through (5.10), as formulated in Hasançebi et al. (2010a). Metropolis test is finalized by generating a random number r between 0 and 1, such that if ($r \leq P$), the candidate is accepted and it replaces the current design. Otherwise ($r > P$), the candidate is rejected and the current design maintains itself.

$$\varphi^{(k)} = \varphi^{(k-1)} \cdot \sqrt[3]{\bar{P}_t^{(k-1)} / \bar{P}_p^{(k-1)}}, \quad 0.9 \leq \varphi \leq 1.1 \quad (5.8)$$

$$\Delta W_{\text{tra}} = \tanh\left(0.35 * \frac{\Delta W}{K}\right) \quad (5.9)$$

$$P = \varphi \cdot \exp\left(-\frac{\Delta W_{\text{tra}}}{K * T^{(k)}}\right) \quad (5.10)$$

In Eqns. (5.8)-(5.10), φ is a correction factor introduced to ensure that the operational average acceptance probability follows the theoretical acceptance

probability in a numerical implementation of the algorithm; $\bar{P}_t^{(k-1)}$ and $\bar{P}_p^{(k-1)}$ are the theoretical and practical (operational) average acceptance probabilities at the $(k-1)$ -th cooling cycle, respectively; ΔW_{tra} is the transformed value of ΔW value using a sigmoid function, $T^{(k)}$ is the temperature at k -th cooling cycle, and finally K is the a parameter called Boltzmann value, which is manipulated as the working average of ΔW_{tra} values, i.e. $K = (\Delta W_{tra})_{ave}$.

It should be noted that a reformulation of acceptance probability function (Eqn. 5.10) has been achieved in Hasançebi et al. (2010a) through the correction factor (ϕ) (Eqn. 5.8). They have stated that in a usual SA algorithm Boltzmann parameter (K) is manipulated as the working average of ΔW values for non-improving candidates (i.e. $K = \Delta W_{ave}$). Therefore, it should be anticipated that if one averages acceptance probabilities of all candidates subjected to Metropolis test at each cooling cycle, he should plot a curve that would roughly match with the theoretical curve $\exp(-1 / T)$. However; this might not be the case in practice if the Metropolis test is employed as originally proposed. Especially for large scale structures, the intended values of acceptance probability do not comply with the theoretical one. Rather, the average acceptance probability calculated according to Eqn. (5.3) in practice reveal much higher values compared to the theoretical acceptance probability. As a result of this poor candidate designs are still accepted at very high rates even in later stages, hampering the convergence of the algorithm to a good-solution. The correction factor (ϕ) formulated in Eqn. (5.8) has been introduced to overcome this problem. In addition, the upper and lower bounds on the correction parameter are introduced to avoid abrupt changes in the value of this parameter. By virtue of this parameter, the average acceptance probability for non-improving candidate designs is kept approximately at the same level with the theoretical acceptance probability.

Similarly, Hasançebi et al. (2010a) proposed an improvement on implementation of Boltzmann parameter (K). Boltzmann parameter has two main functions on the

algorithm. The first one is that, it normalizes the ΔW values during the Metropolis test to eliminate problem dependency. Secondly, it accumulates the search experience by storing the moves through previously sampled candidates in the search space. In this way, acceptance of the next candidates is related to former search experience. During the optimization process, extremely poor candidates may be generated. In that case, ΔW becomes very high value and if this value is utilized directly to update Boltzmann parameter as in the original formulation Eqn. (5.2), it drags the Boltzmann parameter to unfavorably high values, in which case non-improving solutions are accepted at a very high rate even in later stages of optimization process. This may cause the algorithm to lose its search ability to focus on good regions of the search space. Therefore, a transformation of ΔW by using the sigmoid function has been proposed through Eqn. (5.9) to eliminate this problem.

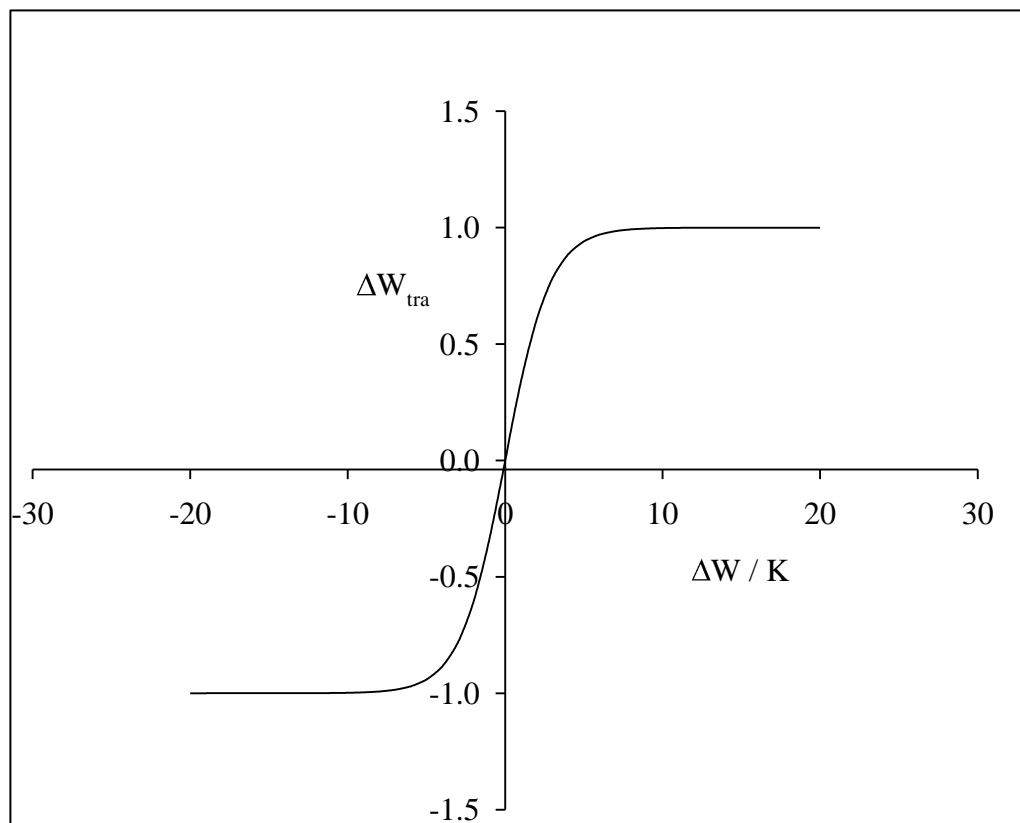


Figure 5.5 Sigmoid transformation function.

Figure 5.5 shows the sigmoid function used in Eqn. (5.9). Accordingly, every time when a candidate design is generated, its ΔW value is calculated in a usual way and proportioned to the current value of Boltzmann parameter, i.e. $\Delta W / K$. For any $\Delta W / K$, Eqn. (5.9) yields a transformed value ΔW_{tra} which always remain in the range 0 and 1. Even if a candidate is extremely poor (say ΔW is infinite), its transformed value ΔW_{tra} is mapped to a value between 0 and 1 by virtue of Eqn. (5.9). Then The Boltzmann parameter is then manipulated as the average value of the transformed values ΔW_{tra} , rather than direct values of ΔW , i.e., $K = (\Delta W_{tra})_{ave}$.

Step 5: Iterations of a Cooling Cycle

A single iteration of a cooling cycle is referred to the case where all design variables are selected once and perturbed to generate candidate designs. Generally, a cooling cycle is iterated a certain number of times in the same manner to ensure that objective function is reduced to a reasonably low value associated with the temperature of the cooling cycle. Having selected the iterations of the starting and final cooling cycles (i_s and i_f), the iteration of a cooling cycle (i_c) is determined by a linear interpolation between i_s and i_f as follows:

$$i_c = \text{int} \left[i_f + (i_f - i_s) \left(\frac{T - T_f}{T_f - T_s} \right) \right] \quad (5.11)$$

In this thesis, the iterations of the starting and final cooling cycles were all taken as 1. This was performed for the sake of reducing the computation time. It was also found that the final design after optimization was not affected significantly by the number of iterations of cooling cycles.

Step 6: Reducing Temperature

When the iterations of a cooling cycle are completed, the temperature is reduced by the ratio of the cooling factor η , and the temperature of the next cooling cycle is set.

$$T^{(k+1)} = T^{(k)} \cdot \eta \quad (5.12)$$

Step 7: Termination Criterion

The steps 3 through 6 are repeated until the whole cooling cycles are implemented.

5.5. Two-Phase Simulated Annealing Algorithm

A standard design procedure of transmission line towers requires that each particular tower is designed with different combinations of body and leg extensions. The various body extensions of a tower are required to increase its height and thus to obtain the required minimum ground clearance as well as clearances for road or river crossings. On the other hand, leg extensions are used to spot the tower on the land according to various geographic and surface conditions along the line. Therefore, during the design process of a particular tower type, a family of finite element (FE) models is generated corresponding to different combinations of body and leg extensions of the tower. The cross-arms as well as tower body that invariably present in every combination are referred to as basic-body, which is jointly shared by all tower family. Different body and leg extensions are added to the basic body of the tower to generate the family. The member groups in the basic body are designed together according to the maximum forces and strength utilization values across the tower family. On the other hand, the members that belong to a particular combination of body and leg extension, should be grouped internally and sized independently during the design process. To this end, a practical design application of a transmission line tower

involves sizing of a high number of member groups, and requires concurrent analyses of finite element models of the entire tower family.

On the other hand, simulated annealing is a non-deterministic search technique, and it partially works on the basis of randomized search of the design space, like every other meta-heuristic approach. A size and shape optimum design of a transmission line tower through the annealing algorithm described above often requires a very long computation time and effort, which makes it impractical to be used in a typical design office.

Hence, a two-phase simulated annealing method was proposed in this thesis as an exclusive method for acquiring optimum design of steel lattice towers more rapidly with an annealing algorithm. In the first phase of this method, only the shape parameters are optimized by the annealing algorithm while the steel members are sized with a fully stressed design based heuristic approach. The objective of the first phase is to improve the initial design rapidly in relatively less number of iterations (cooling cycles). In the second phase, the best design obtained in the prior phase is utilized as the initial design, and the annealing algorithm is implemented anew for both shape and size variables together under a new set of annealing parameters over a much reduced number of cooling cycles. The basic computational steps of the two-phase SA algorithm are summarized below and are also presented in the flowcharts depicted in Figure 5.6 and Figure 5.7.

Phase 1:

Step1. Initialization and setting an annealing (cooling) schedule: The parameters are initialized and a rapid cooling schedule is generated in which the number of cooling cycles N_c can be set to 30.

Step2. Generation of an initial design: An initial design is created in a usual manner by assigning random values to all design variables within the ranges of

their predefined limits, and its modified objective function is calculated using Eqn. (4.20).

Step3. Creating and resizing of candidate designs: A candidate design is then generated by perturbing a shape variable in the current design and resizing all the members deterministically based on a fully stressed based heuristic approach under the new geometry of the truss using the following iterative algorithm.

- a. Initially assign all the members to the smallest section in the profile database by setting all the sizing variables to 1, i.e. $X_{ci} = 1, i = 1, \dots, N_c$. It should be noted once again that the size variables are denoted with the index numbers of the assigned steel sections in the profile database.
- b. Analyze the candidate design using PLS-Tower solver
- c. Check design limit states only (not geometric constraints) for the tower and identify member or member groups which violate design limit state constrains.
- d. For member or member groups that violate design limit state constraints, adopt a larger cross-section from the profile list by incrementing their size variables all at once, and keep the others unchanged using Eqn. (5.13).

$$X_{ci,mod} = \begin{cases} X_{ci} + s_i & \text{if violated} \\ X_{ci} & \text{otherwise} \end{cases} \quad (5.13)$$

In Eqn. (5.13), X_{ci} and $X_{ci,mod}$ refer to current and modified value of a size variable for a member or member group, respectively, and the s_s is the amount of increment (or step size) in the value of the size variable.

- e. Repeat steps b through d until all members or member groups satisfy design limit state constraints or all member groups are set to the largest section in the profile database.

It is worthwhile to mention that the second termination criterion might happen if a candidate design has a very distorted tower geometry at a time, in which case the

design limit states may not be satisfied even if all members are set to the largest section in the profile database. It should also be noted that the maximum number of iterations performed in resizing algorithm is equal to $(N_{\text{sec}}-1)/s_s$, where N_{sec} is the number of steel sections in the profile database. Accordingly, iteration number and execution time of the resizing algorithm are controlled by the step size parameter. A very low value of step size increases accuracy of the resizing algorithm, yet may adversely affect overall execution time of the algorithm, if the discrete profile database includes a high number of steel sections. In this study the s_s is set to a value of 5 for a profile list consisting of around one hundred steel sections. This way it is ensured that resizing algorithm will be completed in a maximum of 20 iterations.

Step 4. Evaluating the candidate design and Metropolis test: The created and resized candidate design in Step 3 is compared with the current design. If the candidate provides a better solution, it replaces the current design, otherwise the winner is determined in the Metropolis test using Eqns. (5.8) through (5.10).

Step 5. Iterations of a cooling cycle: A single iteration of a cooling cycle is completed when all the shape variables are selected once in a random order to generate candidate designs. The cooling cycle may be iterated a number of times according to Eqn. (5.11).

Step 6. Reducing temperature: The temperature is reduced as per Eqn. (5.12).

Step 7. Termination criterion: The steps 3 through 6 are repeated until the whole cooling cycles are implemented.

Phase 2:

In the second phase of the proposed approach, the annealing algorithm described

in Section 5.4 is mainly implemented for both size and shape design variables together. However, instead of initiating the algorithm from a randomly generated design, the best design obtained in phase 1 is utilized as the initial design of the second phase. Accordingly, the search is initiated from a very promising design point unlike before, and the need for an exhaustive cooling schedule is not required any more. Hence, a mild (rapid) cooling schedule is chosen that employs the algorithm over a reduced number of cooling cycles with a new set of annealing parameters. It was shown in the numerical examples that the second phase produced comparable solutions to those of the original SA algorithm, although the former employs a rapid cooling schedule and thus requires much lesser computation time.

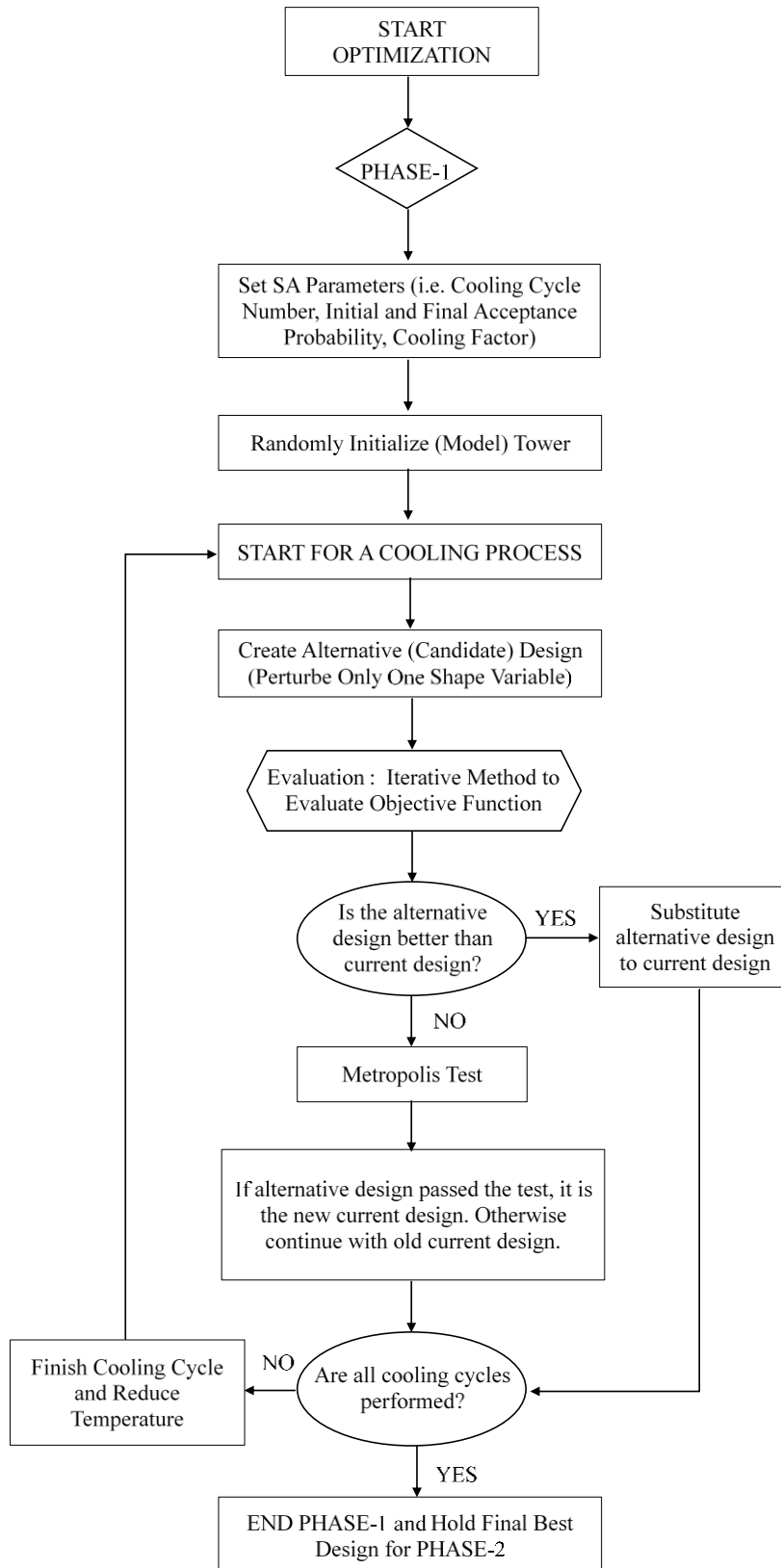


Figure 5.6 A flowchart for Phase-1 of two-phase simulated annealing algorithm.

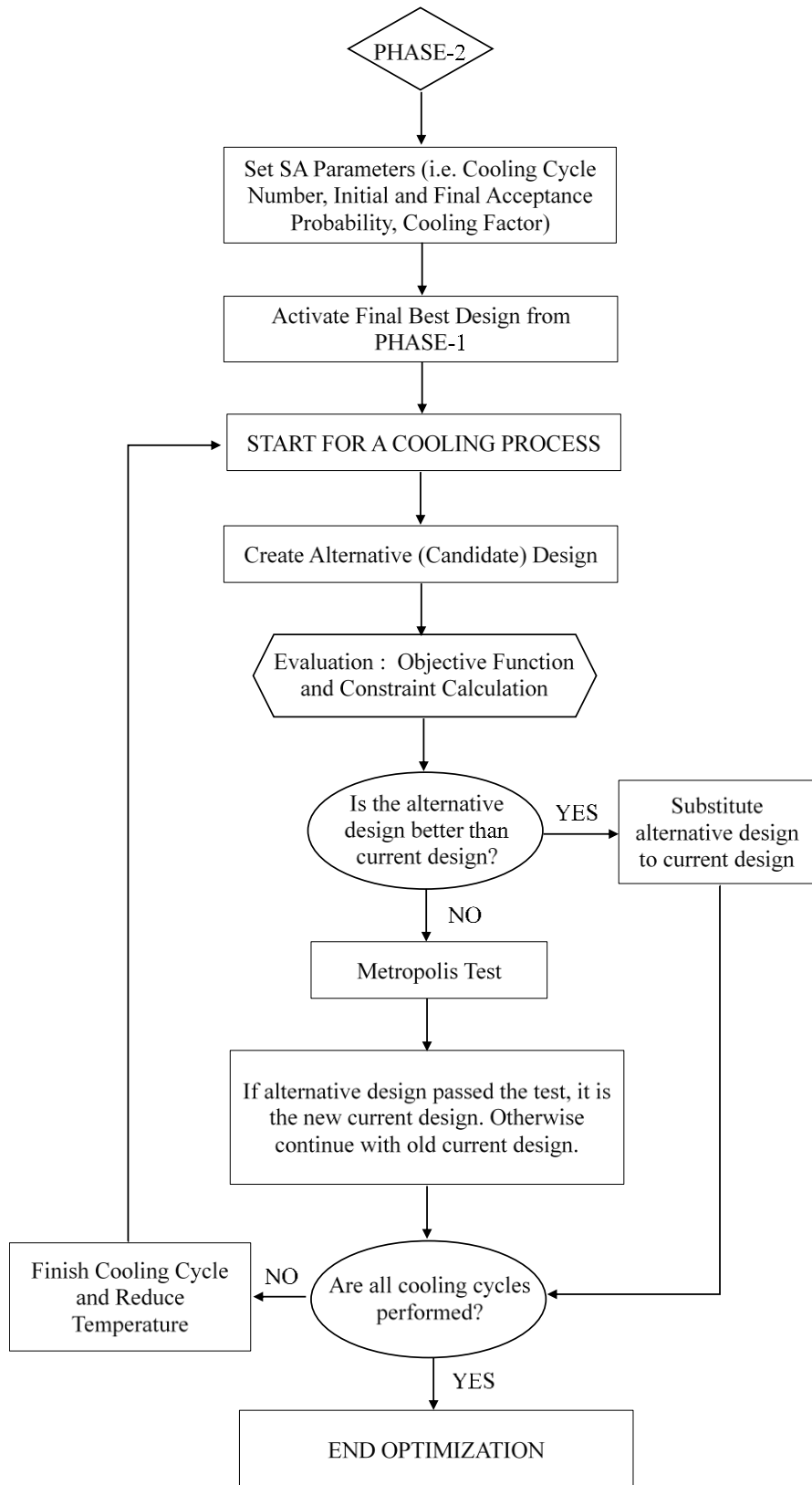


Figure 5.7 A flowchart for Phase-2 of two-phase simulated annealing algorithm.

5.6. Strengths and Weaknesses of Simulated Annealing

SA is a robust and effective stochastic optimization algorithm. One of the superior features of the SA over the classical methods and other local search optimization algorithms is that it can be utilized to optimize a wide range of problems from different disciplines. Although SA was originally developed as a discrete optimization algorithm, it can also be used to handle continuous optimization problems. For instance, Bohachevsky et. al (1986) and Fabian (1997) utilized the SA algorithm for mathematical function optimization problems. In the literature, SA was successfully applied to optimize highly nonlinear models, complicated structures, chaotic data including many constraints, and problems having discrete and/or continuous constraints. The method has been proved to approach the global or near-global optimum solution provided that proper values are selected for initial and final temperatures and cooling cycle parameters. Additionally, since SA is a stochastic search algorithm, it does not require high degree function operations and heavy mathematical computations. Hence, it can easily be implemented into computer codes developed for discrete and continuous design optimization. Finally, the method can be tuned depending on the characteristics of the problems at hand so that the algorithm can take place in different application areas from cost function minimization to structural weight minimization with small modifications.

The main weakness of SA is that similar to all stochastic optimization algorithms, it has a computationally expensive algorithm in terms of its convergence time. Although there are studies to improve convergence time of SA, users are usually in a tradeoff mechanism about the quality of the optimization result and elapsed time.

5.7. Simulated Annealing vs. Other Search Methods

Many search algorithms have been devised in the literature for solution of optimization problems. These methods extend from traditional optimization

algorithms that employ gradient calculations and problem-specific information to metaheuristics that use nature inspired methodologies for search process. A direct comparison between different methods may not be almost impossible. However, it is clear to anyone that an efficient optimization algorithm searching for global optimum should have two main characteristics. Firstly, the algorithm should be able to explore an extensive part of the search space. Secondly, the algorithm should exploit previously visited good solutions to steer the search to better design points.

Hasançebi et al. (2009) compared seven stochastic search algorithms; namely genetic algorithms, evolutionary strategies, particle swarm optimizer, tabu search, ant colony, and simulated annealing, to evaluate performances of the algorithms on the pin jointed structures. Firstly, a benchmark problem (i.e. 25-bar truss) was optimized by using abovementioned algorithms and then optimum designs of four real size design examples were tested. The algorithms were compared according to their solution accuracies, convergence rates and reliabilities. Among the seven optimization algorithms, simulated annealing and evolutionary strategies revealed the best performances. Additionally, in Hasançebi et al. (2010c) performances of abovementioned optimization algorithms were compared in sizing optimization of real sized frame structures. Again, this study pointed out more successful performances of simulated annealing and evolutionary strategies in design optimization of steel frames

Besides the stochastic optimization algorithms, gradient based optimization methods have been widely used in literature for function optimization. The main advantage of the gradient based optimization algorithms is they require only a limited number of iterations to converge to a solution. They employ the information gained from the gradient of the function to follow a direction in the search space. However, if the function is discrete, discontinuous or non-differentiable, the algorithm cannot compute the derivative of the function. On the other hand, SA does not require gradient of the function. Another drawback of the

gradient based algorithms is that if the search space includes a number of local optima or the function is not a unimodal function, the gradient based algorithms may get stuck in local optima easily. On the other hand, one of the main advantages of SA is that it cannot get stuck in local optima easily by allowing occasional uphill moves.

CHAPTER 6

PLS-TOWER INTEGRATED OPTIMIZATION SOFTWARE FOR OPTIMUM DESIGN OF TRANSMISSION LINE TOWERS

The lattice steel towers resist the applied loading in the form of truss action. Therefore, they are modeled and analyzed as space trusses, in which the members are assumed to carry primarily axial compression or tension forces. The structural analysis of a tower is usually performed using finite element method, in which the tower geometry is discretized into a certain number of elements (members) and nodes (joints). Today, various finite element (FE) computer programs and software package are used by the designers working in the industry to analyze towers under ultimate design loads. The PLS-Tower (developed by Power Line Systems, Inc.) is the most well-known and recognized software by the private corporations as well as state authorities (PLS-Tower Manual, 2015). This software has been automated to conduct geometrically linear and nonlinear analysis of lattice steel towers and also to perform strength checks according to the available design specifications around the world.

The simulated annealing based algorithms developed for optimum size and shape design of steel lattice transmission line towers were integrated with PLS-Tower software to offer practicing engineers a useful tool, which gives them ability to utilize full design and analyses features of PLS-Tower during automated optimum design process as well as to pre- and post-process tower models using its graphical user interface. In the following, the PLS-Tower software is briefly overviewed first with its design and analysis capabilities. Next, some information is presented regarding the integration of PLS-Tower with the optimization algorithms discussed in Chapter 5.

6.1. PLS-Tower

PLS-Tower (Figure 6.1) is a powerful and easy to use Microsoft Windows program for the analysis and design of steel lattice towers used in electric power lines or communication facilities. Both self-supporting and guyed towers can be modeled. The program performs design checks of structures under user-specified loads. For electric power structures it can also calculate maximum allowable wind and weight spans and interaction diagrams between different ratios of allowable wind and weight spans.

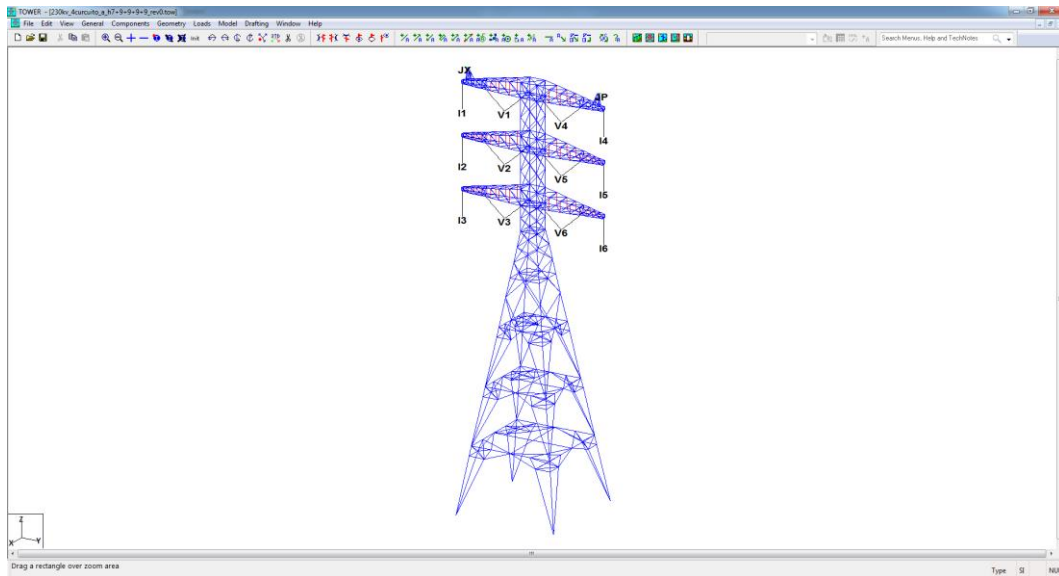


Figure 6.1 Opening screen of PLS-Tower.

In general, the tower structures in PLS-Tower are modeled and defined based on collections of the following components:

- Angle Members;
- Solid Round Members;
- Pipe Members;
- Bolts;
- Guys;
- Cables;

- Equipment (user defined items like antennas, cable conduits, ladders etc.);
- Insulators (clamp, strain, post, suspension, 2-parts).

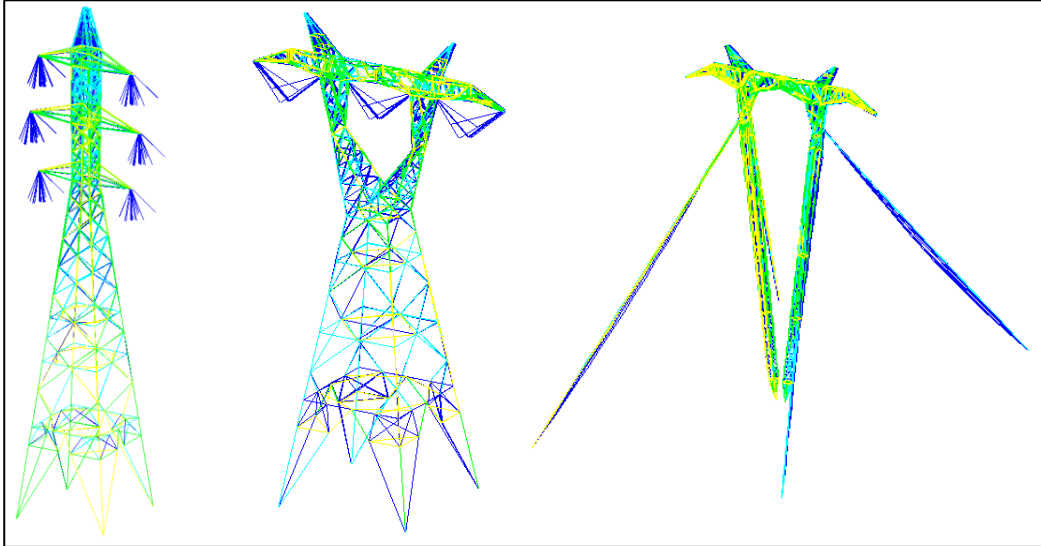


Figure 6.2 Comprehensive structure modeling with PLS-Tower.

Building a structure in PLS-Tower is as simple as defining the overall outline geometry of a tower, selecting intermediate joints and then lacing members or other components up between these joints (Figure 6.2). The user is free to mix and match the various members and components at will. This gives the user the power to create arbitrarily complex structures, including lattice box structures used in many older substations.

Component libraries in PLS-Tower (Figure A.1) define the size, weight, strength and other properties of bolts, guys, members and other equipment. The users are allowed to create their own libraries as well. Using libraries of standard components greatly enhances productivity of the users by significantly reducing the amount of input, which also reduces the chance of error.

PLS-Tower offers pre and post processing features to facilitate the finite element analysis and design for towers. A lattice structure modeled in PLS-Tower is input as a collection of elements and the connections and bracing properties for each member. PLS-Tower takes advantage of symmetry in a structure in both joint and member generation, duplicating symmetrical joints and members about either axis, both axes and even in a triangular format found in many communication structures. Even very large or complicated structures can be modeled in PLS-Tower.

PLS-Tower is capable of performing both linear and nonlinear analyses. Nonlinear analysis allows the user to see P-Delta effects, to detect instabilities, accurately model tension-only members and perform reliable buckling checks. PLS-Tower models guys, cables and 2-part insulators as 3-D cable elements. This sophisticated analysis works even when the elements have large displacements.

Once PLS-Tower calculates the forces experienced in different members and components of a structure, it compares them against automatically calculated code capacities for the code selected. The results of these checks are available in text reports, spreadsheets or color-coded graphics (Figure 6.3).

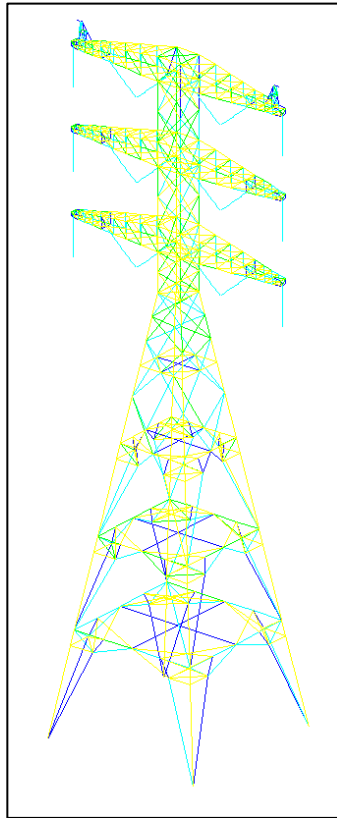


Figure 6.3 The color-coded analysis result graphic.

ASCE-10, ANSI/EIA/TIA 222 (Revisions F and G-1), CSA S37, ECCS, CENELEC (Euro), AS 3995, BS 8100, and other international codes can be used to check a structure. Members are checked against their ultimate strength in accordance with the code selected, with overstressed members easily identified graphically and in the output reports. PLS-Tower performs linear or exact nonlinear analysis depending on the choice made. The PLS-Tower manual describes how these checks are implemented and details the assumptions made.

In addition to these code checks, PLS-Tower can calculate pairs of allowable wind and weight spans, or better yet, determine entire interaction diagrams between the allowable wind and weight spans. Optimum spotting performed with these interaction diagrams will result in a more economical solution than traditional spotting with just a single, or a few, wind and weight span pairs.

PLS-Tower makes extensive use of 3-D graphics to help the user visualize a structure. All elements can be rendered in 3-D and a tower structure can be viewed from any direction making modeling mistakes immediately apparent. When the users see a mistake they simply click on it to edit the problem joint, member, or component.

After an analysis, elements are color-coded based on their utilization with overstressed elements graphically shown in red (Figure 6.4) These elements can be edited with a single click. Overstressed elements are also colored red in text and spreadsheet reports (**Hata! Başvuru kaynağı bulunamadı.**).

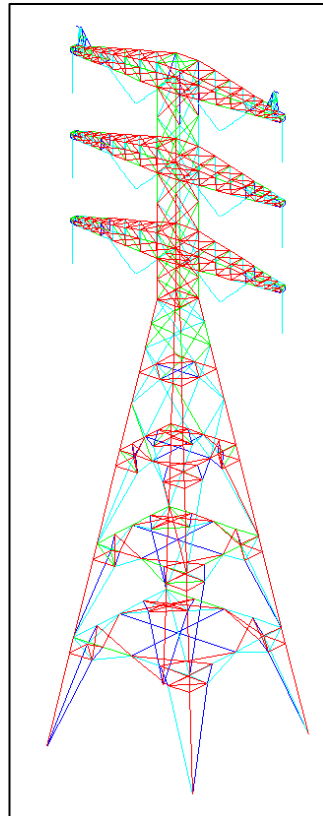


Figure 6.4 The illustration of overstressed elements

Figure 6.5 The table of overstressed elements

Figure 6.6 The table of overstressed elements

Group Label	Group Desc.	Angle Type	Angle Size	Steel Strength (MPa)	Max Usage %	Usage Cont-rol	Max Use In Comp. %	Comp. Control Member	Comp. Force (kN)	Comp. Control Load Case	L/r Capacit (kN)
1	1 MAIN LEG	SAE	L50*50*5	355	92.63	Comp	92.63	g1X	-78.686	9a. Broken Wire OPGW&UCL	84.94
2	2 MAIN LEG	SAE	L80*80*6	355	116.39	Comp	116.39	g4Y	-235.33	9b. Broken Wire UCL&MCL	202.18
3	3 MAIN LEG	SAE	L80*80*6	355	110.87	Comp	110.87	g5X	-268.1	9a. Broken Wire OPGW&UCL	241.82
4	4 MAIN LEG	SAE	L80*80*6	355	91.01	Comp	91.01	g6P	-220.08	8a. Wind & Ice	241.82
5	5 MAIN LEG	SAE	L80*80*6	355	180.97	Comp	180.97	g7P	-437.63	9a. Broken Wire OPGW&UCL	241.82
6	6 MAIN LEG	SAE	L120*120*8	355	126.84	Comp	126.84	g8P	-655.42	9a. Broken Wire OPGW&UCL	516.74
7	7 MAIN LEG	SAE	L120*120*8	355	138.99	Comp	138.99	g9P	-739.86	9a. Broken Wire OPGW&UCL	532.31
8	8 MAIN LEG	SAE	L120*120*8	355	135.78	Comp	135.78	g10P	-722.77	9a. Broken Wire OPGW&UCL	532.31
9	9 MAIN LEG	SAE	L120*120*8	355	133.1	Comp	133.1	g11P	-687.76	8a. Wind & Ice	516.74
10	10 MAIN LEG	SAE	L130*130*12	355	107.93	Comp	107.93	g12P	-974.64	8a. Wind & Ice	903.04
11	11 MAIN LEG	SAE	L130*130*12	355	102.88	Comp	102.88	g13P	-929.08	8a. Wind & Ice	903.04
12	12 MAIN LEG	SAE	L130*130*12	355	116.28	Comp	116.28	g14P	-1050.1	8a. Wind & Ice	903.04
13	13 MAIN LEG	SAE	L130*130*12	355	114.64	Comp	114.64	g15P	-1035.3	8a. Wind & Ice	903.04
14	14 MAIN LEG	SAE	L130*130*12	355	115.07	Comp	115.07	g16P	-1039.2	8a. Wind & Ice	903.04
15	15 MAIN LEG	SAE	L130*130*12	355	130.36	Comp	130.36	g17P	-1177.6	8a. Wind & Ice	903.36
16	16 COMMON BODY BRACING	SAE	L40*40*4	355	0.86	Comp	0.86	g22R	-0.597	9a. Broken Wire OPGW&UCL	69.6
17	17 COMMON BODY BRACING	SAE	L40*40*4	355	1.63	Comp	1.63	g23P	-0.389	9a. Broken Wire OPGW&UCL	23.89
18	18 COMMON BODY BRACING	SAE	L40*40*4	355	1.69	Comp	1.69	g24R	-0.658	6a. High Wind	38.83
19	19 COMMON BODY BRACING	SAE	L40*40*4	355	3.43	Comp	3.43	g25P	-0.508	6b. High Wind (Min. Weight Span)	14.79
20	20 COMMON BODY BRACING	SAE	L40*40*4	355	172.27	Comp	172.27	g26XR	-29.736	8a. Wind & Ice	17.26
21	21 COMMON BODY BRACING	SAE	L40*40*4	355	246.84	Comp	246.84	g27X	-85.217	9a. Broken Wire OPGW&UCL	34.52

Done

Figure 6.7 The table of overstressed elements

While PLS-Tower is a stand-alone program its open design allows it to easily interface with other programs. PLS-Tower provides a well defined XML output file and hooks that enable pre and post-processors to be connected to the program making it the ideal engine of lattice tower analysis process.

Users of PLS-CADD line design program, another software developed by Power Line System Inc., can use PLS-Tower to prepare allowable wind and weight span or interaction diagram files for optimum spotting. They can also take PLS-Tower structures and spot them in a line. PLS-CADD can calculate the loading on a structure at a particular location and display the results of a PLS-Tower check with those loads.

PLS-Tower results are presented in a combination of graphical views, spreadsheets and text reports. All of this information can easily be exported to other programs. Graphical results can be saved in DXF files compatible with most CAD systems. Spreadsheet results may be saved in an XML file, pasted into spreadsheet programs or exported to ODBC compliant databases. Text results can be customized by the user and saved to files or pasted into word processing programs.

6.2. Integration of PLS-Tower with Optimization Algorithms

Figure 6.8 crudely displays the integration of PLS-Tower with the optimization algorithms discussed in Chapter 5.

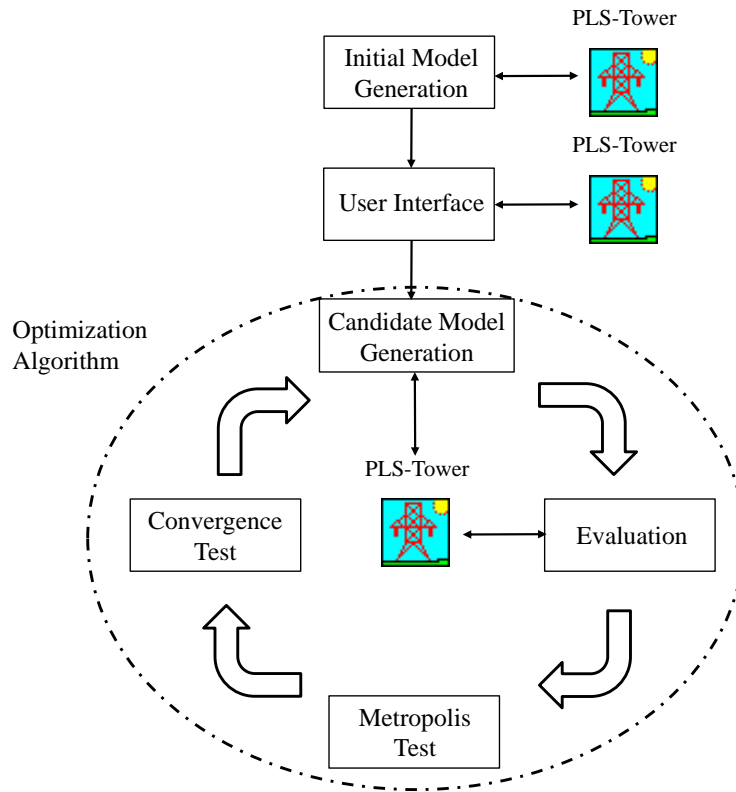


Figure 6.8 Integration of the PLS-Tower and optimization algorithms.

Prior to initiation of an optimum design process with the integrated optimization software, an initial model of the tower with an arbitrary geometry (panel widths) must be formed by the user in PLS-Tower. Due to electrical clearances between conductors and steel members, the tower structures are usually developed with a complex 3D geometry. The PLS-Tower offers unique symmetry features for joint and elements to facilitate a rapid formation of the finite element mesh for the tower. Two types of joints are introduced as either primary or secondary. The primary joints are directly defined with their locations in 3D Cartesian coordinate system. The secondary joints, on the other hand, are specified according to their relative positions with respect to two primary joints. The tower members are generated in the model likewise by specifying their end joints and symmetry conditions. The member properties are assigned next such that for each member, the designer defines eccentricity code, restraint code, unbraced length ratios, connected leg(s) of the member, etc. This is followed by member grouping in

which the individual members are grouped together to have the same angle section due to symmetry, practicality and/or fabrication requirements. For instance, the designer is often required to use the identical angle sections for a number of panels in the leg although the stress levels are lesser in the upper panels. Although it is heavier, the use of identical sections eliminates the need for the splices, which may result in more economical and also convenient designs for manufacturing and erection viewpoints. Once the member groups are introduced, the group properties are specified by indicating material type, group type, element type, etc. for each group. The material type contains information regarding the material properties of steel grades which the group members are manufactured from. The group type indicates structural functions of members in the group, such as leg, redundant, other, etc. On the other hand, element type describes the type of finite element used to model the members in a group, such as beam, truss, etc. Ideally, all members in a tower should be modeled as truss elements in a 3-D truss model, where the joints are idealized as moment-free pins. However, this often gives rise to planar joints and mechanisms at the intersection of members that all lie in one-plane. To surmount this problem, the PLS-Tower offers the use of beam elements with rotational stiffness at the ends. It is a customary practice to model the leg members and struts having intermediate joints between their ends as beam elements, while diagonals and single struts are modeled as truss elements.

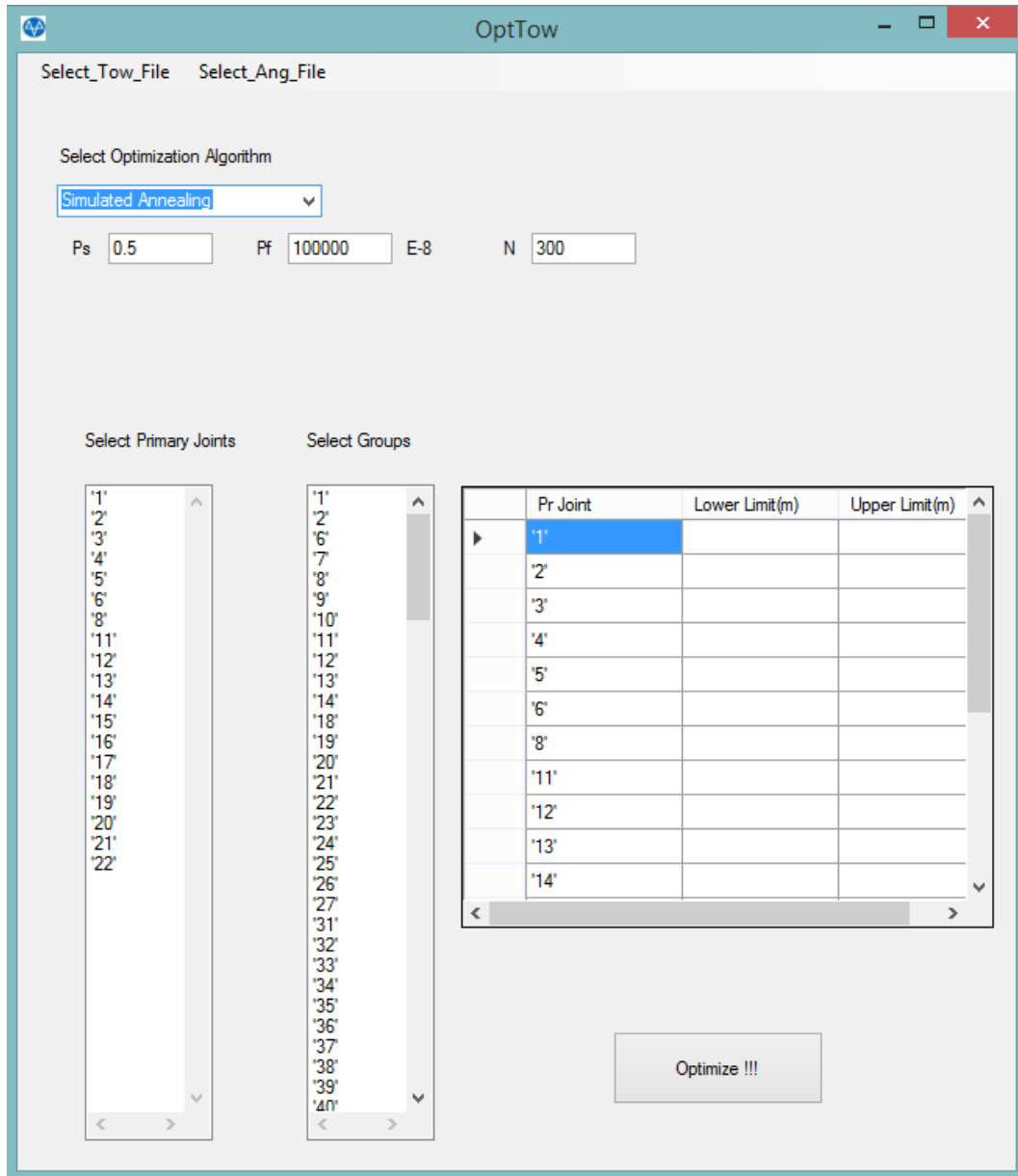


Figure 6.9 The user interface in the integrated optimization software to select the initial PLS-Tower model and angle profile database file.

Once the initial model of the tower is generated in PLS-Tower, the integrated optimization software can be executed. The user interface shown in Figure 6.9 appears on screen and asks the user to select the initial PLS-Tower model and angle profile database file. Then, the initial PLS-Tower input file is searched for primary joints and member group types. This information is reflected in the user interface and listed in two selection windows, as depicted in Figure 6.9. The user

selects the primary joints and member group types to be optimized from these windows. In addition, the upper and lower limits of the primary joint coordinates are also specified in the user-interface. Throughout the optimization, the primary joint coordinates are not allowed to breach these limits.

At each cooling cycle of the optimization algorithm, a number of candidate designs are generated by perturbing design variables in the current solution, as explained in detail in the preceding chapter. Whenever a candidate design is produced, the design variables pertaining to this solution are stored in a vector consisting of primary joint coordinates and index numbers of the angle sections in the profile database selected for member groups. First, the design variables are converted into string format compatible with PLS-Tower. Then, a model-generation module developed in this study scans through the data structure of initial PLS-Tower input file, and it creates a new input file with modified design information, where the primary joint coordinates and selected sections of the member groups are revised according to the candidate design.

In the evaluation stage of this solution, PLS-Tower software is called to run the generated input file of the candidate design on the command line. The results of the analyses include joint displacements and member forces under each load case as well as design checks according to a chosen code of design practice, such as ASCE 10-97 (2000), and they are written into a text file by PLS-Tower. In this text file, a summary of the analyses and design checks are also reported briefly in so-called group summary tables which display the details of member and connection designs only for the most critical member of each group under tension and compression cases separately. The most critical member corresponds to the one that has the largest compression or tension capacity usage amongst all the members in the group considering all the load cases. The displayed information for a critical member of each group consists of assigned angle type (single angle, double angle etc.), assigned angle size, maximum calculated force in the member, member's load capacity, maximum capacity usage, unbraced length ratios of the

member in various axes and their allowable values, number of bolts, hole diameters, connection shear and bearing capacities, etc. The evaluation module developed in this study is automated to retrieve the required values and design checks for each member group from the group summary tables. In addition, the final weight of the resulting tower corresponding to the candidate design is directly extracted from the result file, and the modified (unconstrained) objective function value of the candidate design is calculated using the Eqns. (4.1) through (4.20). In this way the integrated optimization software incessantly enables transfer of the data between the PLS- Tower and optimization algorithm until all the cooling cycles are completed.

CHAPTER 7

NUMERICAL EXAMPLES

The numerical performances of the annealing algorithms discussed in Chapter 5 were investigated on four case studies chosen from the real-world projects. The case studies were selected from suspension and tension towers with different voltage levels commonly utilized for transmission grids as 110 kV, 220 kV and 400 kV. In a transmission line, suspension towers constitute the majority of the line while tension towers are utilized in smaller numbers. However, since the tension towers serve to deviate the line route and also function to prevent mass collapse of the suspension towers, this results in larger design forces and therefore tension tower always have a bigger self-weight compared to suspension towers. The design loads acting on the towers consisted of dead loads of tower, wires (conductors and ground wires) and permanently attached equipment; ice loads on the tower, wires and equipment; wind loads on tower, wires and equipment; loads from wires' tensile forces; erection and maintenance loads; unbalanced loads; and finally failure loads, such as broken wire conditions. In conformity with the original designs of the towers, these loads were calculated and assembled in separate load combinations as per international loading standards, including IEC 60826 (2003) and EN 50341 (2012). In a typical transmission line, for both tension and suspension towers, the critical wind loads were applied to the towers in transverse direction to the line. The wind loads on wires were transmitted to the tower from conductors at the end of the cross-arms and from ground wires at the top of the peak. On the other, the wind load acting on the tower itself should be calculated anew and online for each candidate design sampled in the course of optimization since each candidate design has a different wind area based on cross-sections assigned to member groups in a candidate design.

In each case study considered here, both the annealing algorithm (SA) and its two

phase variant (two-phase SA) developed in this work were employed together to minimize the weight of a lattice tower using three shape variables and a selected number of sizing variables (member groups) in line with the practical design of such structures. The steel sections used for member groups were selected from European angle profile database and the design checks were performed as per ASCE 10-97 (2000) specification. The choice of control parameters in SA algorithm was carried out in line with the recommendations in Hasançebi et al. (2010a), as follows: $P_s = 0.50$, $P_f = 10^{-3}$, $N_c = 300$. This led to the following cooling schedule parameters from Eqn. (5.4): $T_s = 1.4427$, $T_f = 0.1448$ and $\eta = 0.9923$. On the other hand, extensive numerical experimentations were carried out with the two-phase SA to obtain the optimal parameter settings of this algorithm, which would enable it to converge to a reliable solution in a relatively short time. Accordingly, the optimal settings of the control parameters were set as follows: $P_s = 0.50$, $P_f = 10^{-3}$, $N_c = 30$ for phase 1, and $P_s = 0.25$, $P_f = 10^{-4}$, $N_c = 100$ for phase 2.

In each case study, a total of five independent runs were carried out with both SA and two-phase SA algorithms each, considering the stochastic nature of the technique. The numerical performances of the algorithms were reported in terms of the optimized weights of the towers achieved as well as total computing time required for the entire optimization process. It is important to emphasize that all design considerations, such as profile dataset, geometry requirements and loading were kept exactly identical to the design process of the towers in industry practice. Hence, the optimized design weights of the towers were also compared with the results of conventional design process in order to quantify material saving owing to optimization process. In order to achieve an unbiased comparison for execution time of the algorithms, all the optimization runs were carried out with a personal computer having Intel Core i7-4720HQ 2.60 GHz 6 MB L3 processor.

7.1. The 337-Member, 110kV Suspension Tower

The first design example is a 43.5-meter high 110kV suspension tower consisting of 337 members. It is a single circuit tower having a pine-tree type geometry, as shown in Figure 7.1. The electrical phases are held by the three cross-arms in vertical configuration, whereas a single ground wire is placed at the top of the tower. The tower was modeled in PLS-Tower such that it had three primary joints to optimize and 51 member groups, and a total number of 22 load combinations were considered. The steel sections assigned to member groups were selected from a profile database consisting of 67 European equal leg angle profiles in conformity with the original design of the tower in industry practice. Only the steel sections heavier than L50x50x5 were used while sizing the member groups. In addition, the minimum thicknesses of the steel sections assigned to member groups were enforced to be 6 mm for leg members and 5 mm for other members. The steel material quality was assigned as S355JR for all member groups. The configuration of the redundant members as well as their section assignments were carried out the same way as in the original tower design. The wind load applied on the tower structure was calculated per IEC 60826 (2003) and the member groups were sized according to ASCE 10-97 (2000) specification.

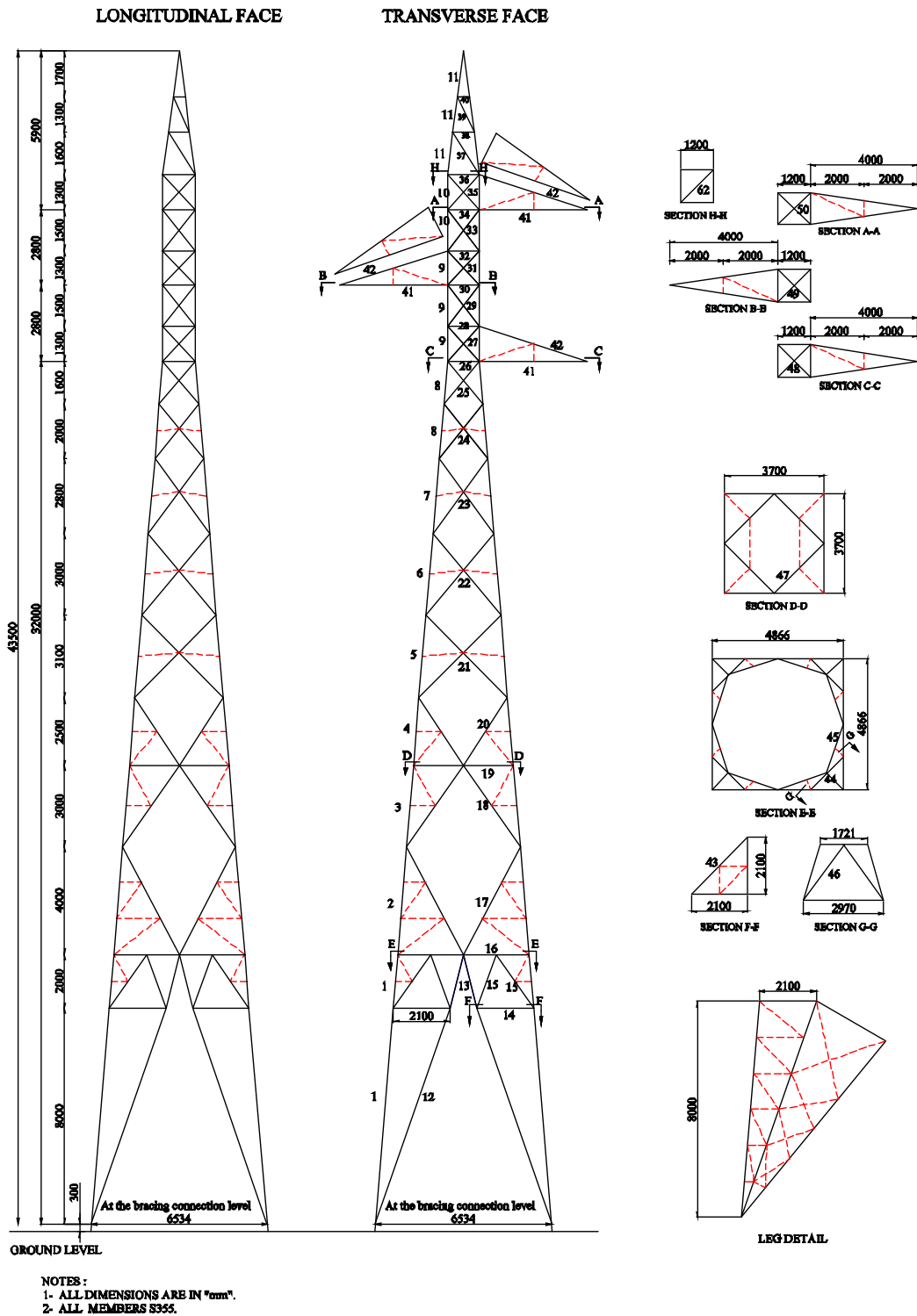


Figure 7.1 The 337-member, 110kV suspension tower (all units are in mm).

The tower was designed using both SA and two-phase SA algorithms by performing five independent runs each by randomizing the initial geometry of the tower. The results were reproduced in Table 7.1 and Table 7.2 in terms of the optimized weight of the tower and computing time in each run of the SA and two-phase SA algorithms, respectively. It can be observed from Table 7.1 that the SA algorithm has yielded optimized weights for the tower between 7235.1-7600.3 kg with a mean of 7373 kg and a standard deviation of 165 kg. The total computing time of the SA algorithm for this example was 445 min on average with a standard deviation of 20 min. On the other hand, the two-phase SA algorithm was implemented in two phases, as shown in Table 7.2. In the first phase the tower weight was quickly dropped to a level between 8964.4 - 8999.5 kg in 20-21 min of computing time. The second phase implemented thereafter resulted in optimized design weights of the tower between 7483.4-7621.6 kg with a mean of 7552 kg and a standard deviation of 59 kg. The overall (phase 1 + phase 2) computing time of the two-phase SA algorithm for this example was 173 min on average with a standard deviation of 9 min. It follows that even though the two-phase SA algorithm results in 2.0% heavier design on average, it achieves a significant reduction in computation time in comparison to the SA algorithm. In Table 7.3, the original design of the tower in conventional industry practice is benchmarked against its optimized design located by both algorithms in their best runs in terms of primary joints (shape variables), section designations assigned to each member group and overall design weights. Considering the fact that the existing tower designed by senior engineers had a design weight of 8262.5 kg, the optimized designs of the tower with SA and two-phase SA algorithms resulted in 12.5% and 9.5% weight reductions, respectively compared to its original design. The best feasible design results obtained from SA and two-phase SA algorithms are figured out in Figure 7.2. Additionally, the analysis models of final best results are shown in Figure 7.3. Since two-phase SA starts with an initially good solution, it starts to generate feasible solutions in first cycles. However; unlike to two-phase SA, SA starts to generate feasible solutions long afterwards due to starting with randomly generated model. Also, if the optimization problem contains lots of

design variables, SA requires much more time to generate the feasible solutions compared to two-phase SA.

Table 7.1 The optimized weight of 110kV suspension tower and computing time in each run of the SA algorithm.

Run#	Optimized Weight (kg)	Time (min)	Mean		Standard Deviation	
			Weight (kg)	Time (min)	Weight (kg)	Time (min)
Run1	7600.3	440				
Run2	7258.6	423				
Run3	7497.3	438	7373	445	165	20
Run4	7275.4	476				
Run5	7235.1	447				

Table 7.2 The optimized weight of 110kV suspension tower and computing time in each run of the two-phase SA algorithm.

Run#	Weight (kg)		Time (min.)			Mean		Standard Deviation	
	Phase 1	Phase 2	Phase 1	Phase 2	Overall Time	Weight (kg)	Overall Time (min)	Weight (kg)	Overall Time (min)
Run1	8999.5	7583.2	22	167	189				
Run2	8994.3	7483.4	20	150	170				
Run3	8979.7	7575.1	21	147	168	7552	173	59	9
Run4	8964.4	7498.5	21	147	168				
Run5	8976.9	7621.6	21	149	170				

Table 7.3 Comparison of the optimized design weights of 110kV suspension tower with its existing design.

Design Variables	Existing Tower	SA Algorithm	Two-phase SA Algorithm
Size Variables (Member Groups)			
G_1	L100*100*10	L100*100*8	L110*110*10
G_2	L100*100*10	L100*100*8	L110*110*8
G_3	L100*100*10	L100*100*8	L110*110*8
G_4	L100*100*8	L100*100*8	L100*100*8
G_5	L100*100*8	L90*90*8	L100*100*8
G_6	L100*100*8	L90*90*8	L100*100*7
G_7	L90*90*8	L90*90*7	L90*90*7
G_8	L90*90*8	L90*90*7	L90*90*7
G_9	L80*80*6	L75*75*6	L70*70*7
G_{10}	L80*80*6	L70*70*5	L70*70*5
G_{11}	L70*70*6	L60*60*5	L60*60*5
G_{12}	L90*90*8	L100*100*6	L100*100*6
G_{13}	L80*80*8	L75*75*6	L80*80*6
G_{14}	L50*50*5	L50*50*5	L50*50*5
G_{15}	L50*50*5	L50*50*5	L50*50*5
G_{16}	L75*75*5	L50*50*5	L50*50*5
G_{17}	L80*80*6	L75*75*6	L75*75*6
G_{18}	L70*70*6	L65*65*5	L65*65*5
G_{19}	L65*65*5	L50*50*5	L50*50*5
G_{20}	L60*60*5	L55*55*5	L55*55*5
G_{21}	L70*70*5	L75*75*5	L70*70*5
G_{22}	L65*65*5	L65*65*5	L65*65*5
G_{23}	L60*60*5	L60*60*5	L60*60*5
G_{24}	L50*50*5	L50*50*5	L50*50*5
G_{25}	L50*50*5	L50*50*5	L50*50*5
G_{26}	L50*50*5	L50*50*5	L50*50*5
G_{27}	L50*50*5	L50*50*5	L50*50*5
G_{28}	L50*50*5	L50*50*5	L50*50*5
G_{29}	L50*50*5	L50*50*5	L50*50*5
G_{30}	L50*50*5	L50*50*5	L50*50*5
G_{31}	L50*50*5	L50*50*5	L50*50*5
G_{32}	L50*50*5	L50*50*5	L50*50*5
G_{33}	L50*50*5	L50*50*5	L50*50*5
G_{34}	L50*50*5	L50*50*5	L50*50*5
G_{35}	L50*50*5	L50*50*5	L50*50*5
G_{36}	L50*50*5	L50*50*5	L50*50*5
G_{37}	L50*50*5	L50*50*5	L50*50*5
G_{38}	L50*50*5	L50*50*5	L50*50*5
G_{39}	L50*50*5	L50*50*5	L50*50*5
G_{40}	L50*50*5	L50*50*5	L50*50*5
G_{41}	L60*60*6	L70*70*5	L70*70*5
G_{42}	L60*60*6	L60*60*5	L60*60*5
G_{43}	L60*60*5	L50*50*5	L50*50*5
G_{44}	L50*50*5	L50*50*5	L50*50*5
G_{45}	L50*50*5	L50*50*5	L50*50*5
G_{46}	L60*60*5	L55*55*5	L55*55*5
G_{47}	L60*60*5	L50*50*5	L50*50*5
G_{48}	L50*50*5	L50*50*5	L50*50*5
G_{49}	L50*50*5	L50*50*5	L50*50*5

Table 7.3 (continued)

Design Variables	Existing Tower	SA Algorithm	Two-phase SA Algorithm
Size Variables (Member Groups)			
G_{50}	L50*50*5	L50*50*5	L50*50*5
G_{51}	L50*50*5	L50*50*5	L50*50*5
Shape Variables (m)			
$x_1 = y_1$	3.27	3.45	3.02
$x_2 = y_2$	0.60	0.50	0.52
$x_3 = y_3$	0.60	0.50	0.50
Weight (kg)	8262.5	7235.1	7483.4

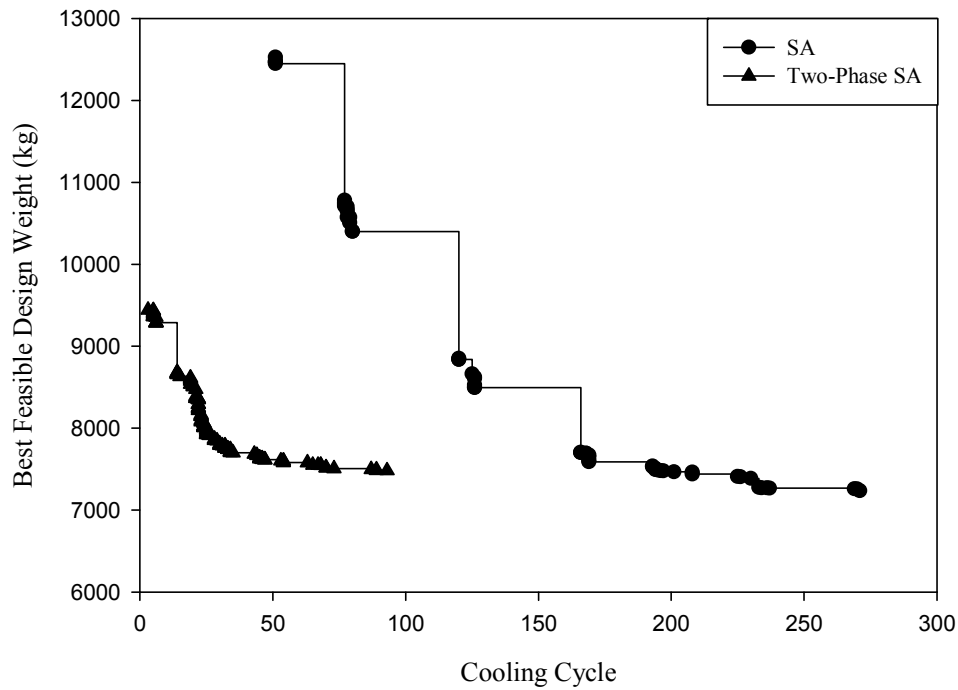
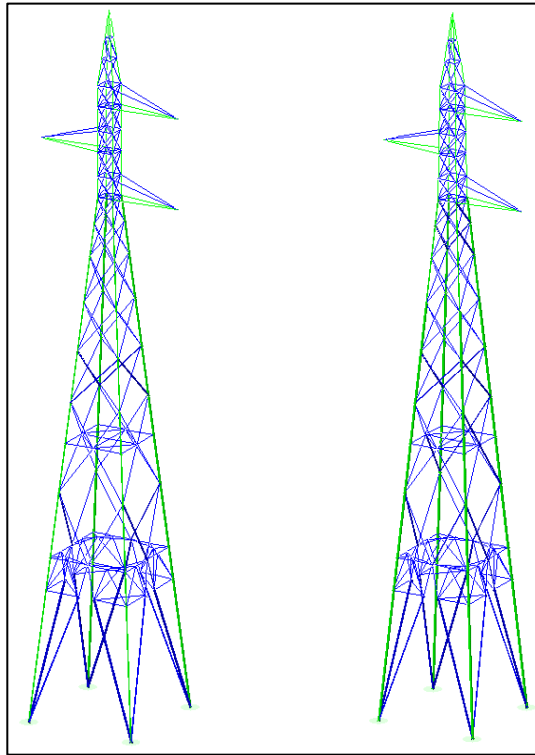


Figure 7.2 Best feasible design weights obtained from SA and two-phase SA for 110 kV suspension tower.



a) SA result b) Two-phase SA result

Figure 7.3 Final best feasible towers obtained from SA and two-phase SA for 110kV suspension tower.

7.2. The 438-Member, 110kV Tension (Angle) Tower

The second design example is a 43.9-meter high 110kV tension tower consisting of 438 members. It is a single circuit tower having a pine-tree type geometry, as shown in Figure 7.4. The electrical phases are held by the three cross-arms in vertical configuration, whereas a single ground wire is placed at the top of the tower. The tower was modeled in PLS-Tower such that it had three primary joints to optimize and 64 member groups, and a total number of 49 load combinations were considered. The steel sections assigned to member groups were selected from a profile database consisting of 67 European equal leg angle profiles in conformity with the original design of the tower in industry practice. Only the steel sections heavier than L50x50x5 were used while sizing the member groups. In addition, the minimum thicknesses of the steel sections assigned to member groups were enforced to be 6 mm for leg members and 5 mm for other members. The steel material quality was assigned as S355JR for all member groups. The configuration of the redundant members as well as their section assignments were carried out the same way as in the original tower design. The wind load applied on the tower structure was calculated per IEC 60826 (2003) and the member groups were sized according to ASCE 10-97 (2000) specification.

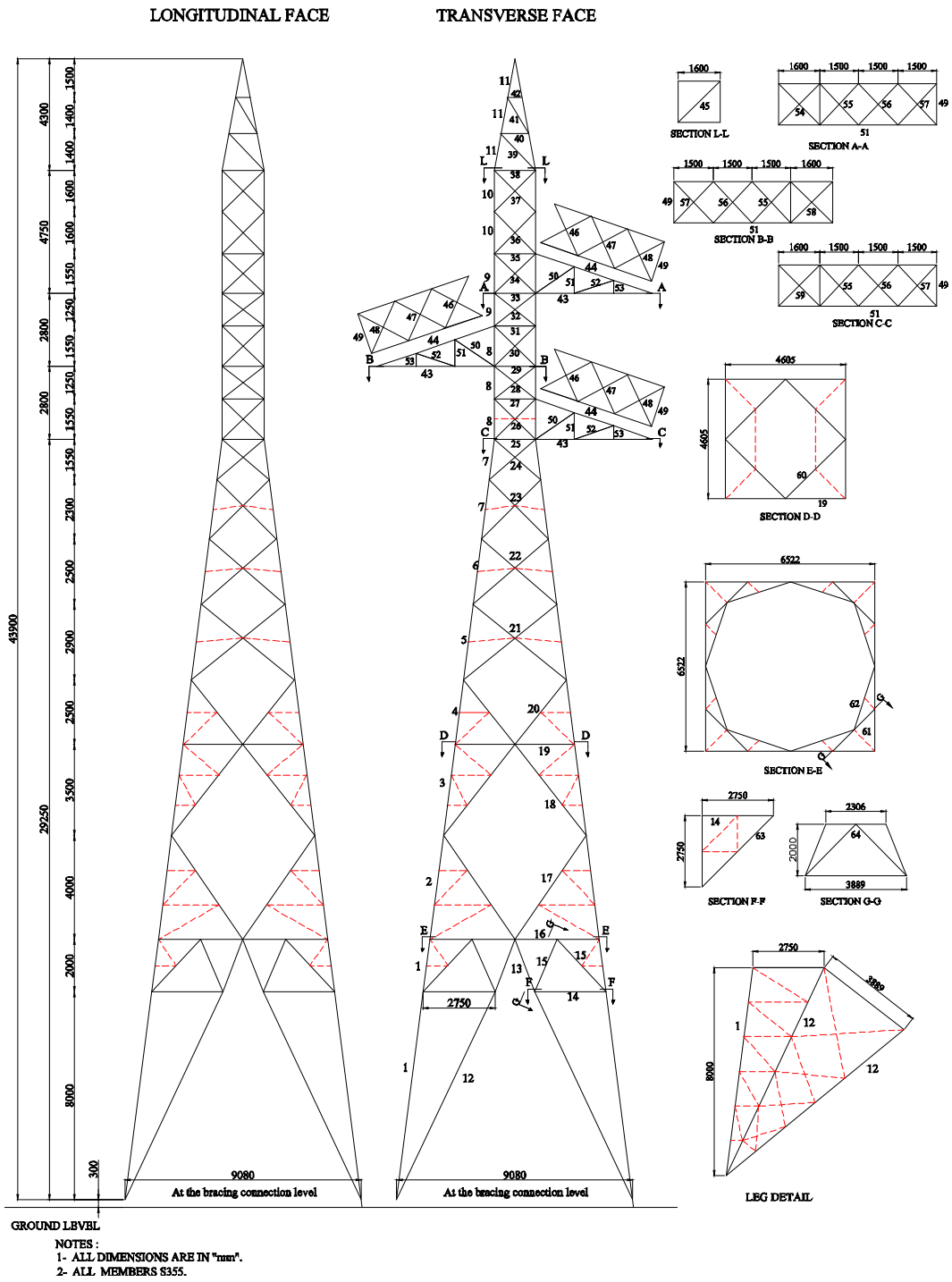


Figure 7.4 The 438-member, 110kV tension (angle) tower (all units are in mm).

Again this tower was designed using both SA and two-phase SA algorithms by performing five independent runs each by randomizing the initial geometry of the tower. The results were reproduced in Table 7.4 and Table 7.5 in terms of the optimized weight of the tower and computing time in each run of the SA and two-phase SA algorithms, respectively. It can be observed from Table 7.4 that the SA algorithm has yielded optimized weights for the tower between 11835.1-12537.2 kg with a mean of 12193 kg and a standard deviation of 280 kg. The total computing time of the SA algorithm for this example was 843 min on average with a standard deviation of 26 min. On the other hand, the two-phase SA algorithm was implemented in two phases, as shown in Table 7.5. In the first phase the tower weight was quickly dropped to a level between 14504.6-15015.1 kg in 37-42 min of computing time. The second phase implemented thereafter resulted in optimized design weights of the tower between 11801.3-12916.7 kg with a mean of 12120 kg and a standard deviation of 458 kg. The overall (phase 1 + phase 2) computing time of the two-phase SA algorithm for this example was 319 min on average with a standard deviation of 13 min. Although the two-phase SA exhibited a comparable performance with respect to that of the SA, it achieved a significant reduction in computation time. In Table 7.6, the original design of the tower in conventional industry practice is benchmarked against its optimized design located by both algorithms in their best runs in terms of primary joints (shape variables), section designations assigned to each member group and overall design weights. Considering the fact that the existing tower designed by senior engineers had a design weight of 13207.1 kg, the optimized designs of the tower with SA and two-phase SA algorithms resulted in 7.7% and 8.2% weight reductions, respectively compared to its original design. The best feasible design results obtained from SA and two-phase SA algorithms are figured out in Figure 7.5. Additionally, the analysis models of final best results are shown in Figure 7.6. Since two-phase SA starts with an initially good solution, it starts to generate feasible solutions in first cycles. However; unlike to two-phase SA, SA starts to generate feasible solutions long afterwards due to starting with randomly generated model. Also, if the optimization problem contains lots of design

variables, SA requires much more time to generate the feasible solutions compared to two-phase SA.

Table 7.4 The optimized weight of 110kV tension (angle) tower and computing time in each run of the SA algorithm.

Run#	Optimized Weight (kg)	Time (min)	Mean		Standard Deviation	
			Weight (kg)	Time (min)	Weight (kg)	Time (min)
Run1	12044.8	845				
Run2	12149.0	814				
Run3	12399.1	885	12193	843	280	26
Run4	12537.2	838				
Run5	11835.1	834				

Table 7.5 The optimized weight of 110kV tension (angle) tower and computing time in each run of the two-phase SA algorithm.

Run#	Weight (kg)		Time (min.)			Mean	Standard Deviation		
	Phase 1	Phase 2	Phase 1	Phase 2	Overall Time	Weight (kg)	Overall Time (min)	Weight (kg)	Overall Time (min)
Run1	14507.5	12916.7	38	275	313				
Run2	14456.9	11801.3	37	304	341				
Run3	14504.6	11827.1	42	270	312	12120	319	458	13
Run4	15015.1	12055.1	37	273	310				
Run5	14361.1	11999.5	38	281	319				

Table 7.6 Comparison of the optimized design weights of 110kV tension (angle) tower with its existing design

Design Variables	Existing Tower	SA Algorithm	Two-Phase SA Algorithm
Size variables (Member Groups)			
G_1	L150*150*12	L150*150*12	L150*150*12
G_2	L150*150*12	L140*140*12	L140*140*12
G_3	L150*150*12	L140*140*12	L140*140*12
G_4	L150*150*12	L140*140*12	L140*140*12
G_5	L150*150*12	L140*140*12	L140*140*12
G_6	L150*150*12	L140*140*12	L140*140*12
G_7	L150*150*12	L140*140*12	L140*140*12
G_8	L130*130*10	L110*110*10	L100*100*12
G_9	L130*130*10	L100*100*8	L100*100*8
G_{10}	L130*130*10	L100*100*7	L100*100*6
G_{11}	L80*80*6	L75*75*6	L75*75*6
G_{12}	L100*100*6	L100*100*6	L100*100*6
G_{13}	L80*80*6	L80*80*6	L80*80*6
G_{14}	L70*70*5	L50*50*5	L50*50*5
G_{15}	L60*60*5	L50*50*5	L50*50*5
G_{16}	L65*65*5	L50*50*5	L50*50*5
G_{17}	L90*90*6	L80*80*6	L80*80*6
G_{18}	L90*90*6	L90*90*6	L90*90*6
G_{19}	L65*65*5	L60*60*5	L60*60*5
G_{20}	L80*80*6	L70*70*5	L70*70*5
G_{21}	L80*80*6	L75*75*5	L75*75*5
G_{22}	L80*80*6	L70*70*5	L70*70*5
G_{23}	L80*80*6	L70*70*5	L70*70*5
G_{24}	L70*70*5	L60*60*5	L60*60*5
G_{25}	L70*70*5	L60*60*5	L70*70*5
G_{26}	L80*80*6	L75*75*8	L75*75*6
G_{27}	L70*70*5	L65*65*7	L65*65*5
G_{28}	L60*60*5	L55*55*5	L50*50*6
G_{29}	L60*60*5	L55*55*5	L55*55*5
G_{30}	L80*80*6	L65*65*5	L60*60*5
G_{31}	L60*60*5	L60*60*5	L55*55*5
G_{32}	L60*60*5	L60*60*5	L60*60*5
G_{33}	L60*60*5	L55*55*5	L55*55*6
G_{34}	L80*80*6	L60*60*5	L55*55*5
G_{35}	L60*60*5	L50*50*5	L50*50*5
G_{36}	L50*50*5	L50*50*5	L50*50*5
G_{37}	L50*50*5	L50*50*5	L50*50*5
G_{38}	L50*50*5	L50*50*5	L50*50*5
G_{39}	L50*50*5	L50*50*5	L50*50*5
G_{40}	L50*50*5	L50*50*5	L50*50*5
G_{41}	L50*50*5	L50*50*5	L50*50*5
G_{42}	L50*50*5	L50*50*5	L50*50*5
G_{43}	L90*90*6	L90*90*6	L90*90*6
G_{44}	L80*80*6	L75*75*6	L75*75*6
G_{45}	L50*50*5	L50*50*5	L50*50*5
G_{46}	L50*50*5	L50*50*5	L50*50*5
G_{47}	L50*50*5	L50*50*5	L50*50*5
G_{48}	L50*50*5	L50*50*5	L50*50*5
G_{49}	L50*50*5	L50*50*5	L50*50*5

Table 7.6 (continued)

Design Variables	Existing Tower	SA Algorithm	Two-Phase SA Algorithm
Size variables (Member Groups)			
G_{50}	L50*50*5	L50*50*5	L50*50*5
G_{51}	L50*50*5	L50*50*5	L50*50*5
G_{52}	L50*50*5	L50*50*5	L50*50*5
G_{53}	L50*50*5	L50*50*5	L50*50*5
G_{54}	L50*50*5	L50*50*5	L50*50*5
G_{55}	L50*50*5	L50*50*5	L50*50*5
G_{56}	L50*50*5	L50*50*5	L50*50*5
G_{57}	L50*50*5	L50*50*5	L50*50*5
G_{58}	L50*50*5	L50*50*5	L50*50*6
G_{59}	L50*50*5	L50*50*5	L50*50*5
G_{60}	L70*70*5	L50*50*5	L50*50*5
G_{61}	L50*50*5	L50*50*5	L50*50*6
G_{62}	L60*60*5	L50*50*5	L50*50*5
G_{63}	L70*70*5	L50*50*5	L50*50*5
G_{64}	L60*60*5	L60*60*5	L60*60*5
Shape variables (m)			
$x_1 = y_1$	4.54	4.25	4.25
$x_2 = y_2$	0.80	0.81	0.80
$x_3 = y_3$	0.80	0.70	0.75
Weight (kg)	13207.1 kg	11835.1 kg	11801.3 kg

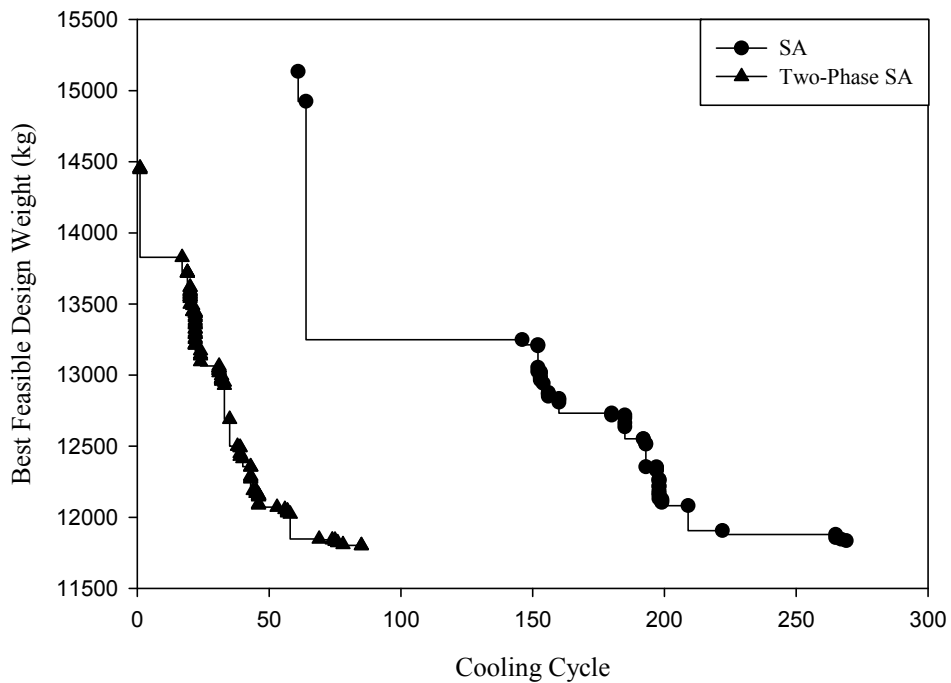
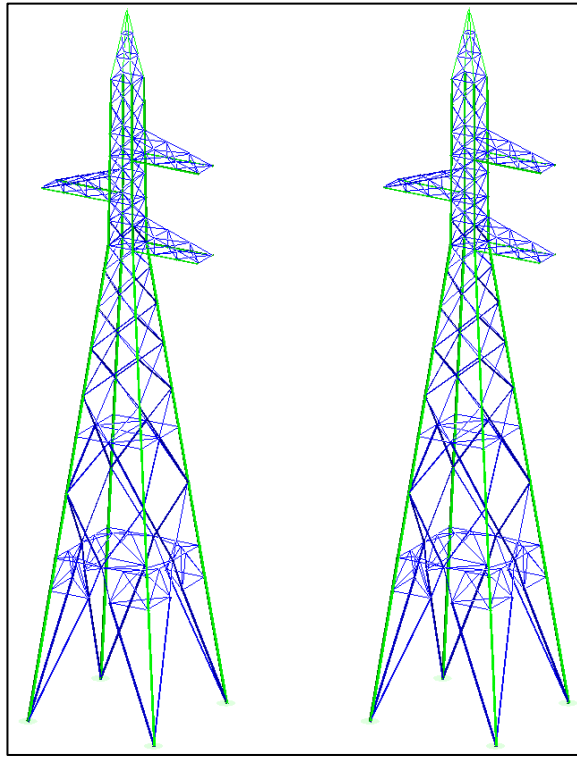


Figure 7.5 Best feasible design weights obtained from SA and two-phase SA for 110 kV tension tower.



a) SA result b) Two-phase SA result

Figure 7.6 Final best feasible towers obtained from SA and two-phase SA for 110kV tension tower.

7.3. The 397-Member, 220kV Suspension Tower

The third design example is a 220kV suspension tower (Figure 7.7) made up of 397 members. It is a 31.5-meter high, double circuit tower having lattice-mast type geometry with two earth-wire peaks to carry the earthing and optical communication wires. The tower was initially intended to be designed as a tubular tower due to landing obstructions, but later was converted into lattice mast type due to economical considerations. While modeling the tower in PLS-TOWER, three primary joints were considered and the 397 members of the tower were grouped into 58 sizing variables (member groups). The tower was subjected to a total number of 11 load combinations, and the member groups were sized according to ASCE 10-97 (2000) specification. The wind loading on the tower were considered as per “SAPS”, which is a wind load calculation procedure ignoring the shielding effect of members on each other. The steel sections assigned to member groups were selected from a profile database consisting of 73 European equal leg angle profiles. The thickness and size limitations imposed in the original design of the tower were also observed here to perform an unbiased comparison with the industry practice. Accordingly, the minimum thicknesses of the steel sections assigned to member groups were selected as 6 mm for leg members and 4 mm for other members. The minimum sections assigned to member groups were not allowed to be lighter than L65x65x6 for leg members and L45x45x4 for other members. No redundant member was utilized for this tower. All members were selected to be A572-Gr50 steel grade.

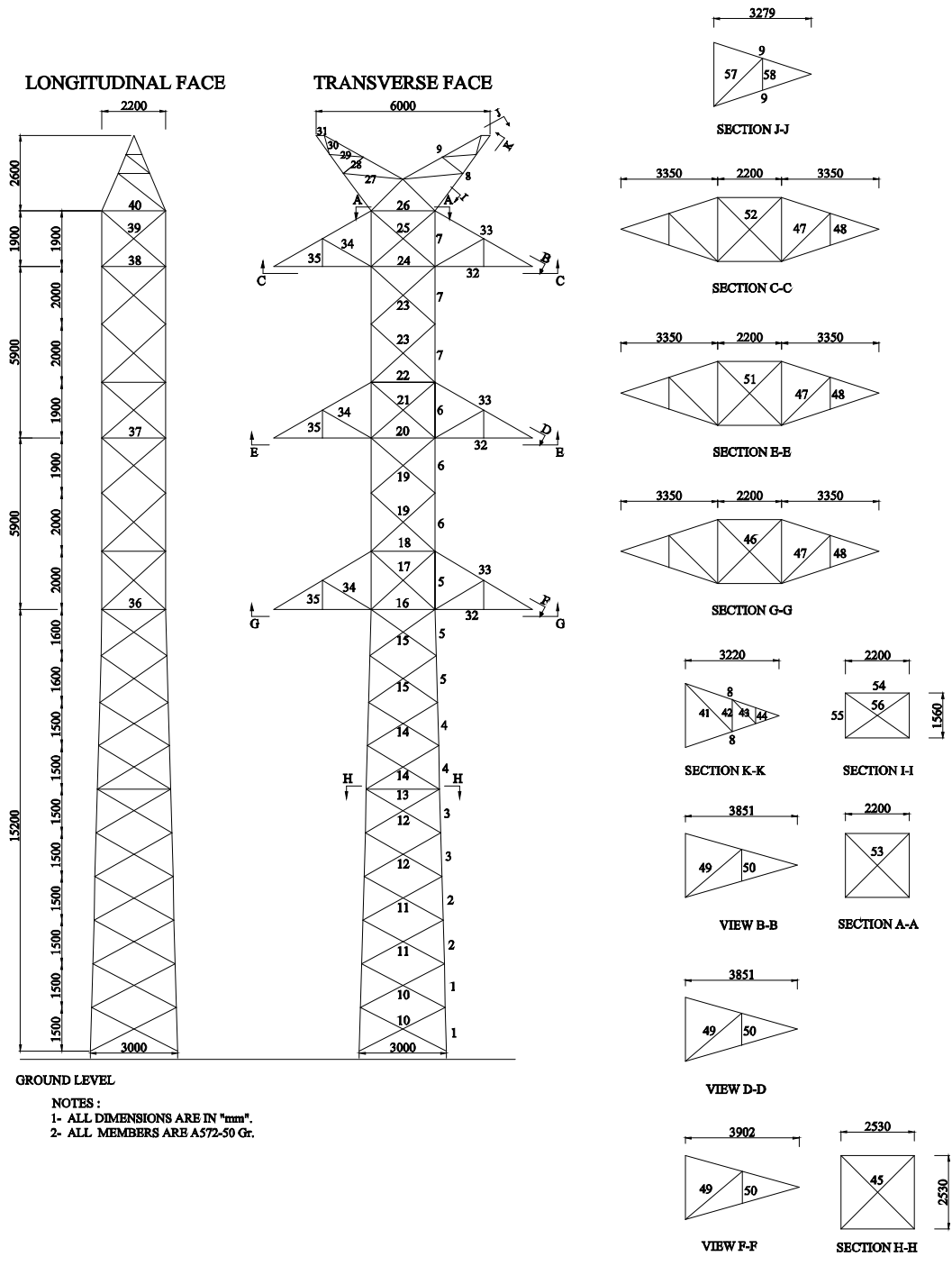


Figure 7.7 The 397-member, 220kV suspension tower (all units are in mm).

The tower was designed using both the SA and two-phase SA algorithms by performing five independent runs each. Table 7.7 and Table 7.8 display the results of the runs in terms of the optimized weight of the tower and computing time in each run of the SA and two-phase SA algorithms, respectively. It can be seen from Table 7.6 that the SA algorithm produced optimized weights for the tower between 4649.4-4845.0 kg with a mean of 4754 kg and a standard deviation of 89 kg. The total computing time of the SA algorithm for this example was 549 min on average with a standard deviation of 30 min. On the other hand, the two-phase SA algorithm was implemented in two phases, as shown in Table 5. In the first phase the tower weight was quickly dropped to a level between 5322.2-5357.8 kg in 20-22 min of computing time. The second phase implemented thereafter yielded optimized design weights of the tower between 4673.5 - 4742.3 kg with a mean of 4701 kg and a standard deviation of 26 kg. The overall (phase 1 + phase 2) computing time of the two-phase SA algorithm for this example was 177 min on average with a standard deviation of 5 min. For this example, the average performance of two-phase SA algorithm was slightly better than that of the SA algorithm, even though the former located the optimum approximately three times faster. In Table 7.9, the original design of the tower in conventional industry practice is benchmarked against its optimized design located by both algorithms in their best runs. Considering the fact that the weight of the existing tower was 6346 kg, the optimized designs of the tower with the SA and two-phase SA algorithms resulted in 26.7% and 26.4% weight reductions, respectively compared to its original design. The best feasible design results obtained from SA and two-phase SA algorithms are figured out in Figure 7.8. Additionally, the analysis models of final best results are shown in Figure 7.9. Since two-phase SA starts with an initially good solution, it starts to generate feasible solutions in first cycles. However; unlike to two-phase SA, SA starts to generate feasible solutions long afterwards due to starting with randomly generated model. Also, if the optimization problem contains lots of design variables, SA requires much more time to generate the feasible solutions compared to two-phase SA.

Table 7.7 The optimized weight of 220kV suspension tower and computing time in each run of the SA algorithm.

Run#	Optimized Weight (kg)	Time (min)	Mean		Standard Deviation	
			Weight (kg)	Time (min)	Weight (kg)	Time (min)
Run1	4778.4	569				
Run2	4649.4	565				
Run3	4672.2	574	4754	549	89	30
Run4	4824.6	527				
Run5	4845.0	507				

Table 7.8 The optimized weight of 220kV suspension tower and computing time in each run of the two-phase SA algorithm.

Run#	Weight (kg)		Time (min.)		Overall Time	Mean		Standard Deviation	
	Phase 1	Phase 2	Phase 1	Phase 2		Weight (kg)	Overall Time (min)	Weight (kg)	Overall Time (min)
Run1	5335.7	4695.5	21	153	174				
Run2	5322.2	4673.5	21	150	171				
Run3	5354.1	4742.3	21	160	181	4701	177	26	5
Run4	5333.8	4704.3	21	158	179				
Run5	5357.8	4688.3	21	160	181				

Table 7.9 Comparison of the optimized design weights of 220kV suspension tower with its existing design.

Design Variables	Existing Tower	SA Algorithm	Two-phase SA Algorithm
Size Variables (Member Groups)			
G_1	L120*120*12	L130*130*10	L110*110*12
G_2	L120*120*12	L130*130*10	L110*110*11
G_3	L120*120*10	L120*120*10	L110*110*10
G_4	L120*120*10	L120*120*8	L110*110*8
G_5	L100*100*10	L110*110*8	L100*100*8
G_6	L100*100*8	L100*100*6	L90*90*8
G_7	L75*75*6	L75*75*5	L70*70*6
G_8	L65*65*6	L50*50*4	L50*50*4
G_9	L65*65*6	L45*45*4	L45*45*4
G_{10}	L60*60*5	L55*55*4	L55*55*4
G_{11}	L60*60*5	L55*55*4	L55*55*4
G_{12}	L60*60*5	L55*55*4	L55*55*4
G_{13}	L75*75*5	L60*60*4	L60*60*4
G_{14}	L65*65*5	L60*60*4	L60*60*4
G_{15}	L75*75*5	L60*60*4	L60*60*4
G_{16}	L65*65*5	L60*60*4	L55*55*4
G_{17}	L60*60*5	L55*55*4	L55*55*4
G_{18}	L60*60*5	L55*55*4	L55*55*4
G_{19}	L65*65*5	L55*55*4	L55*55*4
G_{20}	L65*65*5	L60*60*4	L55*55*4
G_{21}	L65*65*5	L55*55*4	L55*55*4
G_{22}	L60*60*5	L55*55*4	L55*55*4
G_{23}	L65*65*5	L55*55*4	L55*55*4
G_{24}	L65*65*5	L60*60*4	L55*55*4
G_{25}	L50*50*4	L50*50*4	L50*50*4
G_{26}	L60*60*5	L55*55*4	L55*55*4
G_{27}	L60*60*5	L55*55*4	L55*55*4
G_{28}	L45*45*4	L45*45*4	L45*45*4
G_{29}	L50*50*4	L45*45*4	L45*45*4
G_{30}	L45*45*4	L45*45*4	L45*45*4
G_{31}	L120*120*8	L45*45*4	L45*45*4
G_{32}	L65*65*6	L65*65*5	L65*65*4
G_{33}	L65*65*6	L55*55*4	L60*60*4
G_{34}	L60*60*4	L55*55*4	L55*55*4
G_{35}	L45*45*4	L45*45*4	L45*45*4
G_{36}	L65*65*5	L55*55*4	L55*55*4
G_{37}	L65*65*5	L55*55*4	L55*55*4
G_{38}	L65*65*5	L55*55*4	L55*55*4
G_{39}	L50*50*4	L45*45*4	L45*45*4
G_{40}	L60*60*5	L55*55*4	L55*55*4
G_{41}	L60*60*4	L60*60*4	L60*60*4
G_{42}	L50*50*4	L45*45*4	L45*45*4
G_{43}	L45*45*4	L45*45*4	L45*45*4
G_{44}	L45*45*4	L45*45*4	L45*45*4
G_{45}	L75*75*5	L45*45*4	L45*45*4
G_{46}	L70*70*5	L45*45*4	L45*45*4
G_{47}	L60*60*6	L60*60*4	L60*60*4
G_{48}	L50*50*4	L45*45*4	L45*45*4

Table 7.9 (continued)

Design Variables	Existing Tower	SA Algorithm	Two-phase SA Algorithm
Size Variables (Member Groups)			
G_{49}	L60*60*6	L65*65*4	L65*65*4
G_{50}	L50*50*4	L45*45*4	L45*45*4
G_{51}	L70*70*5	L45*45*4	L45*45*4
G_{52}	L70*70*5	L45*45*4	L45*45*4
G_{53}	L70*70*5	L45*45*4	L45*45*4
G_{54}	L100*100*6	L60*60*4	L60*60*4
G_{55}	L60*60*4	L45*45*4	L45*45*4
G_{56}	L50*50*4	L45*45*4	L45*45*4
G_{57}	L60*60*6	L60*60*4	L60*60*4
G_{58}	L45*45*4	L45*45*4	L45*45*4
Shape Variables (m)			
$x_1 = y_1$	1.50	1.24	1.37
$x_2 = y_2$	1.10	1.00	1.05
$x_3 = y_3$	1.10	1.00	1.04
Weight (kg)	6346.1	4649.4	4673.5

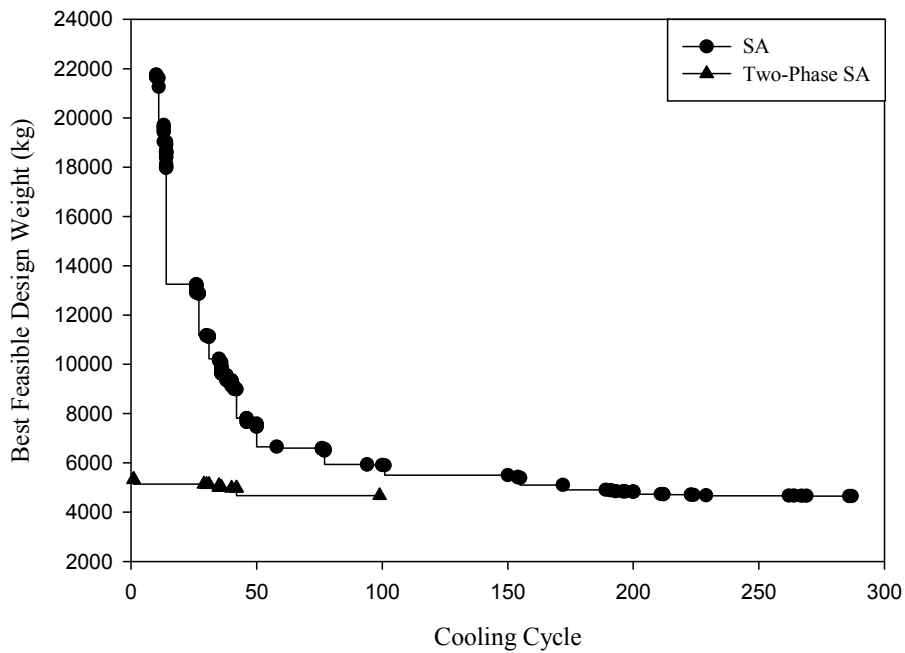
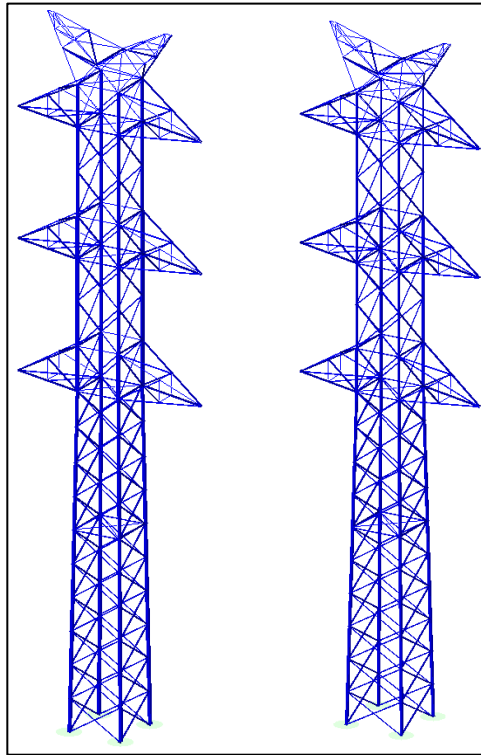


Figure 7.8 Best feasible design weights obtained from SA and two-phase SA for 220 kV suspension tower.



a) SA result b) Two-phase SA result

Figure 7.9 Final best feasible towers obtained from SA and two-phase SA for 220kV suspension tower.

7.4. The 693-Member, 400kV Suspension Tower

The fourth and last example is an 80.4-meter high, 400kV suspension tower consisting of 693 members. The tower was designed to carry double circuits and has a pine-tree type geometry with two earth-wire peaks, as shown in Figure 7.10. Similar to the first and second design examples, three primary joints were defined to modify geometry of the tower for shape optimization, and the 693 members were grouped into 96 sizing variables (member groups). A total number of 44 load combinations were considered in accordance with EN 50341(2012), and the member groups were sized according to ASCE 10-97 (2000) specification. The steel sections assigned to member groups were selected from a profile database incorporating 72 European angle profiles. The minimum thicknesses of the steel sections assigned to member groups were determined as 6 mm for leg members and 5 mm for other members. Additionally, the minimum sections assigned to member groups were not allowed to be lighter than L60x60x6 for leg members and L45x45x5 for other members. The steel material quality was assigned as S355JR for all members. The configuration of the redundant members as well as their section assignments were carried out the same way as in the original tower design.

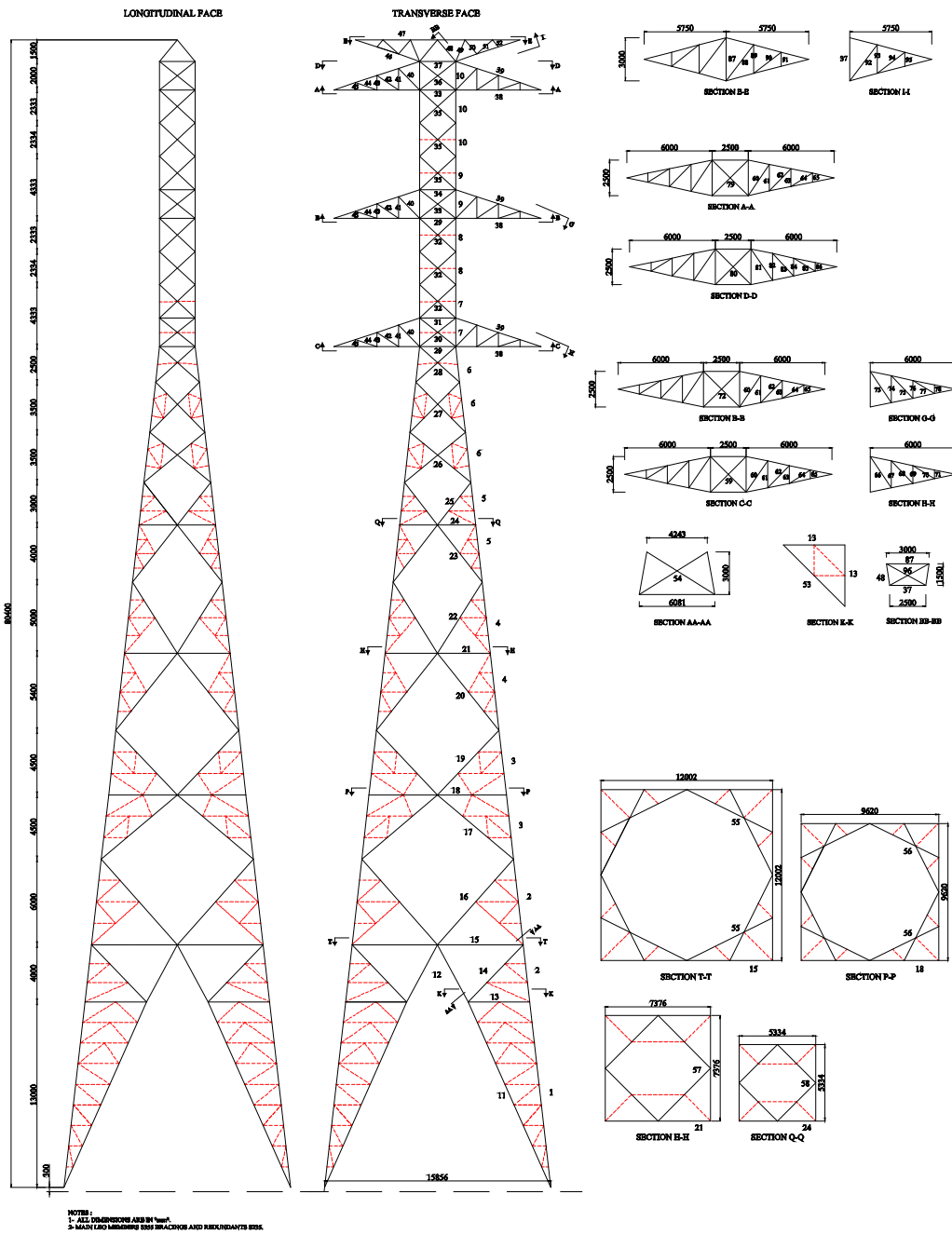


Figure 7.10 The 693-member, 400kV suspension tower (all units are in mm).

The tower was designed using both the SA and two-phase SA algorithms by performing five independent runs each. The results of the runs were displayed in Table 7.10 and Table 7.11 in terms of the optimized weight of the tower and computing time in each run of the SA and two-phase SA algorithms, respectively. It can be seen from Table 7.10 that the SA algorithm produced optimized weights for the tower between 30030.2 - 30701.4 kg with a mean of 30306 kg and a standard deviation of 276 kg. The total computing time of the SA algorithm for this example was 1678 min on average with a standard deviation of 39 min. On the other hand, the two-phase SA algorithm was implemented in two phases, as shown in Table 7.11. In the first phase the tower weight was quickly dropped to a level between 37842.8-38411.8 kg in 58-59 min of computing time. The second phase implemented thereafter yielded optimized design weights of the tower between 30250.1-30646.8 kg with a mean of 30381 kg and a standard deviation of 185 kg. The overall (phase 1 + phase 2) computing time of the two-phase SA algorithm for this example was 609 min on average with a standard deviation of 7 min. Although the two-phase SA exhibited a comparable performance with respect to that of the SA, it achieved a significant reduction in computation time. In Table 7.12, the original design of the tower in conventional industry practice is benchmarked against its optimized design located by both algorithms in their best runs. Considering the fact that the weight of the existing tower was 33561.6 kg, the optimized designs of the tower with the SA and two-phase SA algorithms resulted in 10.8 % and 10.2% weight reductions, respectively compared to its original design. The best feasible design results obtained from SA and two-phase SA algorithms are figured out in Figure 7.11. Additionally, the analysis models of final best results are shown in Figure 7.12. Since two-phase SA starts with an initially good solution, it starts to generate feasible solutions in first cycles. However; unlike to two-phase SA, SA starts to generate feasible solutions long afterwards due to starting with randomly generated model. Also, if the optimization problem contains lots of design variables, SA requires much more time to generate the feasible solutions compared to two-phase SA.

Table 7.10 The optimized weight of 400kV suspension tower and computing time in each run of the SA algorithm.

Run#	Optimized Weight (kg)	Time (min)	Mean		Standard Deviation	
			Weight (kg)	Time (min)	Weight (kg)	Time (min)
Run1	30436.6	1739				
Run2	30030.2	1657				
Run3	30074.2	1652	30306	1678	276	39
Run4	30288.8	1648				
Run5	30701.4	1692				

Table 7.11 The optimized weight of 400kV suspension tower and computing time in each run of the two-phase SA algorithm.

Run#	Weight (kg)		Time (min.)		Overall Time	Mean		Standard Deviation	
	Phase 1	Phase 2	Phase 1	Phase 2		Weight (kg)	Overall Time (min)	Weight (kg)	Overall Time (min)
Run1	38367.4	30257.5	59	545	604				
Run2	37947.4	30646.8	59	553	612				
Run3	38015.2	30250.1	59	542	601	30381	609	185	7
Run4	37842.8	30503.0	58	551	609				
Run5	38411.8	30245.2	58	560	618				

Table 7.12 Comparison of the optimized design weights of 400kV suspension tower with its existing design.

Design Variables	Existing Tower	SA Algorithm	Two-phase SA Algorithm
Size Variables (Member Groups)			
G_1	L160*160*18	L160*160*15	L160*160*15
G_2	L160*160*16	L160*160*15	L160*160*15
G_3	L150*150*16	L160*160*15	L160*160*15
G_4	L150*150*15	L150*150*14	L140*140*15
G_5	L140*140*14	L150*150*14	L140*140*15
G_6	L140*140*14	L150*150*14	L140*140*15
G_7	L130*130*12	L140*140*12	L130*130*12
G_8	L130*130*12	L120*120*12	L130*130*10
G_9	L110*110*8	L120*120*8	L120*120*8
G_{10}	L100*100*6	L100*100*7	L100*100*7
G_{11}	L100*100*6	L100*100*6	L100*100*6
G_{12}	L100*100*10	L130*130*10	L130*130*10
G_{13}	L60*60*5	L50*50*5	L50*50*5
G_{14}	L90*90*6	L90*90*6	L90*90*6
G_{15}	L100*100*6	L70*70*5	L70*70*5
G_{16}	L130*130*8	L130*130*8	L130*130*10
G_{17}	L120*120*8	L110*110*8	L110*110*8
G_{18}	L80*80*6	L70*70*5	L70*70*5
G_{19}	L100*100*8	L100*100*6	L100*100*6
G_{20}	L120*120*10	L110*110*8	L110*110*8
G_{21}	L90*90*6	L55*55*5	L55*55*5
G_{22}	L100*100*6	L100*100*7	L100*100*7
G_{23}	L90*90*7	L100*100*6	L90*90*6
G_{24}	L70*70*5	L60*60*5	L60*60*5
G_{25}	L80*80*6	L75*75*6	L75*75*6
G_{26}	L100*100*7	L100*100*6	L100*100*6
G_{27}	L100*100*7	L100*100*6	L100*100*6
G_{28}	L100*100*6	L90*90*6	L90*90*6
G_{29}	L100*100*6	L90*90*6	L90*90*6
G_{30}	L90*90*6	L80*80*6	L100*100*7
G_{31}	L90*90*6	L80*80*6	L90*90*6
G_{32}	L75*75*6	L75*75*6	L75*75*5
G_{33}	L70*70*5	L70*70*5	L65*65*5
G_{34}	L70*70*5	L65*65*5	L65*65*5
G_{35}	L65*65*5	L65*65*5	L65*65*5
G_{36}	L70*70*5	L70*70*5	L70*70*5
G_{37}	L65*65*5	L55*55*5	L55*55*5
G_{38}	L75*75*6	L75*75*6	L75*75*6
G_{39}	L60*60*6	L45*45*5	L45*45*5
G_{40}	L45*45*5	L50*50*5	L45*45*5
G_{41}	L45*45*5	L45*45*5	L45*45*5
G_{42}	L45*45*5	L45*45*5	L45*45*5
G_{43}	L45*45*5	L45*45*5	L45*45*5
G_{44}	L45*45*5	L45*45*5	L45*45*5
G_{45}	L45*45*5	L45*45*5	L45*45*5
G_{46}	L60*60*6	L60*60*5	L60*60*5
G_{47}	L60*60*6	L55*55*5	L55*55*5
G_{48}	L60*60*5	L50*50*5	L50*50*5
G_{49}	L45*45*5	L45*45*5	L45*45*5

Table 7.12 (continued)

Design Variables	Existing Tower	SA Algorithm	Two-phase SA Algorithm
Size Variables (Member Groups)			
G_{50}	L45*45*5	L45*45*5	L45*45*5
G_{51}	L45*45*5	L45*45*5	L45*45*5
G_{52}	L45*45*5	L45*45*5	L45*45*5
G_{53}	L70*70*5	L60*60*5	L60*60*5
G_{54}	L75*75*5	L70*70*5	L70*70*5
G_{55}	L90*90*6	L80*80*6	L80*80*6
G_{56}	L90*90*6	L80*80*6	L80*80*6
G_{57}	L90*90*6	L60*60*5	L65*65*5
G_{58}	L80*80*6	L70*70*5	L70*70*5
G_{59}	L60*60*5	L45*45*5	L45*45*5
G_{60}	L55*55*5	L50*50*5	L50*50*5
G_{61}	L50*50*5	L45*45*5	L45*45*5
G_{62}	L50*50*5	L45*45*5	L45*45*5
G_{63}	L45*45*5	L45*45*5	L45*45*5
G_{64}	L45*45*5	L45*45*5	L45*45*5
G_{65}	L45*45*5	L45*45*5	L45*45*5
G_{66}	L55*55*5	L50*50*5	L50*50*5
G_{67}	L50*50*5	L45*45*5	L45*45*5
G_{68}	L50*50*5	L45*45*5	L45*45*5
G_{69}	L45*45*5	L45*45*5	L45*45*5
G_{70}	L45*45*5	L45*45*5	L45*45*5
G_{71}	L45*45*5	L45*45*5	L45*45*5
G_{72}	L60*60*5	L45*45*5	L45*45*5
G_{73}	L55*55*5	L50*50*5	L50*50*5
G_{74}	L50*50*5	L45*45*5	L45*45*5
G_{75}	L50*50*5	L45*45*5	L45*45*5
G_{76}	L45*45*5	L45*45*5	L45*45*5
G_{77}	L45*45*5	L45*45*5	L45*45*5
G_{78}	L45*45*5	L45*45*5	L45*45*5
G_{79}	L60*60*5	L50*50*5	L50*50*5
G_{80}	L60*60*5	L45*45*5	L45*45*5
G_{81}	L55*55*5	L50*50*5	L50*50*5
G_{82}	L50*50*5	L45*45*5	L45*45*5
G_{83}	L50*50*5	L45*45*5	L45*45*5
G_{84}	L45*45*5	L45*45*5	L45*45*5
G_{85}	L45*45*5	L45*45*5	L45*45*5
G_{86}	L45*45*5	L45*45*5	L45*45*5
G_{87}	L80*80*6	L80*80*6	L80*80*6
G_{88}	L65*65*5	L65*65*5	L65*65*5
G_{89}	L50*50*5	L45*45*5	L45*45*5
G_{90}	L55*55*5	L50*50*5	L50*50*5
G_{91}	L45*45*5	L45*45*5	L45*45*5
G_{92}	L55*55*5	L50*50*5	L50*50*5
G_{93}	L55*55*5	L45*45*5	L45*45*5
G_{94}	L50*50*5	L45*45*5	L45*45*5
G_{95}	L45*45*5	L45*45*5	L45*45*5
G_{96}	L60*60*5	L55*55*5	L55*55*5

Table 7.12 (continued)

Shape Variables (m)			
$x_1 = y_1$	7.93	7.00	7.02
$x_2 = y_2$	1.25	1.00	1.04
$x_3 = y_3$	1.25	1.00	1.00
Weight (kg)			
	33561.6 kg	30030.2 kg	30245.2 kg

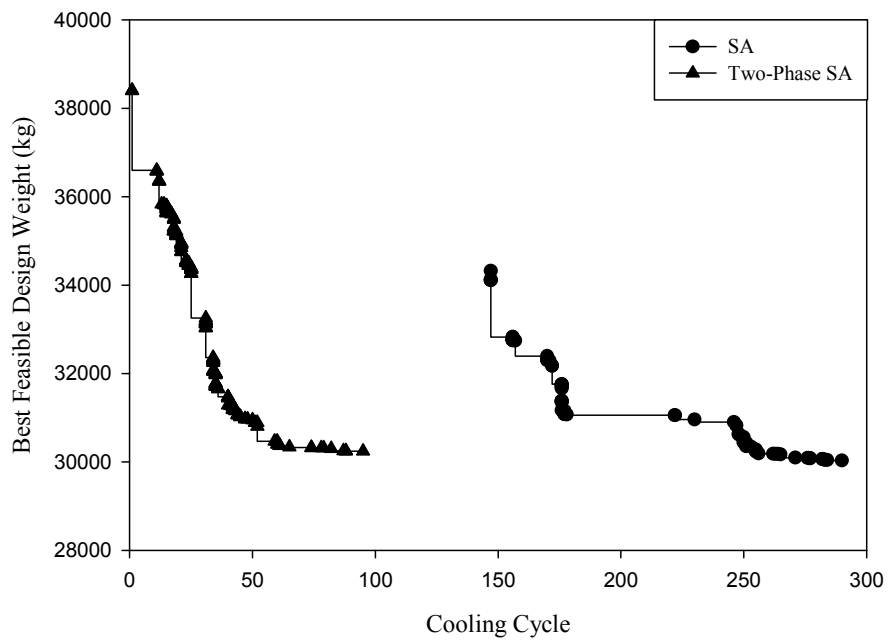
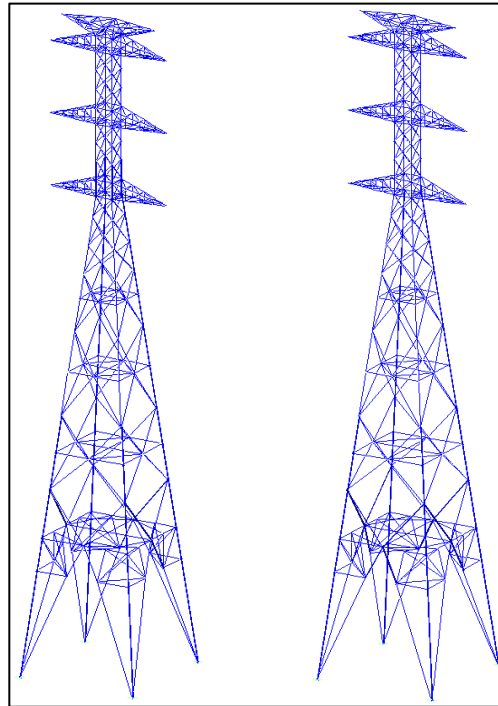


Figure 7.11 Best feasible design weights obtained from SA and two-phase SA for 400 kV suspension tower.



a) SA result

b) Two-phase SA result

Figure 7.12 Final best feasible towers obtained from SA and two-phase SA for 400kV suspension tower.

CHAPTER 8

CONCLUSION

8.1. Overview and Summary of Thesis

Optimization of steel transmission line towers is particularly important in the sense that these structures are designed once as either suspension or tension towers in several different types for each line, yet multitudes of them are erected along transmission lines extending to several hundreds of kilometers. Accordingly, even a small percentage of weight reduction that can be achieved in the design of a single tower may add up to hundreds or thousands of tons of steel material when the entire transmission line is considered. Not only the material but also the design cost of these structures is significant. The towers are formed with combinations of different body and leg extensions. This requires working with several analysis models and member groups. Optimization and detailing the suite of these structures take considerable time. Introducing an automated optimization tool allows engineers to complete the design work in reduced amount of time. This accelerates both manufacturing and assembly time of the transmission time projects.

This thesis is concerned with a simultaneous optimum design steel lattice energy transmission line tower members with respect to the cross-section sizes of the members (size optimization) and the coordinates of the nodal points (shape optimization) to obtain their minimum weight designs. All members are taken into consideration during the size optimization, yet only pre-defined primary joints are involved in shape optimization due to electrical clearance limits as well as design and fabrication requirements followed in practical engineering applications of such systems. The tower members are selected from European steel angle profile

database and their design checks are performed in accordance with provisions imposed by ASCE 10-97 (2000).

The resulting optimization problem is solved using simulated annealing (SA) optimization technique, which is a nature-inspired metaheuristic search technique utilizing concepts from annealing process of physical systems in thermodynamics. Although SA has often been shown as a robust and proven method for optimization of complicated problems encountered in various engineering disciplines, the major drawback of this technique, which is in fact the problem of all other meta-heuristic approaches is that it requires a significant amount of computation time for convergence to near-optimum solutions especially for large-scale structures subjected to numerous load combinations, similar to the problem at hand. Therefore, a two-phase SA algorithm is developed and proposed in this thesis as an exclusive method for acquiring optimum design of steel transmission towers more rapidly with an annealing algorithm. In the first phase of this method, only the shape parameters are optimized by the annealing algorithm while the steel members are sized with a fully stressed design based heuristic approach. The objective of the first phase is to improve the initial design rapidly in relatively less number of iterations (cooling cycles). In the second phase, the best design obtained in the prior phase is utilized as the initial solution, and the annealing algorithm is implemented anew for both shape and size variables together under a new set of annealing parameters over a much reduced number of cooling cycles.

In the context of the thesis, the simulated annealing based algorithms developed for optimum size and shape design of steel lattice transmission line towers are integrated with PLS-Tower software. The objective in this endeavor is to offer practicing engineers a useful tool, which gives them ability to utilize full design and analyses features of PLS-Tower during automated optimum design process as well as to pre- and post-process tower models using its graphical user interface. The PLS-Tower, which is available in every design office working on energy transmission line structures, is the most well-known and recognized software by private corporations as well as state authorities. The software has been specifically

developed for analysis and design of steel lattice towers used in energy transmission lines. It allows for structural analyses of steel towers considering geometric nonlinearities, where the steel members can be sized according to almost all major design specifications in the world. In the study, the integration of simulated annealing algorithms with the PLS-Tower software is performed such that the optimization module modifies the current solution and generates an alternative design with a new set of size and shape variables. A new finite element model (FEM) is generated in PLS-Tower for this new design with the help of model generating module that has been specifically developed by the authors to automate construction of a new model in PLS-Tower without any user interaction. The finite element solver of PLS-Tower is then executed to analyze the new design and obtain member forces, joint support reactions and joint displacements. Depending on the size of the model and type of analyses chosen (i.e., linear or nonlinear), the whole analysis process may take from a fraction of seconds to several minutes. The results of the analyses are collected in group summary tables, which display all details of member and connection design for the most critical element of each member group. The PLS-Tower is also automated to perform all design checks and calculate the resulting weight of the structure. The results obtained from PLS-Tower design module are sent back to optimization module for objective function calculations in conjunction with an integrated penalty function.

The numerical performances of the annealing algorithms were investigated on four case studies chosen from the real-world projects. The case studies were selected from suspension and tension towers in various high-voltage overhead transmission lines between 110 kV and 400 kV; namely (i) a 337-member, 110 kV suspension tower (Figure 7.1), (ii) a 438-member, 110 kV tension tower (Figure 7.4), (iii) 397-member, 220 kV suspension tower (Figure 7.7), and (iv) 693-member, 400 kV suspension tower (Figure 7.10). A summary of the design and geometrical data used in these test problems is given in Table 8.1 in terms of voltage level, tower type, number of tower members, tower height, number of

tower members, number of sizing variables (member groups), number of shape variables, number of angel sections used for sizing tower members, steel grade of tower members, minimum section for leg members, minimum section for other members, number of load combinations.

Table 8.1 Design and geometrical data of example towers.

Design data	Test problem 1	Test problem 2	Test problem 3	Test problem 4
Voltage level	110 kV	110 kV	220 kV	400 kV
Type	Suspension	Tension	Suspension	Suspension
# of members	337	438	397	693
Tower height (m)	43.5	43.9	31.5	80.4
# of sizing variables (member groups)	51	64	58	96
# of shape variables	3	3	3	3
# of angel sections used for sizing tower members	67	67	73	72
Steel grade of tower members	S355JR	S355JR	A572-Gr50	S355JR
Minimum section for leg members	L50x50x6	L50x50x6	L65x65x6	L60x60x6
Minimum section for other members	L50x50x5	L50x50x5	L45x45x4	L45x45x5
# of load combinations	22	49	11	44

Both the annealing algorithm (SA) and its two phase variant (two-phase SA) developed in this thesis are employed together to minimize the lattice steel towers in the test problems. A total of five independent runs were carried out with the SA and two-phase SA algorithms in each case study, considering the stochastic nature of the technique. All design considerations, such as profile dataset, geometry requirements and loading were kept exactly identical to the design process of the towers in industry practice. The numerical performances of the algorithms in these design examples were reported in the respective tables in Chapter 7 in terms of the optimized weights of the towers and computing time in each run. In addition, the optimized design weights of the towers were also compared with the results of conventional design process in order to quantify material saving owing to optimization process. All the results are summarized in Table 8.2 in terms of existing design weight of the tower, the optimized design weight of the tower with SA and two-phase SA, percent reduction of tower weights with SA and two-phase SA, average weight of the tower optimized with SA and two-phase SA, average solution time with SA and two-phase SA.

Table 8.2 Summary of example towers results.

Design data	Test problem 1	Test problem 2	Test problem 3	Test problem 4
The existing design weight (kg)	8262.5	13207.1	6346.1	33561.6
The optimized design weight with SA (kg)	7235.1	11835.1	4649.4	30030.2
The optimized design weight with two-phase SA (kg)	7483.4	11801.3	4673.5	30250.1
% reduction in tower weight by SA	12.5	7.7	26.7	10.8
% reduction in tower weight by two-phase SA	9.5	8.2	26.4	10.2
Average tower weight with SA (kg)	7373	12193	4754	30306
Average tower weight with two-phase SA (kg)	7552	12120	4701	30381
Average solution time with SA (min.)	445	843	549	1678
Average solution time with two-phase SA (min.)	173	319	177	609

The results indicate that the two-phase SA algorithm produces compatible results to those of the SA algorithm even though the former takes much lesser time to converge to the optimum solution. The results also indicate that optimum design process leads to weight reduction in the range of 8-26% as compared to industry practice.

8.2. Future Recommendations

In this study, a certain improvement of SA algorithm is achieved in terms of its computation time for optimum design of transmission line towers in real-life engineering practice. It is shown that a standard typical computation time of SA algorithm can be reduced by half or sometimes to one third by the virtue of two-phase SA without adversely affecting the quality of optimum solutions obtained with annealing search process. However, a further improvement of this algorithm seems possible by hybridizing SA with some gradient based methods, where the latter may be implemented to take care of continuous shape variables during the optimization process for a rapid search process.

Another computational improvement can be achieved with the heuristic approach followed in the first phase of the proposed algorithm. It is noted that the heuristic algorithm constitutes the majority of the optimization time due to significant number of members groups. Hence, alternative optimization strategies might be developed to reduce the computation time of cross-section algorithm in the first phase.

Finally, some soft-computing techniques such as neural networks might be employed for approximate response analyses of designs to accelerate the convergence time of the optimization process.

REFERENCES

- Ahrari, A., & Deb, K. (2016). An improved fully stressed design evolution strategy for layout optimization of truss structures. *Computers & Structures*, *164*, 127-144.
- American Society of Civil Engineers. (2000). *Design of latticed steel transmission structures: (ASCE 10-97)*. Reston, Virginia: American Society of Civil Engineers.
- American Society of Civil Engineers. (2010). *Guidelines for electrical transmission line structural loading: (ASCE 10-74) (Third b.)*. Reston, Virginia: American Society of Civil Engineers.
- Arora, J. S. (2002). Methods of discrete variable structural optimization. *Recent Advances in Optimum Structural Design* (s. 1-40). USA: ASCE.
- Balling, R. J. (1991). Optimal steel frame design by simulated annealing. *Journal of Structural Engineering, ASCE*, *117*(6), 1780-1795.
- Begg, D. W., & Liu, X. (2000). On simultaneous optimization of smart structures - Part II. *Computer Methods in Applied Mechanics and Engineering*, *184*(1), 25-37.
- Belegundu, A. D., & Arora, J. S. (1985). A study of mathematical programming methods for structural optimization part II: Numerical results. *International Journal for Numerical Methods in Engineering*, 1601-1623.
- Belegundu, A. D., & Arora, J. S. (1985). A study of mathematical programming methods for structural optimization part 1: Theory. *International Journal for Numerical Methods in Engineering*, *21*, 1583-1599.
- Bennage, W. A., & Dhingra, A. K. (1995). Single and multiobjective structural optimization in discrete-continuous variables using simulated annealing. *International Journal for Numerical Methods in Engineering*, *38*(16), 2753-2773.
- Bland, J. A. (1994). A tabu search approach to engineering optimisation. *Proc. 9th International Conference on Application of Artificial Intelligence in Engineering* (s. 423-430). University Park PA: WIT Press.

- Bohachevsky, I. O., Johnson, M. E., & Stein, M. L. (1986). Generalized simulated annealing for function optimization. *Technometrics*, 28(3), 209-217.
- Bremicker, M., Papalambros, P. Y., & Loh, H. T. (1990). Solution of mixed-discrete structural optimization problems with a new sequential linearization algorithm. *Computers & Structures*, 37(4), 451-461.
- CENELEC. (2012). *Overhead electrical lines exceeding AC 1 kV - Part 1: General requirements - Common specifications: (BS EN 50341-1)*. Brussels: BSI Standards Publication.
- Ceranic, B., Fryer, C., & Baines, R. W. (2001). An application of simulated annealing to the optimum design of reinforced concrete retaining structures. *Computers & Structures*, 79(17), 1569-1581.
- Cerny, V. (1985). Thermodynamical approach to the traveling salesman problem: An efficient simulation algorithm. *Journal of Optimization Theory and Applications*, 45(1), 41-51.
- Chen, G. S., Bruno, B. J., & Salama, M. (1991). Optimal placement of active/passive members in truss structures using simulated annealing. *AIAA Journal*, 29(8), 1327-1334.
- Chen, T. Y., & Su, J. J. (2002). Efficiency improvement of simulated annealing in optimal structural designs. *Advances in Engineering Software*, 33(7-10), 675-680.
- Chunming, W., Tingting, S., Bin, M., & Jing, G. (2012). Research on the optimal layout of high-strength steel in the transmission tower. *Physics Procedia*, 33, 619-625.
- Coloni, A., Dorigo, M., & Maniezzo, V. (1991). Distributed optimization by ant colonies. *Proceedings of ECAL91-European Conference on Artificial Life* (s. 134-142). Paris: Elsevier.
- Connor, A. M., Seffen, K. A., Parks, G. T., & Clarkson, P. J. (1999). Efficient optimisation of structures using tabu search. *Conference on Engineering Design Optimisation; Product and Process Improvement* (s. 127-134). Bradford: MCB University Press.
- Das, B. M. (1998). *Principles of foundation engineering*. Sacramento: PWS Publishing.

- de Santana Gomes, W. J., & Beck, A. T. (2013). Global structural optimization considering expected consequences of failure and using ANN surrogates. *Computers & Structures*, *126*, 56-68.
- Degertek, S. O. (2007). A comparison of simulated annealing and genetic algorithm for optimum design of nonlinear steel space frames. *Structural and Multidisciplinary Optimization*, *34*(4), 347-359.
- EN 50341. (2012). *Overhead electrical lines exceeding AC*. Brussels.
- Fabian, V. (1997). Simulated annealing simulated. *Computers & Mathematics with Applications*, *33*(1-2), 81-94.
- Fiacco, A. V., & McCormick, G. P. (1990). *Nonlinear programming sequential unconstrained minimization techniques*. Philadelphia: Society for Industrial and Applied Mathematics.
- Flager, F., Soremekun, G., Adya, A., Shea, K., Haymaker, J., & Ficher, M. (2014). Fully Constrained Design: A general and scalable method for discrete member sizing optimization of steel truss structures. *Computers & Structures*, *140*, 55-65.
- Gandomi, A. H., Yang, X. S., Talatahari, S., & Alavi, A. H. (2013). *Metaheuristic applications in structures and infrastructures*. Elsevier.
- Garcia-Lopez, N. P., Sanchez-Silva, M., Medaglia, A. L., & Chateaufneuf, A. (2011). A hybrid topology optimization methodology combining simulated annealing and SIMP. *Computers & Structures*, *89*(15-16), 1512-1522.
- Genovese, K., Lamberti, L., & Pappalettere, C. (2005). Improved global-local simulated annealing formulation for solving non-smooth engineering optimization problems. *International Journal of Solids and Structures*, *42*(1), 203-237.
- Guo, H. Y., & Li, Z. L. (2011). Structural topology optimization of high-voltage transmission tower with discrete variables. *Structural and Multidisciplinary Optimization*, *43*(6), 851-861.
- Hajela, P. (1999). Nongradient methods in multidisciplinary design optimization—status and potential. *Journal of Aircraft*, *36*(1), 255-265.
- Hasançebi, O., & Çarbaş, S. (2011). Ant colony search method in practical structural optimization. *International Journal of Optimization in Civil Engineering*, *1*, 91-105.

- Hasançebi, O., & Erbatur, F. (2002a). Layout optimisation of trusses using simulated annealing. *Advances in Engineering Software*, 33(7-10), 681-696.
- Hasançebi, O., & Erbatur, F. (2002b). On efficient use of simulated annealing in complex structural optimization problems. *Acta Mechanica*, 157(1), 27-50.
- Hasançebi, O., Bahçecioglu, T., Kurç, O., & Saka, M. P. (2011). Optimum design of high-rise steel buildings using an evolution strategy integrated parallel algorithm. *Computers & Structures*, 89(21-22), 2037-2051.
- Hasançebi, O., Çarbaş, S., & Saka, M. P. (2010a). Improving the performance of simulated annealing in structural optimization. *Structural and Multidisciplinary Optimization*, 41(2), 189-203.
- Hasançebi, O., Çarbaş, S., Doğan, E., Erdal, F., & Saka, M. P. (2009). Performance evaluation of metaheuristic search techniques in the optimum design of real sized pin jointed structures. *Computers & Structures*, 87(5), 284-302.
- Hasançebi, O., Çarbaş, S., Doğan, E., Erdal, F., & Saka, M. P. (2010c). Comparison of non-deterministic search techniques in the optimum design of real size steel frames. *Computers & Structures*, 88(17), 1033-1048.
- Hasançebi, O., Erdal, F., & Saka, M. P. (2010b). Adaptive harmony search method for structural optimization. *Journal of Structural Engineering*, 136(4), 419-431.
- Holland, J. H. (1992). *Adaptation in natural and artificial systems*. Cambridge: The MIT Press.
- IEC 60826. (2003). *Loading and strength of overhead transmission lines 3rd edition*. Geneva.
- International Electrotechnical Commission. (2003). *International Standard: Design criteria of overhead transmission lines: (IEC 60826) (Third b.)*. Geneva: IEC.
- Kaveh, A., Gholipour, Y., & Rahami, Y. (2008). Optimal design of transmission towers using genetic algorithm and neural networks. *International Journal of Space Structures*, 23(1), 1-19.
- Kennedy, J., & Eberhart, R. C. (1995). Particle swarm optimization. *Proceedings of IEEE International Conference on Neural Networks*, (s. 1942-1948). Piscataway, NJ.

- Kiessling, F., Nefzger, P., Nolasco, J. F., & Kaintzyk, U. (2003). *Overhead power lines planning, design, construction*. New York: Springer.
- Kirkpatrick, S., Gelatt, C. D., & Vecchi, M. P. (1983). Optimization by simulated annealing. *Science*, 220(4598), 671-680.
- Kocer, F. Y., & Arora, J. S. (2002). Optimal design of latticed towers subjected to earthquake loading. *Journal of Structural Engineering*, 197-204.
- Lamberti, L. (2008). An efficient simulated annealing algorithm for design optimization of truss structures. *Computers & Structures*, 86(19-20), 1936-1953.
- Lamberti, L., & Pappalettere, C. (2007). Weight optimization of skeletal structures with multi-point simulated annealing. *Computer Modeling in Engineering and Sciences*, 18(3), 183-222.
- Lamberti, L., & Pappalettere, C. (2011). Metaheuristic design optimization of skeletal structures: A review. *Computational Technology Reviews*, 4(1), 1-32.
- Lee, K. S., & Geem, Z. W. (2005). A new meta-heuristic algorithm for continuous engineering optimization: Harmony search theory and practice. *Computer Methods in Applied Mechanics and Engineering*, 194(36-38), 3902-3933.
- Leite, J. P., & Topping, B. H. (1998). Improved genetic operators for structural engineering optimization. *Advances in Engineering Software*, 29(7-9), 529-562.
- Leite, J. P., & Topping, B. H. (1999). Parallel simulated annealing for structural optimization. *Computers & Structures*, 73(1-5), 545-564.
- Liu, W., & Ye, J. (2014). Collapse optimization for domes under earthquake using a genetic simulated annealing algorithm. *Journal of Constructional Steel Research*, 97, 59-68.
- Manoharan, S., & Shanmuganathan, S. (1999). A comparison of search mechanisms for structural optimization. *Computers & Structures*, 73(1-5), 363-372.
- Marti, J. V., Gonzalez-Vidosa, F., Yepes, V., & Alcalá, J. (2013). Design of prestressed concrete precast road bridges with hybrid simulated annealing. *Engineering Structures*, 48, 342-352.

- Metropolis, N., Rosenbluth, A. W., Rosenbluth, M. N., Teller, A. H., & Teller, E. (1953). Equation of state calculations by fast computing machines. *The Journal of Chemical Physics*, 21(6), 1087-1092.
- Mitra, G., & Wolfenden, K. (1968). A computer technique for optimizing the sites and heights of transmission line towers - A dynamic programming approach. *The Computer Journal*, 10(4), 347-351.
- Moh, J. S., & Chiang, D. Y. (2000). Improved simulated annealing search for structural optimization. *AIAA Journal*, 38(10), 1965-1973.
- Natarajan, K., & Santhakumar, A. R. (1995). Reliability-based optimization of transmission line towers. *Computers & Structures*, 55(3), 387-403.
- Papadrakakis, M., Lagaros, N. D., & Tsompanakis, Y. (1998). Structural optimization using evolution strategies and neural networks. *Computer Methods in Applied Mechanics and Engineering*, 156(1-4), 309-333.
- Paris, J., Martinez, S., Navarrina, S., Colominas, F., & Casteleiro, M. (2010). Structural optimization of high tension towers. *2nd International Conference on Engineering Optimization*. Lisbon, Portugal.
- Paris, J., Martinez, S., Navarrina, S., Colominas, F., & Casteleiro, M. (2012). Structural optimization of high voltage transmission line towers considering continuum and discrete design variables. *Computer Aided Optimum Design in Engineering XII*, (s. 59-69).
- Park, H. S., & Sung, C. W. (2002). Optimization of steel structures using distributed simulated annealing algorithm on a cluster of personal computers. *Computers & Structures*, 80(14-15), 1305-1316.
- Patnaik, S. N., Guptill, J. D., & Berke, L. (1995). Merits and limitations of optimality criteria method for structural optimization. *International Journal for Numerical Methods in Engineering*, 38, 3087-3120.
- Perez, R. E., & Behdinan, K. (2007). Particle swarm approach for structural design optimization. *Computers & Structures*, 85(19-20), 1579-1588.
- Pezeshk, S., Camp, C. V., & Chen, D. (2000). Design of nonlinear framed structures using genetic optimization. *Journal of Structural Engineering*, 382-388.
- Power Line Systems Inc. (2015). *PLS-TOWER Manual: Analysis and design of steel latticed towers used in transmission and communication facilities*. USA: Power Line Systems Inc.

- Rao, G. V. (1995). Optimum design for transmission line towers. *Computers & Structures*, 57(1), 81-92.
- Ray, S. (2008). *Electrical power systems: Concepts, theory and practice*. New Delhi: PHI Learning Private Limited.
- Reddy, G., & Cagan, J. (1995). An improved shape annealing algorithm for truss topology generation. *Journal of Mechanical Design*, 117(2A), 315-321.
- Saka, M. P. (2007). Optimum design of steel frames using stochastic search techniques based on natural phenomena: A review. In B. H. Topping, *Civil engineering computations: Tools and techniques* (pp. 105-147). Stirlingshire, UK: Saxe-Coburg Publications.
- Saka, M. P. (2009). Optimum design of steel sway frames to BS5950 using harmony search algorithm. *Journal of Constructional Steel Research*, 65(1), 36-43.
- Saka, M. P. (2014). Shape and topology optimization design of skeletal structures using metaheuristic algorithms: A review. *Computational Technology Reviews*, 9, 31-68.
- Saka, M. P., & Dogan, E. (2012). Recent developments in metaheuristic algorithms: A review. *Computational Technology Reviews*, 5(4), 31-78.
- Saka, M. P., & Geem, Z. W. (2013). Mathematical and metaheuristic applications in design optimization of steel frame structures: An extensive review. *Mathematical Problems in Engineering*, 1-33.
- Scholz, D. (2011). *Deterministic global optimization-geometric branch and bound methods and their applications*. New York: Springer.
- Shea, K., & Smith, I. F. (2006). Improving full-scale transmission tower design through topology and shape optimization. *Journal of Structural Engineering*, 132(5), 781-790.
- Shea, K., Cagan, J., & Fenves, S. J. (1997). A shape annealing approach to optimal truss design with dynamic grouping of members. *Journal of Mechanical Design*, 119(3), 388-394.
- Shehata, A. Y., Nassef, A. O., & El Damatty, A. A. (2008). A coupled finite element-optimization technique to determine critical microburst parameters for transmission towers. *Finite Elements in Analysis and Design*, 45(1), 1-12.

- Sheppard, D. J., & Palmer, A. C. (1972). Optimal design of transmission towers by dynamic programming. *Computers & Structures*, 2(4), 445-468.
- Shim, P. Y., & Manoochehri, S. (1997). Generating optimal configurations in structural design using simulated annealing. *International Journal for Numerical Methods in Engineering*, 40(6), 1053-1069.
- Snyman, J. A. (2005). *Practical mathematical optimization-An introduction to basic optimization theory and classical and new gradient-based algorithms* (Vol. 97). New York: Springer.
- Stiny, G. (1980). Introduction to shape and shape grammars. *Environment and Planning B*, 7, 343-351.
- Stromberg, L. L., Beghini, A., Baker, W. F., & Paulino, G. H. (2011). Application of layout and topology optimization using pattern gradation for the conceptual design of buildings. *Structural and Multidisciplinary Optimization*, 43(2), 165-180.
- Szewczyk, Z., & Hajela, P. (1993). Neural network approximations in a simulated annealing based optimal structural design. *Structural Optimization*, 5(3), 159-165.
- Taniwaki, K., & Ohkubo, S. (2004). Optimal synthesis method for transmission tower truss structures subjected to static and seismic loads. *Structural and Multidisciplinary Optimization*, 26(6), 441-454.
- Terai, K. (1974). *Application of optimality criteria in structural synthesis*. University of California. Los Angeles: United States.
- Theodoracatos, V. E., & Grimsley, J. L. (1995). The optimal packing of arbitrarily-shaped polygons using simulated annealing and poly-time cooling schedules. *Computer Methods in Applied Mechanics and Engineering*, 125(1-4), 53-70.
- Venanzi, I., & Materazzi, A. L. (2007). Multi-objective optimization of wind-excited structures. *Engineering Structures*, 29(6), 983-990.
- Zecchin, A. C., Simpson, A. R., Maier, H. R., Leonard, M., Roberts, A. J., & Berrisford, M. J. (2006). Application of two ant colony optimisation algorithms to water distribution system optimisation. *Mathematical and Computer Modelling*, 44(5-6), 451-468.

Zeng, S. K., & Li, L. J. (2012). Particle swarm-group search algorithm and its application to spatial structural design with discrete variables. *International Journal of Optimization in Civil Engineering*, 2(4), 443-458.

APPENDIX A

COMPONENT LIBRARIES OF PLS-TOWER

Component libraries in PLS-Tower (Figure A.1) define the size, weight, strength and other properties of bolts, guys, members and other equipment. The users are allowed to create their own libraries as well. Using libraries of standard components greatly enhances productivity of the users by significantly reducing the amount of input, which also reduces the chance of error.

	Steel Material Label	Modulus of Elasticity	Yield Stress Fy (MPa)	Ultimate Stress Fu (MPa)	Member All. Stress Hyp. 1 (MPa)	Member All. Stress Hyp. 2 (MPa)	Member Rupture Hyp. 1 (MPa)	Member Rupture Hyp. 2 (MPa)	Member Bearing Hyp. 1 (MPa)	Member Bearing Hyp. 2 (MPa)
1	S355JR	199948	355	510	0	0	0	0	0	0
2	S275JR	199948	275	410	0	0	0	0	0	0
3	S235JR	199948	235	350	0	0	0	0	0	0
4	A572-50	199948	345	448	0	0	0	0	0	0

a) Steel Material Library

	Angle Type	Angle Size	Long Leg (cm)	Short Leg (cm)	Thick. (cm)	Unit Weight (N/m)	Gross Area (cm ²)	w/t Ratio	Radius of Gyration Rx (cm)	Radius of Gyration Ry (cm)	Radius of Gyration Rz (cm)	Number of Angles	Wind Width (cm)
1	SAE	L45*45*4	4.5	4.5	0.4	26.88	3.49	8.50	1.36	1.36	0.88	1	4.5
2	SAE	L45*45*5	4.5	4.5	0.5	33.16	4.30	6.60	1.35	1.35	0.87	1	4.5
3	SAE	L45*45*6	4.5	4.5	0.6	39.24	5.09	5.33	1.34	1.34	0.87	1	4.5
4	SAE	L50*50*4	5	5	0.4	30.02	3.89	9.75	1.52	1.52	0.98	1	5
5	SAE	L50*50*5	5	5	0.5	36.98	4.80	7.60	1.51	1.51	0.98	1	5
6	SAE	L60*60*4	6	6	0.4	36.30	4.71	12.00	1.83	1.83	1.18	1	6
7	SAE	L60*60*5	6	6	0.5	44.83	5.82	9.40	1.82	1.82	1.17	1	6
8	SAE	L65*65*4	6.5	6.5	0.4	39.63	5.15	13.00	1.99	1.99	1.29	1	6.5
9	SAE	L65*65*5	6.5	6.5	0.5	48.85	6.34	10.20	1.98	1.98	1.27	1	6.5
10	SAE	L70*70*5	7	7	0.5	52.68	6.84	11.20	2.14	2.14	1.38	1	7
11	SAE	L75*75*6	7.5	7.5	0.6	67.39	8.75	9.83	2.28	2.28	1.47	1	7.5
12	SAE	L80*80*6	8	8	0.6	72.01	9.35	10.67	2.44	2.44	1.57	1	8
13	SAE	L80*80*8	8	8	0.8	94.76	12.30	7.75	2.42	2.42	1.55	1	8
14	SAE	L100*100*8	10	10	0.8	119.68	15.50	10.00	3.06	3.06	1.96	1	10
15	SAE	L100*100*10	10	10	1.0	148.13	19.20	7.80	3.04	3.04	1.95	1	10

b) Steel Profile Library

	Bolt Label	Bolt Diameter (cm)	Hole Diameter (cm)	Ultimate Shear Capacity (kN)	Default End Distance (cm)	Default Bolt Spacing (cm)	Shear Capacity Hyp. 1 (kN)	Shear Capacity Hyp. 2 (kN)
1	M-16 (5.8)	1.60	1.75	60.32	0	0	0	0
2	M-20 (5.8)	2.00	2.15	94.25	0	0	0	0
3	M-24 (5.8)	2.40	2.55	135.72	0	0	0	0
4	M-30 (5.8)	3.00	3.15	212.06	0	0	0	0
5	M-16 (6.8)	1.60	1.75	72.38	0	0	0	0
6	M-20 (6.8)	2.00	2.15	113.10	0	0	0	0
7	M-24 (6.8)	2.40	2.55	162.86	0	0	0	0
8	M-30 (6.8)	3.00	3.15	254.47	0	0	0	0
9	M-16 (8.8)	1.60	1.75	96.46	0	0	0	0
10	M-20 (8.8)	2.00	2.15	150.72	0	0	0	0
11	M-24 (8.8)	2.40	2.55	217.15	0	0	0	0
12	M-30 (8.8)	3.00	3.15	339.29	0	0	0	0

Save Save As Merge Report Cancel

c) Bolt Library

	Label	Stock Number	Area (mm ²)	Modulus of Elasticity (MPa)	Diameter (mm)	Unit Weight (N/m)	Drag Coef.	Thermal Expansion Coeff. (/deg C)	Ultimate Tension (kN)	Allowable % of Ultimate
1	28	#28 - GR 1500	1000	150000	29	79.07	1	1.20E-05	1350	85
2	40	#40 - GR 1500	1780	150000	39	141.26	1	1.20E-05	2400	85
3	1/2	1/2 - HQ	97	160000	12.7	7.845	1	1.15E-05	133	85
4	2x1/2	1/2 - HQ	194	160000	12.7	15.69	1	1.15E-05	266	85
5	2x5/8	5/8 -HQ	302	160000	15.9	23.536	1	1.15E-05	428	85
6	13/16	13/16 -HQ	256	150000	20.6	20.594	1	1.15E-05	356	85
7	42589	7/8 -HQ	296	150000	22.2	23.536	1	1.15E-05	409	85
8	15/16	15/16 -HQ	340	150000	23.8	27.459	1	1.15E-05	480	85
9	1	1 -HQ	387	150000	25.4	30.401	1	1.15E-05	543	85
10	1-13/16	1-13/16-HQ	1271	135000	46	101.01	1	1.15E-05	1800	85
11	1-15/16	1-15/16-HQ	1452	135000	49.2	114.74	1	1.15E-05	2050	85
12	2	2-HQ	1548	135000	50.8	122.58	1	1.15E-05	2180	85

Save Save As Merge Report Cancel

d) Cable Library

	CAN Property Label	Stock Number	Strength Factor	Strength Check	Resultant Capacity (kN)	Long. Shear Cap. (kN)	Tran. Shear Cap. (kN)	Vert. Shear Cap. (kN)	Long. Pos. Cap. (kN)	Long. Neg. Cap. (kN)	Tran. Pos. Cap. (kN)	Tran. Neg. Cap. (kN)	Vert. Pos. Cap. (kN)	Vert. Neg. Cap. (kN)
1														
2														
3														
4														
5														
6														
7														
8														
9														
10														

Save Save As Merge Report Cancel

e) Connection and Anchor Library

	Equipment Property Label	Stock Number	Weight (N)	Wind Area (m ²)	Ice Area (m ²)	Shape or EIA Antenna Type	Drag Coef.	Diameter (m)	Height (m)	Vertical Offset (m)
1	T1000		44482	4.65	0.00		1	0.00	0.00	0.00
2	T2000		88964	9.29	0.00		1	0.00	0.00	0.00
3	Microwave Antenna		444.82	0.46	0.19	EIA Microwave	1	0.76	0.76	0.00
4										

Save Save As Merge Report Cancel

f) Equipment Library

	Label	Stock Number	Holding Capacity (N)
1	TST1		4.45E+06
2	C-EX1		222411
3	C-EX2		88964.4
4	C-EX3		88964.4
5	C-EX4		222411
6	C-EX5		100085
7	C-EX6		499998
8	C-EX7		88964.4
9	C-EX8		111206
10	C-EX12		59999.8

Save Save As Report Cancel

g) Clamp Library

	Label	Stock Number	Length (m)	Weight (N)	Wind Area (m ²)	Tension Capacity (N)	Energized Length (m)	Energized Diameter (m)
1	ST-EX1	edf	2.00	444.82	0	222411	0	0
2	ST-EX2		1.83	444.82	0	222411	0	0
3	400 TEN	1	4.01	2650	0	160000	0	0
4	220 TEN	1	2.87	3600	0	160000	0	0
5	DSus_1	1	5.00	2470	0	120000	0	0

Save Save As Report Cancel

h) Strain Insulator Library

	Label	Stock Number	Length (m)	Weight (N)	Wind Area (m ²)	Tension Capacity (N)	Top Rect Width (m)	Top Rect Height (m)	Bot. Rect Width (m)	Bot. Rect Height (m)	Vert. Rect Width (m)	Vert. Rect Height (m)
1	SUSP-EX3		2.59	444.82	0	88964.4	0.3048	0.3048	0.0305	0.1219	0.3048	0.6096
2	SUSP-EX4		2.29	934.13	0	88964.4	0	0	0	0	0	0
3	SUSP-EX5		3.96	1779.29	0	155688	0	0	0	0	0	0
4	SUSP-EX6		2.11	889.64	0	44482.2	0	0	0	0	0	0
5	SUSP-EX7		1.52	667.23	0	111206	0	0	0	0	0	0
6	SUSP-EX8		4.11	0.00	0	155688	0	0	0	0	0	0
7	SUSP-EX12		3.50	1425.00	0	120000	0	0	0	0	0	0

Save Save As Report Cancel

i) Suspension Insulator Library

	Label	Stock Number	Length Side A (m)	Length Side B (m)	Wind Area Side A (m ²)	Wind Area Side B (m ²)	Weight Side A (N)	Weight Side B (N)	Tension Cap. Side A (N)	Tension Cap. Side B (N)
1	2part-EX4		3.23	3.23	0	0	934.1	934.1	133447.0	133447.0
2	2part-EX3		2.91	2.91	0	0	444.8	444.8	88964.4	88964.4
3	2part-EX7A		1.75	2.14	0	0	1334.5	1334.5	155688.0	155688.0
4	2part-EX7B		1.37	1.01	0	0	1334.5	1334.5	155688.0	155688.0
5	2part-EX7C		0.87	1.22	0	0	1334.5	1334.5	155688.0	155688.0
6	2part-EX7D		3.35	3.49	0	0	444.8	444.8	88964.4	88964.4
7	2part-EX7E		1.77	1.68	0	0	444.8	444.8	88964.4	88964.4

Save Save As Report Cancel

j) 2-Part Insulator Library

	Label	Stock Number	Has Brace	Horz. Projection (m)	Vert. Projection (m)	Weight (N)	Interaction Capacity	Cantilever Capacity (N)	Tension Capacity (N)	Comp. Capacity (N)
1										
2										
3										
4										
5										

k) Post insulator library

Figure A.1 Component libraries of PLS-Tower.

CURRICULUM VITAE

Serkan SAHIN has a 10-year experience in structural engineering, design, and consulting. With the knowledge of structural design, he involved various types of structural design projects such as Overhead Transmission Line Towers design, Industrial Buildings design, Research and Development projects (e.g., Wind Turbine Towers, Solar Panels).

He has acquired proficiency especially in the analysis and design of the steel lattice towers, substation structures, and wind turbine towers, steel buildings. Serkan SAHIN holds a Master of Science degree in Structural Engineering since 2009. His research was based on the comparison of AISC-360 (AISC-LRD) and Eurocode 3 specifications in terms of strength limit states. Since 2009, he has been studying for his PhD degree on weight optimization of steel lattice energy transmission line towers using stochastic optimization algorithms.

PERSONAL INFORMATION

Surname, Name : Şahin, Serkan
Nationality : Turkish (T.C.)
Date of Birth and Place : 16 May 1983, Ankara
Marital Status : Single
e-mail : drsahinserkan@gmail.com

EDUCATION

Degree	Institution	Year of Graduation
Ph.D.	METU Civil Engineering	2016
MSc.	METU Civil Engineering	2009
BSc.	METU Civil Engineering	2006
High School	Başkent High School, Ankara	1997

WORK EXPERIENCE

Senior Structural Design Engineer and Project Manager; July 2007 - Present

Miteng Engineering Computer Consultancy Inc.

- Design of steel structures, transmission line towers, substation steel structures, wind turbine towers, and solar systems.
- Design of foundations for steel structures, transmission line towers, substation steel structures, wind turbine towers, and solar systems.
- Participating in research & development projects.
- Coordinating the preparation of workshop and erection drawings as per client specifications.
- Participating in full-scale load tests of the transmission line towers.

Structural Design Engineer; June 2006 - June 2007

Promer Consultancy Engineering Ltd. Inc.

- Design of steel industrial buildings.
- Design of foundations for industrial buildings and industrial machines.
- Coordinating the preparation of workshop and erection drawings as per client specifications

FOREIGN LANGUAGES

English (advanced level), Spanish (elementary level), German (beginner level)

PUBLICATIONS

1. Topkaya, C., & Şahin, S. (2011). A comparative study of AISC-360 and EC3 strength limit states. *International Journal of Steel Structures*, 11(1), 13-27.

SOFTWARE AND PROGRAMMING SKILLS

- Microsoft Office
- Visual Basic.NET
- Mathcad
- CSI - Sap2000
- CSI - Etabs
- CSI - Safe
- Response2000
- PLS-Tower
- PLS-CADD
- Tekla Structures
- AutoCAD

HOBBIES

Reading, History, Computer Technologies, Tennis, Table Tennis, Swimming, Football, Basketball, Squash, Movies